NASA CONTRACTOR REPORT

NASA CR-616

A "CRITICAL" TRACKING TA: FOR MAN-MACHINE RESEARCH RELATED TO THE OPERATOR'S EFFECTIVE DELAY TIME

PART I: THEORY AND EXPERIMENTS WITH A FIRST-ORDER DIVERGENT CONTROLLED ELEMENT

by H. R. Jex, J. D. McDonnell, and A. V. Phatak

Prepared by
SYSTEMS TECHNOLOGY, INC.
Hawthorne, Calif.
for Ames Research Center

NATIONAL AERONAUTICS AND SPACE ADMINISTRATION • WASHINGTON, D. C. • NOVEMBER 1966

NASA CR-616

A "CRITICAL" TRACKING TASK FOR MAN-MACHINE RESEARCH RELATED TO THE OPERATOR'S EFFECTIVE DELAY TIME

PART I: THEORY AND EXPERIMENTS WITH A FIRST-ORDER DIVERGENT CONTROLLED ELEMENT

By H. R. Jex, J. D. McDonnell, and A. V. Phatak

Prepared under Contract No. NAS 2-2288 by
SYSTEMS TECHNOLOGY, INC.
Hawthorne, Calif.

for Ames Research Center

NATIONAL AERONAUTICS AND SPACE ADMINISTRATION

For sale by the Clearinghouse for Federal Scientific and Technical Information
Springfield, Virginia 22151 - Price $3.00

FOREWORD

This report was prepared under Contract NAS2-2288 between Systems Technology, Inc., Hawthorne, California, and NASA. The NASA project monitor was George Rathert. The STI technical director was Duane T. McRuer and the project engineer was Henry R. Jex.

The experimental work was carried out jointly at The Franklin Institute Laboratory for Research and Development, Philadelphia, Pennsylvania. The principal investigator there was William C. Reisener under the technical direction of E. S. Krendel.

ABSTRACT

A closed-loop compensatory tracking task has been developed which yields a measure of the human operator's time delay characteristics while tracking, constrains his behavior to within very narrow limits, and provides a low-variability indicator of the operator's tracking ability. The task is called the "Critical Task" because the operator is required to stabilize an increasingly unstable controlled element up to the critical point of loss of control.

In the present report, a first-order divergence is used as the controlled element to obtain certain theoretical advantages. Based on recent human response research, a theoretical analysis of this man-machine system is performed, and an experimental program is described which enables describing function and critical task measures to be compared. A specific critical task mechanization and operating procedure is developed which yields consistent and reliable measurements of the critical levels of instability.

An analysis of the describing function results shows that, when operating near criticality, the subject's behavior is adequately represented by recently developed human operator describing function models and adaptation laws. Further, the extrapolation of describing function data to the critical level of instability shows that the operator consistently loses control at small, but finite, mean stability margins. The just-controllable first-order divergence is shown to be related dominantly to the operator's effective time delay, and secondarily to the nominal variations of his average tracking characteristics and to mid-frequency phase lags due to long period kinesthetic adaptation effects.

CONTENTS

TABLES

FIGURES

SYMBOLS

a_T	Threshold value of the indifference threshold nonlinearity
$c(t)$	Operator output time function, limb position
$C(j\omega)$	Fourier transform of operator output
$e(t)$	Error time function
e_c	Autopacer error criterion level for adjustment rate switching
$E(j\omega)$	Fourier transform of error
$F(t)$	Limb-applied force
G	Total open-loop describing function, Y_pY_c
G_{ie}	Closed-loop describing function, error/forcing function
G_{im}	Closed-loop describing function, system output/forcing function
$i(t)$	Forcing function time function
$I(j\omega)$	Fourier transform of forcing function
$j\omega$	Imaginary part of the complex variable, $s = \sigma \pm j\omega$
k_1	Initial autopacer root adjustment rate
k_2	Final autopacer root adjustment rate
K	Open-loop gain
K_c	Controlled element gain
K_{GM}	Gain at maximum gain margin condition
K_p	Human operator static gain

K_{PM}	Gain at maximum phase margin condition
K_T	Gain of indifference threshold describing function
K_π	Mid-frequency operator gain, $= K_p T_K / T_K'$
$\mathcal{L}$	Laplace transform
$m(t)$	System output time function
$M(j\omega)$	Fourier transform of system output
$\overline{n^2}$	Mean-squared remnant, $\frac{1}{2\pi}\int_0^\infty \Phi_{nn}\, d\omega$
$n_c(t)$	Operator remnant time function
N	Number of subjects
$N_c(j\omega)$	Fourier transform of operator remnant
RT	Reaction time
s	Complex variable, $s = \sigma \pm j\omega$; Laplace transform variable
t	Time
T	Time constant
T_c	Critical or limiting time constant as obtained from the autopacer, $T_c = 1/\lambda_c$
T_f	Autopacer switching circuit filter time constant
T_I	General lag time constant of human pilot describing function
T_K, T_K'	Low frequency lead and lag kinesthetic time constants in precision model of human pilot describing function
T_L	General lead time constant of human pilot describing function
T_N	First-order lag time constant approximation of the neuromuscular system
T_{N_1}	First-order lag time constant of the neuromuscular system
T_R	Run length
Y	Transfer function
$Y_c(s)$	Controlled element (machine and display) transfer function

Y_{CL}	Closed-loop transfer function
Y_{OL}	Open-loop transfer function
Y_p	Pilot describing function
Y_{p_P}	Precision pilot model describing function
Y_{p_S}	Simple pilot model describing function
$Y_{p_{XC}}$	Extended crossover pilot model describing function
α	Low frequency phase approximation parameter, $\alpha = 1/T_K' - 1/T_K$
ζ	Damping ratio
ζ_{CL}	Closed-loop damping ratio
ζ_N	Damping ratio of second-order component of the neuromuscular system
ρ_a	Relative remnant at pilot's output, $\sqrt{1 - \overline{n^2}/\overline{c^2}}$
σ	Standard deviation, real part of complex variable, $s = \sigma \pm j\omega$
σ_i	RMS value of the forcing function
σ_T	RMS value of input to the indifference threshold
λ	Value of unstable root of first-order critical task
λ_c	Critical or limiting root value as obtained from the autopacer, $\lambda_c = 1/T_c$
τ	Pure time delay
$\Delta\tau$	Incremental time delay
τ_d	Physiological time delay
τ_e	Effective time delay
$\tau_r(t)$	Time-varying time delay, source of operator remnant
φ	Phase angle
$\Delta\varphi$	Incremental phase angle
φ_M	Phase margin
$\Phi_{cc}(\omega)$	Pilot's output power spectral density
$\Phi_{ee}(\omega)$	Error power spectral density

Φ_{ec}	Cross power spectral density between e and c
Φ_{ic}	Cross power spectral density between i and c
Φ_{ie}	Cross power spectral density between i and e
Φ_{ii}	Forcing function power spectral density
Φ_{mm}	System output power spectral density
Φ_{nn}	Closed-loop remnant spectral density, at pilot's output
Φ_{nn_c}	Open-loop remnant spectral density, at pilot's output, $\lvert 1 + Y_p Y_c \rvert^2 \Phi_{nn}$
χ	Chi-squared distribution variable
$\overline{\chi}$	Mean value of χ
ω	Angular frequency, rad/sec
ω_c	System crossover frequency, i.e., frequency at which $\lvert Y_p Y_c \rvert = 1$
ω_{CL}	A closed-loop inverse time constant or frequency
ω_i	Forcing function bandwidth
ω_N	Undamped natural frequency of second-order part of the neuromuscular system
ω_{PM}	Frequency of maximum phase margin (where $d\varphi/d\omega = 0$)
ω_u	Crossover frequency for neutral stability
$\doteq$	Approximately equal to
$\angle$	Angle of
dB	Decibels; 20 $\log_{10}$ ( ) if an amplitude quantity, e.g., $\lvert Y_p \rvert$
$\lvert\ \rvert$	Magnitude
$\lvert\ \rvert_{dB}$	Magnitude in dB
$(\bar{})$	Mean value

A "CRITICAL" TRACKING TASK FOR MAN-MACHINE RESEARCH RELATED TO THE OPERATOR'S EFFECTIVE DELAY TIME

Part I. Theory and Experiments with a First-Order Divergent Controlled Element

SECTION I

INTRODUCTION

Recent research in man-machine systems (refs. 1-5) shows that several important system characteristics (such as closed-loop stability, bandwidth, etc.) are critically dependent on the value of the pilot's effective delay time, τ_e. Effective delay time is defined herein as an apparent "pure time delay," "dead time," or "transmission lag" which is, in actuality, a low frequency approximation to the sum of several high frequency effects. The primary constituents of τ_e are neural transmission delays, effective lags due to neural coding, any delay time involved in the human pilot's equalization activities, and an effective delay approximating the higher order terms in the neuromuscular response of a particular limb. (An additional component in τ_e results when the system is such that the equalization lead, T_L, can be used for partial compensation of high frequency lags.) While some components of τ_e are involved in the classical step reaction-time delay, others, such as the cerebral equalizing and processing delays, are different. Furthermore, during continuous tracking of randomlike inputs, modes of human subsystem operation different from those used for discrete movements are brought into play,

e.g., contrast the saccadic (jump) movements of the eyeball versus its smooth pursuit movements for respective step or smooth changes in the desired point of regard (ref. 6). Consequently, a simple psychomotor test for measuring the effective delay time during continuous tracking would be of great practical value.

Such a tracking test, for use in programs related to man–machine integration and piloted vehicles should have the following attributes:

1. Provide a clear measure of tracking behavior which is related to other tracking tasks and to the subject's psychomotor capabilities.

2. Be sensitive enough to reveal significant changes in psychomotor performance due to the applied experimental variables or stress conditions.

3. Can be validated rapidly to achieve a high level of confidence, meaningfulness, and baseline data.

4. Be usable under a wide variety of test conditions.

This report summarizes exploratory research on a critical task technique (involving compensatory tracking of a certain type of controlled element) in which a single experimentally varied parameter will reveal the pilot's effective delay time during tracking tasks essentially free from experimental artifacts. In applying servomechanism techniques to the analysis of pilot–vehicle systems we have discovered that, by proper choice of a first- or second-order divergent "controlled element," the pilot's tracking behavior can be artificially constrained to simple

forms, in which τ_e is the dominant parameter and is measured by the critical divergence time constant, beyond which closed-loop control becomes impossible.

The theoretical basis for the concept resulted from aircraft handling qualities investigations in references 7 and 8. The use of a constraining aircraft stabilization task was originally proposed as a critical task by Ashkenas in an unpublished memorandum (ref. 9), and verification of the theoretical predictions was published in reference 10. A simplification of the task from the complex dynamics of an aircraft to a simple first-order controlled element was proposed by Durand in 1961 and was verified as an unpublished byproduct of the work reported in reference 10. The large scale investigations of reference 2 included two simpler unstable controlled elements to determine the human operator's describing function under subcritical operation, and these results indicated that the underlying assumptions would probably be met near critical conditions.

The present program was started to develop the critical task concept into a usable psychomotor test. This includes laying a firm analytic foundation for its justification, developing a specific test configuration, and verifying the indicated measurements by independent measurements of an operator's describing function under conditions closer to criticality than reported in reference 2.

The report starts with a description of the human response parameters affecting effective delay time, leading to the critical task concept and its theoretical basis, all drawing heavily on the background of reference 2. There follows the evolution of a specific critical task configuration and

procedure, including some early results. Next comes the experimental validation of the test, which was performed in the Human Response Facility at The Franklin Institute Laboratory for Research and Development. Finally, the implications and conclusions of this phase of the program are summarized. Certain mathematical analyses and data are contained in the Appendix.

SECTION II

THEORY

A. THE HUMAN OPERATOR MODEL

In this section the current mathematical model of the human operator will be summarized to form a basis for subsequent theoretical analyses of the critical task. The emphasis will be on those features affecting the operator's apparent delay time.

The critical task is a single-loop compensatory tracking task, for which the important parameters are defined in figure 1. Two key features are the solitary operator stimulus (the error) and the random-appearing nature of the forcing function (the system input). Numerous experiments (e.g., those summarized in refs. 1 and 2) serve as the data base for the analytical model describing human operation and adaptation for compensatory tracking with a visually presented, random-appearing forcing function.

The model of figure 1 comprises three elements:

1. A general quasi-linear describing function form.
2. A series of "adjustment rules" which specify how to "set" the parameters in the generalized describing function so that it becomes an approximate model of human behavior for the particular situation of interest.
3. A set of remnant power spectra related to the parameters in Item 2.

The most precise form of operator describing function* for compensatory control tasks is (see ref. 2 for details):

$$Y_p(j\omega,t) \doteq \underbrace{K_p e^{-j\omega[\tau_d+\tau_r(t)]}}_{\text{Gain}\ \text{Time Delays}} \underbrace{\frac{\left(T_K j\omega+1\right)K_T\left(\frac{a_T}{\sigma_T}\right)}{\left(T'_K j\omega+1\right)\left(T_{N_1} j\omega+1\right)\left[\left(\frac{j\omega}{\omega_N}\right)^2+\frac{2\zeta_N j\omega}{\omega_N}+1\right]}}_{\text{Neuromuscular system}} \underbrace{\left[\frac{\left(T_L j\omega+1\right)}{\left(T_I j\omega+1\right)}\right]}_{\text{Equalization}} \qquad (1)$$

A slightly modified form of this equation is used to facilitate comparison between the operator gain in this and various simpler or earlier models. This form is:

$$Y_p(j\omega,t) \doteq K_\pi e^{-j\omega[\tau_d+\tau_r(t)]} \frac{\left(j\omega+\frac{1}{T_K}\right)}{\left(j\omega+\frac{1}{T'_K}\right)} \frac{K_T\left(\frac{a_T}{\sigma_T}\right)}{\left(T_{N_1} j\omega+1\right)\left[\left(\frac{j\omega}{\omega_N}\right)^2+\frac{2\zeta_N j\omega}{\omega_N}+1\right]} \left[\frac{\left(T_L j\omega+1\right)}{\left(T_I j\omega+1\right)}\right] \qquad (2)$$

where $K_\pi = K_p(T_K/T'_K)$ = "mid-band pilot gain"

The operator is able to adjust his mid-band gain, K_π, and equalization parameters, T_L and T_I, within a fairly wide range for suitable loop closures. These adjustments have been firmly validated by experiment and their application is treated in numerous other references (e.g., 2–5 and 7–10) and need not be further discussed at this point. The term $K(a_T/\sigma_T)$ in the describing function refers to the indifference threshold describing function. This is nearly unity for difficult tracking tasks, because the serial thresholds are consciously reduced

*Because this describing function is strictly valid only in the frequency domain, it is herein represented as a function of the frequency operator ($j\omega$) instead of the Laplace operator(s).

to their nominal levels, while the rms inputs to the thresholds (the displayed error, etc.) are relatively large.

Next, consider the time delay terms. The pure time delay represented by the $e^{-j\omega\tau_d}$ term is due to sensory excitation (the retina in the visual case), nerve conduction transport lags, computational lags, and other latencies in the central nervous system. τ_d can also include sampling lags associated with multiple display scanning. It appears to be essentially invariant with forcing function and controlled element dynamics for random-appearing input tasks. However both intersubject and intrasubject τ_d variations occur. Empirically the minimum value for τ_d seems to lie in the range from about 0.06 to 0.10 sec for single-loop tracking situations.

The operator's time delay variation, $\tau_r(t)$, is not thoroughly understood at this time, but is believed to be a good way to describe one source of remnant. In that case, it would be a function of attention level, task difficulty, etc. Any variation in τ_r results in an apparent phase lag fluctuation and sets one fundamental limit on the minimum phase margin required for closed-loop stability during a long duration tracking task. Over long tracking runs (1 – 5 minutes) the mean value of $\tau_r(t)$ is zero, but over very short periods (on the order of a few seconds) it may drift somewhat. This point will be discussed later in interpreting the experimental results.

The neuromuscular (NM) system is represented here by a formidable array of parameters. A detailed description is beyond the scope of this report, but is currently in preparation. The pair of terms $(j\omega + 1/T_K)/(j\omega + 1/T_K')$ is a tentative model of the effects of kinesthetic sensory adaptation (or "washout") in the neuromuscular subsystem. T_K is the time constant of sensory adaptation, on the order of tens of seconds, and is analogous to the

time it takes for the feel of newly put-on clothing to disappear. T_K' is associated with a closed-loop root resulting from T_K and is usually much longer than T_K. Consequently, $1/T_K$ and $1/T_K'$ constitute a very low frequency lag–lead pair in the frequency domain. They are usually below the bandwidth of measurement, leaving only a small residual amplitude rise but appreciable phase lag at the lower input frequencies. An important observation about kinesthetic adaptation is that the low-frequency phase lag increases under difficult tasks, where concentration and neuromuscular system tension are maximum (ref. 2).

The remaining third-order characteristics of the NM portion of equation (1) are associated with a high frequency first-order lag, T_{N_1}, and an underdamped second-order lag, ω_N, ζ_N. The T_{N_1} term is related to the viscous damping terms in the closed inner NM loops, while the second-order terms reflect the combined stiffness, inertia, and damping in the arm-plus-stick system. Direct measurements of the second-order characteristics were made in reference 12, where, during a continuous tracking task, the complete arm-plus-manipulator was struck and the ω_N and ζ_N were inferred from the resulting transient response. Generally speaking, most of these dynamics occur at or beyond the frequency of followable inputs (about 10 rad/sec). Thus they can be represented via simpler terms by combining the main effects of the third-order model (a phase lag) into a single first-order NM lag term $(T_N j\omega + 1)^{-1}$, where

$$T_N = T_{N_1} + \left(\frac{2\zeta_N}{\omega_N}\right) \tag{3}$$

or even to merely include T_N as an additional time delay to be added to τ_d.

One frequently used term should be clarified at this point. "Unity-gain crossover frequency" or just crossover frequency, ω_c, is defined as that frequency where the open-loop amplitude ratio (output/error) equals 1.0. The crossover frequency is important because it approximates the closed-loop bandwidth of the compensatory tracking loop, because it defines the frequency region where most of the dynamic interactions of feedback occur, and because it provides the dividing criteria between relatively high ($> \omega_c$) or low ($< \omega_c$) frequencies. As reference 13 clearly demonstrates, it is only near crossover frequencies that accurate pilot describing functions are required, and it is in the crossover region that the effective delay time is defined.

B. EFFECTIVE DELAY TIME

Consider a sine wave of a given frequency, ω, operated on by a pure time delay, τ. A fixed value of τ will not alter the amplitude of the output, but will shift its angular phasing with respect to the input by an amount, $\Delta\varphi$, which increases with the applied frequency:

$$\Delta\varphi = -\tau\omega \qquad (4)$$

where $\Delta\varphi$ is in radians (negative for lag) and ω is in radians/second

In reverse, considering a frequency response plot, a phase lag which varies as a linear increase with frequency (and with unity amplitude ratio) represents an effective time delay.

The definition of the operator's "effective delay time" while tracking a continuous random input is related to the mid-band lags in the complete describing function (eq. 1). The breakpoints occurring at frequencies greater than the crossover frequency are ω_N and $1/T_{N_1}$, and $1/T_L$ will lie in this same frequency region if low frequency lead equalization is not required in the system. The phase lag corresponding to these high frequency components is:

$$\Delta\varphi_{hi} = -\omega\left[\tau_d + \tau_r(t)\right] - \tan^{-1} T_{N_1}\omega - \tan^{-1} \frac{\frac{2\zeta_N\omega}{\omega_N}}{1 - \left(\frac{\omega}{\omega_N}\right)^2} + \tan^{-1} T_L\omega \qquad (5)$$

At frequencies in the mid-band region (near ω_c), this becomes:

$$\Delta\varphi_{hi} \doteq -\left[\tau_d + \tau_r(t) + T_{N_1} + \frac{2\zeta_N}{\omega_N} - T_L\right]\omega$$

whence the effective delay time is defined as:

$$\tau_e \equiv \tau_d + \tau_r(t) + T_{N_1} + \frac{2\zeta_N}{\omega_N} - T_L \qquad (6)$$

The effective time delay, τ_e, is the sum of the "near crossover" lead and lag time constants plus the basic transport delays.

Changes in τ_e imply changes in one or more of its constituents. It is from this consideration that measures of τ_e have promise as integrated indicators of the pilot's physiological integrity in a tracking task. The adequacy of any such differential measure (i.e., $\tau_{e_{actual}} - \tau_{e_{nominal}}$) is thereby dependent on the stationarity of τ_e in the normal organism.

τ_e appears to be stable (with small variance) over a small number of trials, yet exhibits learning effects via slight reductions over a large number of trials. It appears to be critically dependent on those physiologigal and psychological factors involved in the attainment of high grade skill. It offers potential as a general measure of psychomotor performance when only a few runs are taken, while terminal values after many runs indicate maximal tracking performance. Further, since current values can be compared with either absolute minima previously obtained or average population values, the measure provides some indication of probable proficiency on difficult tracking tasks.

C. THE CRITICAL TASK CONCEPT

The measurement of τ_e while tracking is normally a very difficult procedure, in which one of two main approaches can be used:

1. The pilot's quasi-random input describing function is first obtained, using Fourier analysis or a cross-spectral analyzer. Then the frequency response amplitude and phase are simultaneously curve-fitted to remove the linear response terms. From the residual phase versus frequency, the τ_e is found using the following relationship:

$$\tau_e = \frac{d(\varphi \text{ residual})}{d\omega} \tag{7}$$

2. A parameter tracker, or "mimic," is operated in parallel with the pilot, and contains an approximation to a pure time delay (possibly a first- or second-order Padé polynomial). This delay, as well as other parameters, is adjusted to minimize the difference between the pilot and mimic outputs, and the "best fit" value taken as τ_e.

It should not be surprising that very few accurate data on τ_e exist; such sophisticated measuring and data analysis procedures preclude any large scale sampling τ_e by these methods.

The critical task technique can be explained as follows, using a simplified pilot describing function. The complete model alters the details but not the main essentials. Consider a compensatory closed-loop tracking task with a low frequency randomlike input, and a controlled element having a variable first-order divergence (fig. 2), $Y_c = -K_c/(-Ts + 1)$. The appropriate pilot describing function for this controlled element (ref. 2) is a pure gain, K_p, and an effective delay time, τ_e. The latter is approximated by a first-order Padé polynomial, giving for Y_p:

$$Y_p = K_p e^{-\tau_e j\omega} \doteq K_p \frac{\left(\frac{-\tau_e}{2} j\omega + 1\right)}{\left(\frac{\tau_e}{2} j\omega + 1\right)} \tag{8}$$

The system survey* of figure 2 shows that there is a minimum gain, K_{min}, which must be reached to stabilize the system (at ①), and a maximum gain, K_{max}, at which it again goes unstable (at ③). At K_{opt} (near ②) the system is stable, but only marginally so. If $-T$ is now decreased (more unstable), then it can be seen that both the phase margins and gain margins vanish as T approaches τ_e. Furthermore, the pilot cannot help his control by adopting low frequency lead or lag equalization; lead gives less gain spread and lower gain margins, while lag gives more phase lag and thus reduces the phase margin. Consequently, the pilot is constrained to adopt a nearly pure gain response in the crossover region, and in the ideal limit $T_{min} \doteq \tau_e$. Further systems analyses and data for first- and second-order divergent controlled elements of this type, using human pilot models, are given in reference 2.

*A "system survey" is a systems analysis, considering both the performance and stability aspects of a loop closure, using simultaneously the root locus, conventional jω-Bode, and "Siggy" Bode techniques included in the Unified Servo Analysis Method of reference 14.

As an alternative to the graphical solution, consider the analytical solution, which is particularly simple in this case. With Y_p in terms of s for analytical purposes, the open-loop transfer function is:

$$Y_{OL}(s) = Y_p(s)Y_c(s) = -K\frac{e^{-\tau_e s}}{(-Ts + 1)}$$

$$\doteq \frac{-K\left(-\frac{\tau_e}{2}s + 1\right)}{(-Ts + 1)\left(\frac{\tau_e}{2}s + 1\right)} \quad ; \quad K = K_pK_c \tag{9}$$

After some algebra, and using the basic closed-loop relationship that $Y_{CL}(s) = Y_{OL}(s)/[1 + Y_{OL}(s)]$, the closed-loop transfer function is:

$$Y_{CL}(s) = \frac{-\frac{-K}{T}\left(s - \frac{2}{\tau_e}\right)}{s^2 + \underbrace{\left(\frac{2}{\tau_e} - \frac{1}{T} - \frac{K}{T}\right)}_{2\zeta_{CL}\omega_{CL}}s + \underbrace{\frac{2(K-1)}{\tau_e T}}_{\omega_{CL}^2}} \tag{10}$$

Note that in this simplified case $\omega_{CL} \rightarrow 0$ at the critical condition (point ①, dashed root locus in fig. 2). Then, from the ω_{CL}^2 term in equation (10), the result is $K_{limit} = 1.0$. Putting this in the total damping term, $2\zeta_{CL}\omega_{CL} = 0$, gives:

$$\frac{2}{\tau_e} - \frac{1}{T} - \frac{(1.0)}{T} = 0 \text{ at } T_{critical} \equiv T_c$$

Therefore: $$T_c = \tau_e$$

With the more complete neuromuscular system and finite stability margin effects included, the numerical results are modified, as will be shown later. Still preserved, however, are the essential constraining effects on the

pilot's behavior (to pure gain near the shaded phase region of fig. 2) and the close correspondence between τ_e and T_c.

The critical task concept is, then, to provide a divergent controlled element of a form that tightly constrains the allowable pilot equalization near the region of crossover, leaving the effective delay time, τ_e, as the sole determinant of system stability. The divergence is then slowly increased until control is lost, whereupon the critical divergence time constant, T_c, is a measure of τ_e.

D. EFFECTS OF OPERATOR MODEL REFINEMENT

Stability.– The definitive results on pilot describing functions in reference 2 demonstrate that the precision pilot model [represented by eq. (1)] represents the measured operator describing function data with remarkable accuracy over a two-decade range of frequency. Unfortunately, a ten parameter model is too cumbersome for routine data analysis, and it is not really necessary to represent every detail of the data to get a good understanding or measurement of τ_e, as the subsequent analyses will prove. We will now make three loop closures around a near-critical controlled element, using successively simpler pilot models: first, the complete "precision" model; second, an "extended crossover" model; and, third, the "simple crossover" model (all are derived and explained in detail in reference 2). The small errors in the closed-loop roots, stability margins, and error spectra resulting from the simplifications will then become apparent. The objective is to justify the use of these more tractable models for the subsequent analytical investigations.

The controlled element to be examined is:

$$Y_c = \frac{m(s)}{c(s)} = \frac{4}{s - 4} \tag{11}$$

which is near the observed limit for continuous tracking of a relatively wide band input, having a bandwidth of $\omega_i = 4.0$ rad/see.

The precision model parameters, actually based on measured describing function data to be shown later in figure 17, are as follows:

$K_\pi = 1.9$ cm/cm

$t_d = 0.065$ sec

$T_L = 0.02$ sec $\qquad 1/T_L = 50$ sec^{-1}

$T_I = 0$

$T_K = 2.5$ sec $\qquad 1/T_K = 0.40$ sec^{-1}

$T_K' = 25$ sec $\qquad 1/T_K' = 0.04$ sec^{-1}

$T_{N_1} = 0.0625$ sec $\qquad 1/T_{N_1} = 16.0$ sec^{-1}

$\omega_N = 23$ rad/sec

$\zeta_N = 0.1$

The complete precision describing function for this case is thus:

$$Y_{p_P} = \frac{c(j\omega)}{e(j\omega)} = \frac{1.9e^{-.065j\omega}\left(j\omega + .40\right)\left(\frac{j\omega}{50} + 1\right)}{\left(j\omega + .04\right)\left(\frac{j\omega}{16} + 1\right)\left[\left(\frac{j\omega}{23}\right)^2 + \frac{2(.1)}{23}\, j\omega + 1\right]} \tag{12}$$

The extended crossover model of reference 2 is a much simpler form of equation (1), reasonably accurate over a range of frequencies of more than one decade spanning the crossover region, in which the high frequency

neuromuscular dynamics are represented only by their phase lag, i.e., as increments of effective delay time, while the low frequency kinesthetic lags are represented by a single inverse delay time, α. Thus,

$$Y_{p_{XC}} \equiv K_p e^{-j\left[(\alpha/\omega) + \tau_e\omega\right]} \frac{(T_L j\omega + 1)}{(T_I j\omega + 1)} \tag{13}$$

where

$$\alpha = 1/T_K - 1/T_K' \tag{14}$$

$$\tau_e = \tau_d + T_{N_1} + 2\zeta_N/\omega_N \tag{15}$$

T_L, T_I as in equation (1)

K_p here corresponds to the mid-frequency gain, K_π

Often, when T_L is small and $1/T_L$ is beyond the crossover region, as here, it is also included in τ_e. With these simplifications the previous parameters for eq. 12 yield, for the extended crossover model:

$$Y_{p_{XC}} \doteq 1.9e^{-j\left[(.36/\omega) + .116\omega\right]} \tag{16}$$

This is the form which has been found best suited for fitting of first-order critical task data.

The simple crossover model merely ignores the low frequency kinesthetic lags and thus is represented, in general, by:

$$Y_{p_S} \doteq K_p e^{-\tau_e j\omega} \frac{(T_L j\omega + 1)}{(T_I j\omega + 1)} \tag{17}$$

For the specific numbers here, and noting that $T_I = 0$ and including the small value of T_L in τ_e:

$$Y_{p_S} \doteq 1.9e^{-.116j\omega} \tag{18}$$

This is the simplest model capable of demonstrating the significant aspects of critical tasks, and lends itself to analytic manipulation more readily than the extended crossover model.*

The comparative loop closures can now be made. Root-locus and Bode plots for each case are compared in figure 3, where the closed-loop roots corresponding to K_π or $K_p = 1.9$ are designated by the □. (Here, exact expressions for the phase lags from τ_e and α were used.) Figure 3 and Table I demonstrate the following points:

1. The dominant closed-loop imaginary roots near $\omega_{CL} \doteq 8$ rad/sec are closely given by all three pilot models.

2. The dominant closed-loop frequency is near the unity-gain crossover frequency shown on the Bode plots; $\omega_{CL} \doteq \omega_c$.

3. The simple model, having the least phase lag near crossover, results in the highest damping ratio of the dominant roots, and highest phase margin.

4. The main effect of the more precise models is to make the minimum unstable frequency rise from zero (as on previous fig. 2) to the crossover region. The precise low and high frequency instability points, ω_{u_1} and ω_{u_2}, are closely approximated by the extended crossover model.

5. The damping of the second-order neuromuscular dynamics is increased when the loop is closed.

---

*One additional approximation made in most analyses is to represent the time delay terms by their first- or second-order Pade approximations. Thus:

$$e^{-\tau_e j\omega} \doteq \frac{\left(-\frac{\tau_e}{2} j\omega + 1\right)}{\left(\frac{\tau_e}{2} j\omega + 1\right)} \quad ; \quad \omega \ll \frac{1}{\tau_e} \tag{19}$$

$$e^{+\alpha/j\omega} \doteq \frac{\left(\frac{\alpha}{2j\omega} + 1\right)}{\left(-\frac{\alpha}{2j\omega} + 1\right)} \quad ; \quad \omega \gg \alpha \tag{20}$$

6. It can be inferred by inspection of figure 3, and demonstrated by computation, that the optimum crossover frequency, ω_c, (with respect to stability and performance) drops only slightly as 1/T is increased (more instability), and ends up near the crest of the phase curve hump when the stability margins vanish. For the simple model, ω_c follows the precise value at first, then continues to suddenly decrease toward zero as 1/T approaches the critical value. Nevertheless, down to the very low stability margins shown here, the simple model gives correct trends in most of the closed-loop parameters.

This numerical example demonstrates that the extended crossover model gives a remarkably accurate approximation to the precision model, and even the simple model shows the correct trends in the closed-loop stability characteristics.

TABLE I

SUMMARY OF LOOP CLOSURE RESULTS

MODEL	PRECISION	EXTENDED CROSSOVER	SIMPLE CROSSOVER
Dominant Root:			
ω_{CL} (rad/sec)	7.7	7.4	7.9
ζ_{CL}	0.31	0.32	0.36
Crossover Region:			
ω_c (rad/sec)	6.5	6.7	6.7
ω_{u_1} (rad/sec)	1.7	1.8	0
ω_{u_2} (rad/sec)	11.0	11.2	11.4
Phase margin (deg)	13	14	17
Gain margins (dB) at ω_{u_1} ..	5	5	6
Gain margins (dB) at ω_{u_2} ..	3	4	4

Performance.– As a performance consideration, the closed-loop error/input response will now be compared for each model. The error/input response is given by:

$$G_{ie}(j\omega) = \frac{E(j\omega)}{I(j\omega)} = \frac{1}{1 + Y_{OL}(j\omega)}$$

The Padé approximations of equations (19) and (20) were used to approximate the delay terms, and the resulting closed-loop factored transfer functions in terms of the Laplace variable, s, are:

With Precision Model

$$G_{ie_P}(s) = \frac{(s + .04)(s - 4)(s + 16)(s + 31)\left[s^2 + 2(.1)(23)s + (23)^2\right]}{(s + .90)(s + 32.4)\left[s^2 + 2(.31)(7.7)s + (7.7)^2\right]\left[s^2 + 2(.23)(20.7)s + (20.7)^2\right]} \tag{21}$$

With Extended Crossover Model

$$G_{ie_{XC}}(s) = \frac{(s - .18)(s - 4)(s + 17.2)}{(s + .65)\left[s^2 + 2(.32)(7.4)s + (7.4)^2\right]} \tag{22}$$

With Simple Model

$$G_{ie_S}(s) = \frac{(s - 4)(s + 17.2)}{\left[s^2 + 2(.36)(7.9)s + (7.9)^2\right]} \tag{23}$$

The power spectral density, or simply "error spectrum" of the error for a specified input, is obtained by multiplying $|G_{ie}|^2$ by the input spectrum. The mean square error relative to the mean square input is given by the integral over the input bandwidth of this spectral density, as follows:

$$\Phi_{ee}(\omega) = \Phi_{ii}(\omega)\ |G_{ie}(j\omega)|^2$$

$$\frac{\overline{e^2}}{\overline{i^2}} = \frac{\int_0^\infty \Phi_{ee}(\omega)\,d\omega}{\int_0^\infty \Phi_{ii}(\omega)\,d\omega} \tag{24}$$

For a rectangular input spectrum of bandwidth ω_i,

$$\frac{\overline{e^2}}{\overline{i^2}} = \frac{1}{\omega_i} \int_0^{\omega_i} |G_{ie}(j\omega)|^2 d\omega \tag{25}$$

Rather than assume an input spectrum at this point, just the square modulus $|G_{ie}|^2$ is plotted, in figure 4, for each case. Also noted in the figure are the bandwidths corresponding to $\omega_i = 1.5$ and 4.0 rad/sec. This comparison shows that:

1. The error spectra for the three radically different appearing models are quite similar, especially in the range of frequencies below 4 rad/sec where most inputs are concentrated.

2. For inputs cut off at moderate frequencies like $\omega_i = 1.5$ to 4.0 rad/sec, the main difference is slightly less error at the low end of the spectrum for the more precise models.

3. The large peaks are sensitive to the slight changes in closed-loop damping ratio of the dominant root at ω_{CL}. Consequently, the higher frequency components of the error will be more sensitive to the model used than the low frequency portions of the error.

4. The dip in the precision case near 23 rad/sec is due to the neuromuscular system dynamics, ω_N and ζ_N.

Generalizing these and similar results, we conclude that, compared with the precision pilot model, the more analytically tractable extended crossover pilot model will reveal most of the significant theoretical

implications of critical tasks. Even the very approximate simple pilot model will reveal the main trends of such loop closures down to the point of very small stability margins.

E. SOME THEORETICAL IMPLICATIONS

Simple model.– The reason for seeking simpler theoretical pilot describing function forms than the precision model is to permit parametric analyses of the stability and performance in the critical task. In the previous section the simple pilot model for the first-order critical task has been shown to yield reasonably accurate trends in the mid-frequency dynamics, the stability margins, and the error spectrum. Let us now look at some of the theoretical implications which can be drawn by using the simplest operator model.

First, consider the behavior-constraining effects of the critical task as the divergent root is made more unstable.* As mentioned previously, a first-order divergent controlled element is such that no pilot equalization is required in the crossover region. Low frequency lead equalization would increase the phase margin, but only at the expense of gain margin, and conversely for lag equalization. The final test of this theoretical result (that no equalization is required in the crossover region) will have to rest on experiment.

The narrowing range of gain and phase margins as λ is increased toward criticality (incipient loss of control) can be easily shown analytically using the simple crossover model.

---

*For convenience the inverse time constant will henceforth be given a single symbol, $\lambda \equiv 1/T$.

Study of figures 2 and 3 would be helpful before starting this discussion. From the denominator of equation (10), the open-loop static gains necessary for the system to be unstable, $\omega_{CL} > 0$ and $\zeta_{CL} > 0$, are:

$$\begin{aligned} K_{min} &= 1.0 \\ K_{max} &= \frac{2T}{\tau_e} - 1 = \frac{2}{\tau_e \lambda} - 1 \end{aligned} \tag{26}$$

Gain margin is defined as the ratio (expressed in dB) of a specified gain to the gain for neutral stability. For the situation here, there are two gains for neutral stability; hence the optimum closure gain to maximize both gain margins is that gain which lies in the middle of K_{max} and K_{min} expressed in dB. In other words, the gain for maximum gain margins, K_{GM}, is the geometric mean of K_{min} and K_{max}. Thus,

$$K_{GM} = \sqrt{K_{min} K_{max}} = \left(\frac{2}{\tau_e \lambda} - 1 \right)^{1/2} \tag{27}$$

The maximum phase margin and the corresponding gain can also be computed. Using the actual delay time in equation (9), the phase angle in radians is given by:

$$\varphi = -\pi - \tau_e \omega + \tan^{-1} T\omega \tag{28}$$

Thus, the phase margin is:

$$\varphi_M = \pi + \varphi = -\tau_e \omega + \tan^{-1} T\omega \tag{29}$$

At the maximum phase margin point, the slope with respect to frequency is zero:

$$\frac{\partial \varphi_M}{\partial \omega} = 0 = \frac{T}{1 + (T\omega)^2} - \tau_e$$

Solving this for the frequency for maximum phase margin, ω_{PM}:

$$\omega_{PM} = \frac{1}{T}\sqrt{\frac{T}{\tau_e} - 1} \quad ; \quad T \geq \tau_e \tag{30}$$

This value of ω_{PM} may be put back in equation (29) to compute φ_M, and can be used to compute K_{PM} or to locate it graphically. Remember that the simple model represented by equation (30) is not completely accurate in the limit as $T/\tau_e \rightarrow 1$, where the above equation indicates that $\omega_{PM} \rightarrow 0$, whereas in the more precise models ω_{PM} remains at a finite frequency.

To illustrate the constraints on these parameters, figures 5 and 6 show some results from the more extensive computations in reference 15. In figure 5 are plotted the gains for the various stability margins as the open-loop instability, λ, is made more unstable, with the effective time delay held constant at a typical value of $\tau_e = 0.2$ sec. There is a very rapid decrease in all the stability margins as the critical condition is approached. More specifically:

1. K_{GM}: The gain for maximum gain margins is between the gain for maximum phase margin and the gain for minimum rms error. The maximum gain margins, K_M, are marked along the K_{GM} curve.

2. K_{PM}: The gain for maximum phase margin is on the low side of K_{GM}, but is very similar. The maximum achievable phase margins marked along this curve become quite low (< 20 deg) well before the critical point is approached.

3. K_{10^o}: The gain for a practical minimum phase margin of 10 deg is near the stable gain limit at noncritical conditions, but departs appreciably from it for $\lambda > 3$ (in general, for $\lambda\tau_e > 0.6$).

4. $K_{e_{min}}$: The gain for minimum rms error with a rectangular-plus-shelf spectrum of the B6 type (ref. 16) and $\omega_i = 2.5$ rad/sec is very near the maximum stable gain. Because this criterion corresponds to a phase margin less than 10 deg and gain margin less than a few dB, it is doubtful that the theoretical minimum error will be approached under most near-critical conditions. This analysis ignores the effect of remnant, which will generally increase the total errors and reduce $K_{e_{min}}$.

Except for the $K_{e_{min}}$ curve (which depends on a given ω_i and input spectrum shape), the stability margin curves can be normalized to any τ_e in terms of the ratio of T to τ_e (or its inverse, $\tau_e/T = \lambda\tau_e$) as shown at the top of figure 5 .

Next, consider the theoretical error performance implications of the simple model, as shown in figure 6. Here, the normalized error,* e_{rms}/i_{rms}, is shown versus the instability, λ, for gain adjusted to K_{GM}

*The normalized error is computed with standard procedures as outlined near equations (24) and (25) herein and in references 2 and 15.

(maximum gain margin). Two key conclusions may be drawn from the error analysis represented by figure 6:

1. The tracking error rises very steeply as the instability is increased beyond approximately two-thirds of the ideal critical value.
2. The rms tracking error exceeds the rms input by a factor of 5 to 10 as criticality is approached.

The practical implications of these last two theoretical findings are very important. First, they imply that, in order for the displayed error to remain within bounds, the input level must be very small compared to the display range. (There will be further discussion of this point in the section on "Critical Task Development.") Second, it must be remembered that the pilot remnant will induce further errors, which will be similarly magnified during closed-loop operation. This compounds the display problem. These predictions, made well before the experiments to be described in later chapters, were verified in practice.

Extended crossover model.- The residual mid-frequency effects of the low frequency phase lags from the T_K, T_K' effects detract from the phase margin which would be computed from the simple model alone (see fig. 3), and reduces the ideal λ at which all stability margins disappear. This theoretical limit is rederived in Appendix A using the extended crossover model, or "α-model," of the operator. The result is:

$$\frac{\lambda_{c_{ideal}}}{1/\tau_e} \doteq 1 - \sqrt{\alpha\tau_e} \quad ; \quad \alpha \ll \tau_e\omega_c^2 \tag{31}$$

For a typical value of $\alpha\tau_e \doteq 0.04$ it can be seen that the zero margin limit is reduced to $\lambda \doteq 0.8/\tau_e$ compared with $\lambda = 1.0/\tau_e$ for the simple case. The exact proportionality between the limiting λ and $1/\tau_e$ in the simple model case is also modified by the α term, but this is a second-order effect for reasonable values of the parameters. However, the refined limiting case may not be of too much importance if finite stability margins are required for control, since the simple model results have been shown to be valid under these conditions.

F. SUMMARY OF THEORETICAL PREDICTIONS

At this point we will recapitulate the particular theoretical assumptions and predictions which are to be validated by the subsequent experiments. It is assumed that the basic assumptions applying to continuous compensatory tracking by a human operator are met (e.g., random-appearing input, well-trained operator, proper display and control gains, etc.).

The main special assumption of this theory is: While tracking with a simple first-order divergent controlled element having a slowly adjusted divergent root, the operator's behavior remains quasi-stationary and can be represented by the same describing function forms as proven valid for constant-λ conditions.

From these basic (and one special) assumptions, the analysis of operator behavior has led to the following derived predictions, which are to be tested experimentally:

1. Low run-to-run variance in all measured parameters is expected because of the constraining nature of the first-order critical tasks.
2. As the instability λ approaches its critical value, the tracking errors will drastically increase and the stability margins will decrease.

3. The neuromuscular system will be forced to its "tightest" mode of operation, to achieve minimum neuromuscular contribution to τ_e at high frequencies, with an increase in α at low frequencies (from ref. 2).

4. The magnitude of Y_p should be nearly constant, i.e., a "pure gain" over the stable range of crossover frequencies, i.e., over roughly a decade from ω_{u1} to ω_{u2}.

5. The limiting level of λ which can be tracked for more than a few seconds will be less than the theoretical ideal critical value, $\lambda \doteq 1/\tau_e$, because of the requirement for small finite stability margins, the need to limit the tracking errors to remain on the display, and due to secondary effects of the α phase contributions.

6. For a given operator, the exact value of instability, λ_c, at which control is lost will depend primarily on τ_e and secondarily on α, as well as the limiting phase and gain margins required by that individual's random deviations around his mean parameters. If these margins and α are relatively invariant, then a calibratable relationship should exist between τ_e and λ_c.

The development of a device for automatically determining the critical instability will be described next before going on to the experimental program.

SECTION III

DEVELOPMENT OF THE AUTOPACED CRITICAL TASK

It has been shown in the first section that a measure of the subject's effective time delay, τ_e, can be obtained by noting the value of the unstable root at which the subject can no longer maintain control in a tracking situation. It is a primary objective of this program to evolve a method and test configuration for increasing the unstable root from an easily controlled value to the critical value while the operator tracks continuously. An obvious approach is an automatic adjustment which not only relieves the experimenter of the job, but also prevents his bias from contaminating the data. Some of the key considerations in the development of the final test configuration will be reviewed in this section.

A. CRITERIA

The main criterion is that the measured value of the critical divergent root, λ_c, should be dependent only on the human operator's effective time delay, τ_e, and not on the detailed mechanization of the critical task. Specifically, the value measured should not depend significantly on the selected display parameters, the adjusting device operation, or the modus operandi. Variations in λ_c with secondary task variables such as run length, input characteristics, and control gains are expected; hopefully, these variations can be minimized or standardized by proper selection of the task parameters. Other criteria included:

- Simplicity of mechanization, to facilitate its exact duplication in other laboratories and to maximize its reliability.
- Suitability for untrained as well as trained operators without experimenter adjustment.

B. ROOT ADJUSTMENT SCHEMES

During exploratory phases of this program, documented in references 17 and 19, several root adjusting schemes were tried with varying success. Adjustment by the experimenter, as originally used in the 1961 critical task development, was eliminated as too cumbersome and unrepeatable. Self-adjustment of λ by the subject himself was found to be unworkable because no workload margin exists for the adjustment process as criticality is approached. The most successful schemes are those depending on the predicted (and observed) sudden increase in tracking error performance as λ nears the critical value for a particular operator.

Three performance feedback schemes for changing the root increase rate, $\dot{\lambda}$, were:

$$\text{Scheme A:} \qquad \dot{\lambda} = k\left(e_c - |e|\right) \tag{32}$$

$$\text{Scheme B:} \qquad \dot{\lambda} = k\left(e_c - |e|\right)^2 \operatorname{sgn}\left(e_c - |e|\right) \tag{33}$$

$$\text{Scheme C:} \qquad \dot{\lambda} = k\left[e_c - \frac{|e|}{(T_f s + 1)}\right] \tag{34}$$

where "e" is the tracking error (seen by the subject as a vertical displacement of a horizon-bar-like line on a CRT, $|e|$ is its rectified value, and e_c is a preselected "criterion" error level. Scheme A mechanizes the concept that, for very small errors the subject is certainly not near his stability limit and λ should thus be increasing, while for excessively large errors the subject is just losing control and therefore λ should be decreasing. The divergent root should stabilize at the subject's average *minimum* controllable value, $\lambda = \lambda_c$, and hence be proportional to $1/\tau_e$. A number of difficulties with this scheme became apparent as the experiments proceeded, and are discussed in the following paragraph.

The principal difficulty with Scheme A was the large range in the rate of increase, $\dot{\lambda}$. For the initial values of λ the rate was too low, while near terminal values the rate was too high. The total effect, then, is that the subject is required to spend the majority of his tracking time just in getting the root out near the "critical" region. The number obtained in this manner is undesirable from two standpoints: during the long initial time the subject can tire, and a fast final rate gives an optimistic (or high) value for λ_c. This last point can be demonstrated by using an adjustment rate so high that, even with hands-off control, a significant λ_c is obtained before the display diverges to its limits.

Scheme B was evaluated in hopes of correcting the rate deficiency, but a new problem arose — that of interaction. When the gain was high enough to get a good adjustment rate, considerable coupling existed between the control loop and the adjustment loop (the divergent root "chased" the error level).

Smoothing the error (Scheme C) was of no help since the additional lag created stability problems in the coupled subject–adjustment loop.

The best solution to these problems was found to be an adjusting law which was not a feedback function of the error. A two-rate law was evolved, of the form:

$$\text{Scheme D:} \quad \begin{cases} \dot{\lambda} = k_1 \quad ; \quad \dfrac{|e|}{T_f s + 1} < e_c \\ \\ \dot{\lambda} = k_2 \quad ; \quad \dfrac{|e|}{T_f s + 1} > e_c \end{cases} \qquad k_1 > k_2 \tag{35}$$

The subject tracks while the root moves rapidly towards instability. When the filtered absolute error reaches a predetermined level, the rate is decreased to a creeping, but irreversible, rate and continues until the subject loses control. This is similar to the action of an experimenter manually adjusting λ toward the critical limit.

The value of λ at which control is lost can be considered to represent the short-term average of λ_c over the last few seconds of a run. Notice that the operation represented by Scheme D is equally valid for both the trained and the untrained operator since it depends only on the point at which performance deteriorates. Scheme D was used for the final experiments, and was termed the "autopaced test."

Before discussing the parameter selection for the autopaced test, it will be helpful to discuss some error considerations. It is shown in the theory section that if the conventional pilot models are assumed with a fixed time delay, and if a maximum stability measure (such as gain margin) is maintained, the system rms-error-to-input ratio as a function of λ will characteristically increase suddenly as shown in Sketch A.

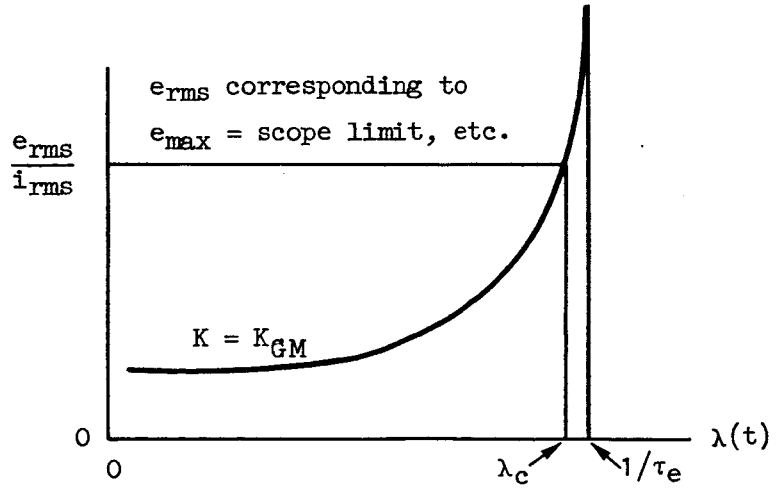

Sketch A. Characteristic error performance for critical task

Consequently, the error criterion e_c, scope size, input, or visual angle limits can all place upper bounds on e_{rms}. If the results of any experimental program are to be independent of the mechanization of the experiment and equipment used, one must insure that these bounds are operator-centered (e.g., eyeball limits), and not machine-centered (e.g., scope size).

C. PARAMETER SELECTION

An attempt was made to desensitize the resulting λ_c obtained from the critical task to the crucial parameters of the configuration. Figures 7-10 show, respectively, the sensitivity to error angle seen by the eye, controlled element gain, amplitude of the input, and the input bandwidth. The knee is quite apparent in each set of figure 7 (two different adjustment "laws" were used) and the available error display angle should obviously be greater than 10 deg. These runs had no input except operator remnant, so it is quite important that this minimum display angle be observed, because any input will further increase the error.

During these runs to determine error limits, which involved various combinations of eye-to-CRT distance and CRT masking apertures, it was observed that the eye remains fixated on the null point, and **the eyeball does not move** to track the error display. Though the error bar traveled beyond ±30 deg of visual angle and, in some cases, the eye was only 5 cm from the CRT, the eye remained centered.

Figure 8 shows that λ_c is fairly insensitive to control gain over a range of two orders of magnitude. (Remember that the operator

must compensate for the control gain to keep the loop gain within narrow limits.) The nominal value had been chosen earlier from operator opinion rating, and was borne out by these data. The input amplitude, figure 9, has a small but linear effect on λ_c, as does the bandwidth (fig. 10) of the input. Zero input seems to give the "best," i.e., most consistent and highest values of λ_c, but this setup is not feasible if describing function data are to be obtained. The input selection was then made on the basis of past human operator response studies (ref. 2) so that a direct comparison could be made between past τ_e data, data taken for this project, and autopaced λ_c values.

The parameters k_1, k_2, e_c, and T_f of Scheme D were selected on the basis of λ_c data and operator opinion. The optimum combinations seem to be readily apparent to the subject. He is quite aware of when the rates are fast enough to give the optimistic reading mentioned below and when the rates are too slow he immediately complains and the data become erratic. An optimistic λ_c can be obtained by raising the root adjustment rate too high. The extreme case would be demonstrated by having a rate so high that, even for a "hands-off" condition, a significant λ is obtained before the divergence causes the task to cease. This condition was avoided by making subjective measures, as noted above.

An additional feature found very desirable is a dot operated by a second gun in the CRT, which moves to the right from the origin proportional to λ, analogous to the root location in the s-plane. The subject can thus observe an increase in λ and monitor his score (the dot holds at λ_c). Good operator incentive is provided by this feature, combined with instructions to "equal or better his previous score."

1. Mechanization

The final configuration for the critical task test based on the development just discussed is shown in block diagram form in figure 11, while the parameters are given in Table II. The gains were chosen on the basis of the appropriate angle at the eye, which is, of course, directly related to the scope size (maximum displacement of the CRT used is ±4 cm). The value of e_c should be about 10 to 20 percent of the maximum scope deflection. This allows the operator to get to within 1 or 2 rad/sec of λ_c before the adjustment rate k_2 switches in. Although the operator should track at the rate k_2 for at least 10 sec before he loses control to insure a nonoptimistic reading, tracking for much more than 100 sec would probably bring the onset of fatigue and other undesirable long term variations.

TABLE II

NOMINAL AUTOPACED CRITICAL TASK PARAMETERS

K_1 = 0.366 cm scope deflection/volt

$K_d \doteq 57.3/d$, degrees display displacement at eye per centimeter of scope deflection

K_s = 2.42 v/Newton

e_c = 0.38 cm

k_1 = 0.2 rad/sec/sec

k_2/k_1 = 0.25

T_f = 1 sec

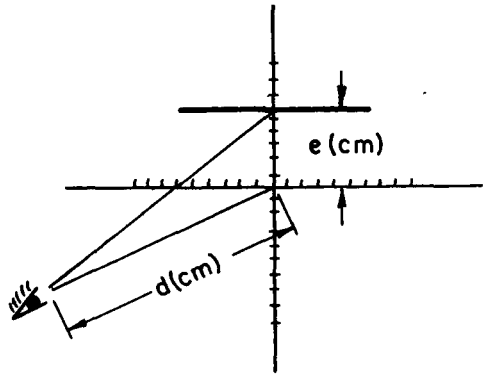

To minimize the neuromuscular lags and to provide an isometric (no deflection) restraint on the operator's muscles, a rigid force stick is preferred. The force stick used for the tests reported herein is a Measurement Systems, Inc., Model 435 control stick. Its low mass and sensitive response allowed relatively high frequency responses to be measured.

This test configuration has been mechanized on general purpose analog computers at both Systems Technology, Inc., and The Franklin Institute. About 17 amplifiers, 11 potentiometers, 1 multiplier, and 5 relays are required for the complete circuit (shown in Appendix B).

D. OPERATION

An autopaced critical task test begins with the operator in place and grasping the stick. The root instability is initially set at a finite low value to insure operator attention. When the rectified and filtered error builds up to the preselected value, the rate of increase of λ decreases but λ continues to creep outward until control is lost. When control is lost, the error goes off-scale and the computer holds, giving a reading for λ_c.

Figure 12 shows typical time histories of autopaced runs with and without an input. Points of note are the relatively random appearance of the input, the very random appearance of the error and its sudden increase past e_c followed by the decrease in $\dot{\lambda}$, the similar appearance of the traces with and without an input, and the moderate time required for the complete run (less than 1 min).

The final system proved to be very reliable and satisfactory for a number of different subjects of various skill levels who tried it out.

SECTION IV

EXPERIMENTS

There are essentially two objectives to the experiments reported herein. The primary objective is to establish that the autopaced critical task indeed provides some measure of τ_e. Second, an explanation and description of the operator's behavior near incipient instability are desirable to further extend the work of reference 2. In attaining these objectives, the experiments are aimed at

- Observing λ effects on the human operator's behavior, as measured by describing function and performance data
- Correlating autopaced data with describing function data

The experimental program was carried out in three phases:

1. An exploratory group of experiments was performed as just described, using the STI simulator, to determine the optimum controlled element configurations, the best adjusting scheme for λ, and the optimum parameters. In addition, some very rough checks of intersubject differences and task learning times were made (ref. 19).
2. A group of preliminary describing function runs was made at The Franklin Institute to verify the duplication of the STI test configuration, and to provide a check on the similarity between the behavior of the test subject and past subjects in similar tasks.
3. The main experiments, performed at The Franklin Institute, included both autopaced λ_c and describing function data, with emphasis on variations in λ and input.

In the remaining portions of this rather lengthy section the most important results of Phases 2 and 3 will be covered (the exploratory

Phase 1 work has been documented in references 17 and 19, and was discussed briefly in the previous section). After reviewing the over-all experimental design, the autopaced data will be presented, then the describing function measurements, their curve fits, and resulting parameter trends will be given. The interpretation of these combined results will be discussed in the final main section.

A. EXPERIMENTAL DESIGN

The scope of this program was too small to consider a massive, statistically designed experimental program to cover all variables of immediate interest, i.e., subjects, number of trials, input bandwidth and level, degree of instability, run length, etc. In fact, not enough was known at the start to even guess at the levels and replications required for a rational statistical design. Consequently, emphasis was placed on key preliminary experiments which would validate the crucial assumptions and provide sufficient insight and data on which to base subsequent theoretical analyses and detailed experiments.

While the exploratory experiments of Phase 1 showed distinct individual differences in the achievable autopaced λ_c scores, these and the previous experiments on subcritical first-order tracking tasks indicated that the basic forms of various operator's describing functions were similar and reasonably well constrained by this task (see ref. 2). Consequently, it was decided to use a single subject, provided that the describing function form was shown to be similar to that of other operators under previously tested conditions. As will be shown later, this

agreement was established, and therefore the limited experimental time could be used to increase the reliability of one subject's data.

The most important variable was the unstable root, λ. For the describing function runs, four values of λ (2, 3, 4, and 5 rad/sec) were chosen to span the region between the previous data of reference 2 and the limit at which runs of reasonable length could be made.

Based on the Phase 1 experiments and on the results for subcritical tasks in reference 2, it was felt that the input bandwidth would have a secondary effect; most of the describing function and autopaced data were measured with one basic low-bandwidth ($\omega_i = 1.5$) input spectrum, but a few describing functions were measured at a higher bandwidth ($\omega_i = 4.0$). Of course, no describing function data could be measured with zero input, because cross-correlation of the signals with the input is required. Because the Phase 1 autopaced data, as well as the theory, indicated that there would be some effect of input level, the main autopaced runs were made with and without the basic input.

A matrix of experimental variables and the number of replications made at each condition is given in Table III.

TABLE III

MATRIX OF EXPERIMENTAL CONDITIONS

INPUT BANDWIDTH, ω_i (rad/sec)	LEVEL OF INSTABILITY, λ (rad/sec)				
	2	3	4	5	Maximum Achievable
	No. of Describing Function Runs				No. of Autopaced Runs
0	–	–	–	–	45
1.5	3	2	9	3	46
4.0	–	–	4	–	–

The procedural design consisted of a series of several simple experiments in which one variable was changed during each day's testing. Thus, λ was the dominant variable on one day and ω_i on another. One set of conditions was established as a "base run" case which was included in each day's runs. By this means it was possible to obtain a large number of replications of one case to establish its intrinsic variability, while permitting a more economical number of runs across the variables of interest.

During each day's testing, the autopaced critical task was run (with and without inputs) at the start and end of the day. To balance out fatigue and presentation order effects, the describing function runs (which were limited to less than a dozen per day by the complex procedures involved) employed a randomized order of presentation of the dominant variable in the morning, and the reverse of this in the afternoon. A detailed run log is included in Appendix C showing the chronology of the data reported herein.

B. AUTOPACED λ_c DATA

The first data to be presented are the results of the autopaced runs. The automatically paced and scored setup described in an earlier section was used for all these trials. Near the end of the Phase 1 experiments at STI, the subject, an engineer and private pilot, was given a large number of trials to insure thorough learning of the task. It has been found that the autopaced critical task provides an excellent training device because it demands constant attention, always progresses to the subject's skill limits, and engenders strong motivation to achieve a high

score. For simplicity, these trials were all made without a command input; the subject's remnant was ample excitation, as is shown in figure 12.

Experience with the exploratory trials of Phase 1 had shown that from three to five autopaced runs should be made in one samping of λ_c. Averaged over five subsamples, the mean for successive samples, $\bar{\lambda}_c$, is quite stable over a large number of trials in any given time interval on the order of an hour or two. The five-trial means and standard deviations for λ_c during the learning trials are shown in figure 13.

No statistical analyses of these training data were attempted, but the following points were apparent:

1. The initial learning time, to get out to a critical instability of $\bar{\lambda}_c \doteq 5$, was quite rapid — on the order of a few trials.
2. Subsequently, over a month's time and over 170 trials, the controllable divergence gradually rose to a level near $\bar{\lambda}_c \doteq 6.5 \pm 0.7$ and leveled off.
3. The trial-to-trial variance (as evidenced by the trend in the standard deviations) was appreciable, being partly attributed to the lack of warmup and loosely controlled training procedures.
4. Although some large fluctuations in the five-trial means were noticed, no attempt was made to formally correlate these particular data against time of day or other subject-centered variables which might conceivably have an effect on λ_c because no pattern is evident among the coded points of figure 13.

Other unpublished learning curves show similar trends, i.e., that initial learning is quite rapid and λ_c stabilizes at a reasonable level after several dozen trials.

During the course of the main experiments at The Franklin Institute, which spanned several days, five-trial autopaced data were taken at the start and end of each day. These data are shown plotted chronologically in figure 14. Runs were made with and without a standard random-appearing input, and a small but consistent difference in $\bar{\lambda}_c$ is apparent. Except for the first set of runs (with input), the levels of $\bar{\lambda}_c$ appear to be essentially the same as the previous set made at STI (note the mark on figure 14 indicating the terminal level of the learning trials from figure 13). These data, as well as the subject's reports, suggest that the autopaced test configuration and data can be duplicated easily even in widely different facilities.

Some simple statistical analyses of the main data were made to establish the distribution of variance, to determine the independence of run-to-run variations in $\bar{\lambda}_c$, and to check any trends in the data. First, a standard RUNS test was made to verify that the variations about the mean within each five-trial sample were randomly ordered (ref. 20, Table II, p. 298). The test showed that the deviations were random. (In the worst case, the test statistic $u = 25$ was within the 90 percent confidence interval.) Histograms of the individual trial differences from their five-trial mean are shown in figure 15. A χ^2 test of goodness of fit was made on each set to verify whether or not these deviations could be considered normally distributed (Gaussian). The test showed that with 26 degrees of freedom in each case, χ^2 was well within the 95 percent confidence interval, and that the two sets of data are normally distributed (with no input, $\chi^2 = 11.27$; with input, $\chi^2 = 13.8$; while the 5 percent reject levels are $\chi^2 = 30.1$ and 38.9,

respectively.) The reason for choosing λ_c rather than $1/\lambda_c \doteq \tau_e$ for analysis is as follows: The recent large scale, simple reaction time (RT) measurements reported in reference 21 show definitely that 1/RT, rather than RT itself, is normally distributed. The reason given is that the RT deviations should depend primarily on the velocity of propagation of signals along neurons, which might be expected to be normally distributed about a mean velocity. The average velocity would be measured by (distance/RT), thus 1/RT should have a normal distribution. If an analogy between RT and τ_e is drawn, then λ_c, which is roughly proportional to $1/\tau_e$, might also be normally distributed about its mean value. The results herein support that hypothesis.

One further conclusion can be drawn from the histogram data: the standard deviation of a typical trial value of λ_c from its sample mean is a reasonably small percentage of the mean. Taking the over-all test means for each input case as a reference, the specific values are:

	Mean	Standard Deviation	$\left(\frac{\text{Std. Dev.}}{\text{Mean}}\right)$
No input.....	6.58	±0.31	4.74%
With input (B6'−1.5−1/8)..	6.00	±0.39	6.50%

These percentages are lower than those experienced in most simple response time measurements, where the standard deviations are typically 10−13 percent of the mean under the best of conditions (ref. 22, p. 38). Consequently, fewer trials are needed to establish a mean to specified precision with the autopaced critical task, and it should be an efficient substitute for reaction time measurements in situations where tracking is important.

From inspection of figure 14 it is apparent that, except for a couple of samples, the level of λ_c remained remarkably constant across all the test days. Consequently, the over-all means for each input case can be tested for the significance of their different means. Since the distributions have been established as normal, the normal statistic (t = difference in means $\div$ standard error) was used. This test gave a value of t = 5.25, which is far beyond the value of t (t = 2.57) for a 99 percent confidence interval. It is concluded that the small systematic reduction in $\bar{\lambda}_c$ due to input is statistically very significant.

In fact, it turns out that almost all five-trial sample means are probably different, albeit slightly, from the over-all mean (as determined by Student's t test). Except for the obvious low initial set and anomalously high (but carefully checked) last two sets of runs in figure 14, the implications of this last finding are that the day-to-day, and even morning-to-afternoon, differences in τ_e might be readily detectable by this technique. This interesting possibility should be studied further.

The interpretation of the measured λ_c in terms of τ_e, and its correlation with other data, will be done in a later section.

In closing this subsection, the following conclusions are drawn:

1. The autopaced critical task developed herein, as well as the resulting λ_c scores for a given well-practiced subject, can be closely duplicated at various facilities.
2. Five-trial sample means for λ_c are very stable, and the variance is remarkably low. This precision implies that the autopaced critical tasks would be a very efficient psychomotor test.

3. Learning is rapid, with several dozen trials being sufficient to reach the asymptotic score level. An essentially constant level of λ_c was observed throughout the experimental program.

4. The test can be run without a command input, using the subject's remnant "noise" to excite the system. Although the test seems subjectively the same as with an input, the λ_c scores without an input are about 10 percent higher than with a standard $B6'-1.5-1/8$ input spectrum.

C. DESCRIBING FUNCTION MEASUREMENTS

Technique. — To validate the theoretical model and assumptions, measurements of the operator's describing function were made. The subject tracked a random input with a first-order divergent controlled element at various fixed levels of instability up to the limiting level which he could track continuously for 2 to 4 min. The describing functions were measured by the cross-spectral analysis technique, using the watthour meter (WHM) analyzer at The Franklin Institute. A complete description of the cross-spectral analysis method and the WHM analyzer is beyond the scope of this report, and the reader is referred to references 2 and 23 for details on the method and equipment. By directly measuring the time-averaged cross-spectra between the displayed error and the command input, $\Phi_{ie}(\omega)$, and between the pilot's control output and the command input, $\Phi_{ic}(\omega)$, the pilot's describing function is computed from

$$Y_p(j\omega) = \frac{\Phi_{ic}(\omega)}{\Phi_{ie}(\omega)} \tag{36}$$

A run length of 4 min. is used for most measurements to provide an adequate number of the low frequency cycles over which to perform the averaging required by the cross-spectral technique.

Input. — Some input is required for describing function measurements, and a sum of many sinusoids is required for the WHM analyzer. By using nonharmonic frequencies and random phases, random appearance of the input and resulting displayed error are assured, thus guaranteeing pure compensatory behavior by the human operator. Inputs are required at each frequency at which the describing function data are desired, yet too large an input bandwidth will cause the operator to "regress" and to smooth over any large high frequency inputs. The solution, originally used in reference 16, is to employ a set of dominant low frequency waves to provide the effective input bandwidth, plus a number of very small high frequency waves which the operator can barely detect but which he cannot avoid responding to.

The specific input consisted of the sum of ten sinusoids. The spectral shape is shown in Sketch B, and approximates a dominant rectangular bandwidth whose highest frequency is ω_i. This particular shape has been identified by the code B6' – ω_i – σ, where B6' refers to the shape (ref. 16), ω_i is the bandwidth, and σ is the rms value in display units. The rectangular-plus-shelf type of input spectra typified by the B6' input have been used previously in human response programs, and have been found to be good approximations to a random input. For example, the data in reference 2 show that the input amplitude distributions are essentially Gaussian, and that the resulting closed-loop error distributions, which are what the pilot actually sees, are also Gaussian.

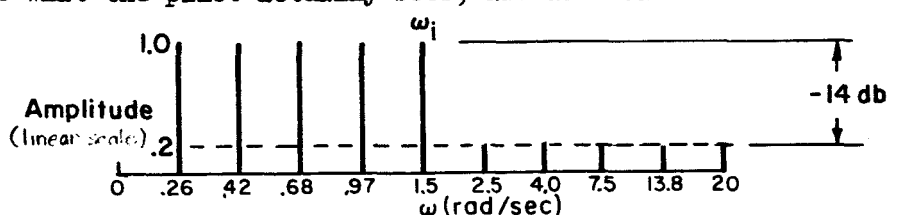

Sketch B. Input spectrum (B6' shape, ω_i = 1.5 rad/sec)

Experimental Setup and Procedure.— The describing function measurements were performed with the same experimental apparatus as the autopaced critical tasks (see section IV-B and Appendix B). The operator was started at an easy subcritical level of instability, which was then moved out to a preset level of λ = 2, 3, 4, or 5 for each run by the autopacer. At this point the WHM measurements started and continued for 4 min. (except for λ = 5, where only 2 min. runs could be completed). About a dozen or so runs were obtained during a morning and afternoon session each day. Mean-squared tracking error and mean-squared control force were also measured during the run. As mentioned previously, the order of presentation of each level of λ was randomized and counterbalanced during each day's running. A run log of the test conditions is contained in Appendix B.

Tie-in with previous data.— Because the experimental design was confined, for economic reasons, to a sampling in depth of one typical operator, it was important to verify that this operator was typical of others. Figure 16 compares typical describing function data (plotted as Y_{OL}, the open-loop describing function during the closed-loop tracking task) of four pilots and one engineer during the similar subcritical tasks of reference 2 (open symbols) with those of the present operator (solid diamonds). The task differences were mostly limited to the apparatus, as follows: (a) The control stick in the current experiments was a rigid force-pickoff pencil stick operated fore and aft; whereas, a light, stiffly sprung handle operated about the lateral (roll) axis was used in the previous cases. (b) The error was displayed by vertical displacement in the

present case, versus horizontal displacement in the previous experiments. (c) The input had a lower rms level in the present experiments; otherwise the inputs were essentially identical.

The difference between the present and the previous data (fig. 16) is small and is consistent with the tighter neuromuscular loop permitted by the isometric force stick. This is evidenced by slightly larger gain and phase shift at low frequencies and a higher frequency for the neuromuscular second-order term. It is concluded that the present experimental subject is typical of the population of pilots for which this critical task is intended.

Some idea of the subject-to-subject variability is also apparent from figure 16. The wide phase scatter at the lowest frequency is due primarily to intrinsic measurement accuracy limitations imposed by run length. The lower variability near the crossover region is apparent, and is partly explained by the "selective variability" hypothesis of reference 2, (which states that the operator's behavior is the least variable in the crossover region) especially if the system closed-loop stability is marginal, as it is here.

Describing function data. — In order to verify the theoretically predicted trends in the parameters describing the operator's behavior, as the instability was increased toward criticality, the raw describing function data were averaged and curve-fitted. To show the run-to-run variability expected among runs taken at various times, the four individual Y_p data plots comprising one data set are shown in figure 17a. This condition ($\lambda = 4$ and $\omega_i = 4$ rad/sec) provided a very consistent set of runs, and the small scatter shown is usually within the accuracy of

the WHM cross-spectral analyzer.* Again, the reduced variability in the crossover region is notable.

The averaged data from figure 17a are shown in figure 17b along with the resulting standard deviations. The data of figure 17a are also curve-fitted, using the three previously described human operator models. The parameters for these three curves have already been given in eqs. (12), (16), and (18). The data points show features requiring the precision model of the operator (solid line) to account for the entire frequency range, since there is some low frequency lag and amplitude rise and a high frequency second-order peak. However, the extended crossover model (dashed line), hereinafter called the "α-model" for brevity, fits the data in the crucial stable region around crossover frequency. It is used for the remainder of the data because it has fewer parameters to adjust and yet covers enough of the frequency domain to validate the theory. First, the mean pilot describing functions $Y_p(j\omega)$ were fitted for phase (using special templates for combined τ and α effects), giving α and τ_e contributions; then the amplitude was fitted near ω_c, giving the pilot gain, K_p. Next, the corresponding open-loop Y_pY_c curves were drawn through the open-loop describing function data, permitting analysis of the various stability margins. "Best fit," but somewhat arbitrary, fairings were also put through the actual Y_pY_c data points to check the consistency of the actual and fitted trends.

*It has been noticed in previous and present work that the input $\omega_i = 4.0$ cases usually have lower scatter than the $\omega_i = 1.5$ cases, but it is not clear whether this is due to the input bandwidth, the larger number of waves in the $\omega_i = 4.0$ case, or to apparatus errors resulting from the different WHM analyzer power levels used in each case.

The remainder of the averaged describing function data taken at other values of λ are presented in figures 18 through 21, first plotted as Y_p and then as Y_pY_c in order to facilitate assessment of both the model fits and loop closure criteria. It is obvious that neither the α-model nor any other model will fit some of the erratic phase points, yet the values of the actual and fitted stability parameters are fairly consistent. Detailed discussion of these describing functions will be delayed until the collection of fitted data parameters has been reviewed.

Data parameters. — Table IV contains a summary of all the fitted parameters, while figures 22–25 show the comparison between the actual and fitted data. The reader should mentally weight the $\lambda = 2$ and 4 data points more heavily, since the $\lambda = 3$ data are an average of only two runs and the $\lambda = 5$ data are made up of three short runs (2 min. and less). The short run lengths mainly increase the low frequency variability. Note, in figure 23, that ω_{u_1} seems to demonstrate contrary trends between actual and model data. This is not considered significant because the measured points are very sensitive to the fairing of the mid-frequency phase curve. Although scatter exists in the other data, most of the trends are consistent. One conclusion is, then, that the α-model provides a sufficiently accurate fit to human operator describing functions measured while performing subcritical and critical tasks.

The parameter adjustments exhibited by the operator can now be extracted from these cross-plots. In view of the remarks made above (regarding weighting of data in favor of the $\lambda = 2$ and 4 runs), we can conclude that α, to a first-order approximation, is constant. The

TABLE IV

FITTED PILOT MODEL PARAMETERS, LOOP CLOSURE CRITERIA, AND TRACKING PERFORMANCE MEASURED DURING SUBCRITICAL TASKS

Instability, λ (rad/sec)	2.0	3.0	4.0		5.0
Input bandwidth, ω_i (rad/sec)	1.5	1.5	1.5	4.0	1.5
α-model parameters					
Pilot gain, K_p (linear).....	2.60	2.65	1.73	1.90	1.67
Effective time delay, τ_e (sec)	0.121	0.111	0.110	0.116	0.100
Low frequency parameter, α (1/sec).....	0.35	0.41	0.35	0.36	0.31
Stability criteria					
Crossover frequency, ω_c (rad/sec).....	5.0	7.5	5.1	6.7	7.1
Lower stable frequency, ω_{u_1} (rad/sec).....	0.99	1.40	1.65	1.8	1.44
Upper stable frequency, ω_{u_2} (rad/sec).....	11.0	10.9	10.5	11.2	11.3
Lower stable gain, K_{u_1} (linear).....	1.11	1.11	1.07	1.15	1.05
Upper stable gain, K_{u_2} (linear).....	5.4	3.8	2.9	2.7	2.3
Gain margin, K_M (dB).....	6.5	3.0	4.0	4.0	3.0
Phase margin, Φ_M (deg).....	30	16	14	14	12
Performance					
RMS: error/input, e_{rms}/i_{rms} (cm/cm).....	0.80	0.93	1.79	2.08	2.34
RMS: control/input, c_{rms}/i_{rms} (cm/cm).....	2.53	2.58	3.08	3.73	3.32
RMS coherence, ρ_a.....	0.74	0.47	0.67	0.74	0.78
Normalized parameters					
Relative instability, $\lambda\tau_e$	0.242	0.333	0.440	0.464	0.500
Relative α; $\alpha\tau_e$	0.042	0.046	0.038	0.042	0.031

variation of τ_e with λ appears to be almost linear. Note that the model fits to the data make no implications on the limiting or minimum value of τ_e achievable by the subject, but only provide a basis for extrapolating beyond the conditions for long continuous runs, as required for the describing function measurements. Other considerations, to be discussed later, are involved in determining the minimum τ_e attainable by the subject.

The carefully considered, but somewhat arbitrary, extrapolation of the data to the limiting value of λ_c in the autopaced experiments is also shown on each of the cross-plots for use in later discussions.

The relative tracking error, as measured by the ratio of the rms tracking error to the rms command input (both referred to the display CRT), increases with λ as shown in figure 26a. Similarly, the control effort, as measured by the ratio of rms pilot output (in force units referred to the display) to rms command input also increases with λ. Noting that the majority of the pilot output is represented by a nearly constant gain amplitude ratio in the describing function plots, it might be expected that $c_{rms}/e_{rms} \doteq K_p$, even if remnant were present. This comparison is made in figure 26b, where it can be seen that the trend of each with λ is similar and that the magnitude of measured [control/error] (rms), approximates the loop gain.

This correspondence offers an extremely easy way of checking that K_p is in the prescribed region. In experiments where the critical task is used to constrain the operator's behavior, but where describing function or parameter tracking measurements are not available, either c_{rms}/r_{rms} or $\overline{|c|}/\overline{|e|}$ could be used to give a close estimate of K_p.

Figure 27 shows the variation of the relative coherence coefficient, ρ_a, which is a measure of the portion of pilot output linearly correlated with the input relative to the total pilot output. As shown in reference 2,

$$\rho_a^2 = \frac{\overline{c_i^2}}{\overline{c^2}} = \frac{\overline{c^2} - \overline{n^2}}{\overline{c^2}} = 1 - \frac{\overline{n^2}}{\overline{c^2}} \qquad (37)$$

where $\overline{c^2}$ = the mean square total pilot output

$\overline{n^2}$ = the mean square remnant (i.e., that portion not accounted for by the describing function acting on the input)

Remember that, by definition, the describing function accounts for any simple nonlinearity in the operator's behavior. The remnant is left to account for the effects of random variations in the operator's adjusted parameters, and especially the variations in delay time [$\tau_r(t)$ of eq. (1)]. Thus, ρ_a is an indicator of the relative remnant in the operator's control signal in an rms sense.

It is apparent from figure 27, where ρ_a varies from 0.5 to 0.8, that the remnant constitutes a relatively large fraction of the operator's output in these experiments, which is probably due to the relatively small input ($\sigma_i \doteq 0.32$ cm here, as compared to 1.3 cm in reference 2 where $\rho_a = 0.8-0.9$). Weighting the $\lambda = 2$ and $\lambda = 4$ data gives a slight decrease in ρ_a as the instability is increased. The level of ρ_a in figure 27 at $\lambda = 2$ is slightly lower than the value measured in reference 2 for the comparable case with $Y_c = 2/(s - 2)$(0.74 versus 0.8^+).

This concludes the presentation and analysis of the describing function data. These results will now be compared with the autopaced λ_c data and the theoretical analyses in order to interpret the results, test the original assumptions, and refine the basic theory.

SECTION V

INTERPRETATION OF RESULTS

A. VALIDATION OF THE THEORY

In this section the experimental data will first be interpreted from the standpoint of the key theoretical assumptions and derived predictions presented at the end of the "Theory" section. Finally, some refinements to the theory required by experimental results will be discussed.

The six theoretical predictions in Section II-F will be assessed in successive order. The first relates to the low run-to-run variance to be expected on the basis of the narrow range of Y_p permitted by stability considerations. As shown by the variances marked on the describing function data of figures 17-21, in the important crossover frequency region between 1 and 10 rad/sec the run-to-run variance is relatively small (on the order of a few symbol widths) for a given λ. Figure 16 showed that the variations from operator to operator are comparably small (especially when it is noted that the controlled element gains were changed for each operator in the previous experiments, requiring compensating operator gain adjustments). As regards the trend in the inter-run or interoperator variances with level of instability, the different number of runs at each λ makes numerical comparison difficult. Purely on the basis of a subjective evaluation of figures 18-21, it is felt that there is no really significant increase in variance with λ. Thus, the first set of theoretical predictions seems to be supported by the data.

The second prediction was that the tracking errors should increase and stability margins would decrease as the instability approached its critical value. A comparison between the theoretical curves of figure 5 and the observed stability criteria of figures 24 and 25 shows there is a clear validation of the prediction of decreasing stability margins. From figure 26a it is also apparent that the relative tracking error increases as λ approaches its critical value, as predicted in figure 6. The second set of theoretical predictions has thus been clearly validated.

The third theoretical prediction was that a tight neuromuscular loop would result from the stress of controlling an unstable element. A tighter kinesthetic (force feedback) loop would lead to increased ω_N, lower ζ_N, higher $1/T_N$, and higher α (due to a larger difference between $1/T_K$ and $1/T_K'$). The present data indicate that α lies between 0.3 and 0.4, a relatively high value compared with that of $\alpha \doteq 0.2$ given in reference 2 for $Y_c = 2/(s - 2)$. The apparent decrease of α with λ shown in figure 22a may only be scatter, as noted previously, because the data variance increases at frequencies below ω_{u1}, where the α phase contribution is fitted. According to the precision-fit data shown in figure 17, for $\lambda = 4$, the values of ω_N, ζ_N, T_N, and τ_e are all consistent with a tighter neuromuscular loop than the $\lambda = 2$ values in reference 2. (Part of this difference may be due to the very stiff force stick employed for the present experiments as

compared with the spring-loaded stick used in reference 2). Taking into consideration the operator's subjective impression of increasing his muscular tenseness during the autopaced runs, the third prediction is considered firmly supported by these experiments.

Prediction No. 4 was that for $Y_c = K_c/(s-\lambda)$ the operator's adaptation would be pure gain (nonequalized) in the broad crossover region and would be constrained to a narrow range of gains. The describing functions for Y_p plotted in figures 17a – 21a clearly demonstrate the predicted constant-amplitude behavior in the broad crossover region. As was shown previously, the differences at very high and low frequencies are well accounted for by the neuromuscular terms in the precision model. The gain adopted by the pilot (K_π in the precision model, or K_p in the α-model and simple model) is well within the stability limits predicted theoretically in figure 5, as shown in figure 25. Even the limiting values of stable gain, which are measured from the describing functions, agree surprisingly well with the predictions of the simple model (using the observed τ_e's in conjunction with figure 5 or equation 26 to establish K_{u_2}). The differences are easily explainable too. The lower gain limit occurs at a higher gain because of a slight adverse effect of the low frequency phase on the lower gain limit (e.g., trace out the phase for the simple model and α-model curves in figure 17b). The upper gain limit is reduced because of the amplitude departure from that of the simpler models as the neuromuscular second-order peak is approached.*

*A slight additional overestimate in the theoretical K_{u_2} was found to result from using the first-order Padé expression to approximate τ_e in the analysis of equation (26), on which figure 5 is based.

Of the possible pilot closure criteria suggested by theory (i.e., K_{GM}, K_{PM}, $K_{e_{min}}$, K_{100}, etc.), comparison of figures 5 and 25 indicated that the maximum gain margin criteria are used, since K_p roughly follows K_{GM}. The very clear proof of the predicted constraining effect of the critical task on operator adaptation is one of the most important results of these experiments.

The fifth prediction was that the maximum instability which can be tracked for a given length of time would be less than the theoretical limit of $\lambda \doteq 0.8/\tau_e$ because of finite gain and phase margin requirements. This is obviously true for the describing function runs, where the maximum instability which could be continuously tracked for 2 min. on 50 percent of the attempts was only $\lambda = 5$ for a fitted $1/\tau_e \doteq 10$.

Consider next the extrapolations of the τ_e data in figure 22, and of the phase and gain margin data of figure 24, to the critical short term instability, $\bar{\lambda}_c \doteq 6$, as measured by the autopacer. It is apparent that finite margins must still exist during the final few seconds of the autopaced runs. The value of $\bar{\lambda}_c = 6$ is consistent with the non-zero stability margins, according to figures 5 and 25. A somewhat tenuous further extrapolation of these stability margins to their zero point would give an intercept around $\lambda = 10$ to 12, which would be consistent with $1/\tau_e = 10$ to 11. The theoretical implications of finite stability margins are thus borne out, but the surprisingly high margins still apparent for the autopaced data require further explanation. This will be given in the final subsection.

The final theoretical prediction was that the autopaced limiting λ_c would depend primarily on $1/\tau_e$ and only secondarily on the effects of α and stability margins, i.e., there should be a calibratable dependence of λ_c on τ_e. The validity of this prediction depends on the smallness and relative invariance of τ_e, and the stability margins required as λ is increased to λ_c. If the operator could track for several seconds with zero stability margins, and if α were constant for all λ near λ_c, then λ_c would approach the ideal limit which could, in turn, be precomputed from the typical values of α from equation (31). However, these experiments show that appreciable stability margins exist even at λ_c, so the universality of any functional dependence of λ_c and τ_e then depends on the universality and consistency of the limiting stability margins and the level of α. The present data are too limited to draw any firm conclusions at this point. The slight variation of α versus λ in figure 22a may or may not be significant for reasons noted previously. If it is assumed constant for a given experimental setup, then only the variations in stability margins from run to run, from operator to operator, and for various rates of change of λ need to be examined. The present data indicate a fairly stable phase margin requirement for 4 min. runs at a given λ, but the observed variation in φ_M with λ in figure 24 makes extrapolation to a given λ_c less certain. Analysis of the variations in stability margin with run length encounters an uncertainty-principle limitation; the shorter the run length, the less accurate the cross-spectral measurement, and thus the intrinsic variation of stability margin at short run lengths cannot be resolved.

Average describing function data fits for several operators at nearly critical λ would be required to determine the universality of the margins required at λ_c. This was beyond the scope of the present program, but is an urgent matter for future investigation. In short, the final prediction was not investigated in sufficient depth to permit its firm validation, and the few applicable data are vague.

In summary, all of the assumptions and predictions of the critical task theory have been proven valid, except for one final point. Some of the reasons behind the apparently large discrepancy between $\bar{\lambda}_c$ and $1/\tau_e$ will be discussed next.

B. THE DIFFERENCE BETWEEN λ_c AND $1/\tau_e$

A major experimental result is the difference between the autopaced control limit of $\bar{\lambda}_c$ and the fitted describing function value of $1/\tau_e$. As previously discussed in the "Theory" section, some of this difference is to be expected on the basis of low frequency phase effects. Let us now check this refined prediction. Extrapolating the measured describing function data of figure 22 to the autopaced limit of $\bar{\lambda}_c = 6.0$ gives $\alpha\big|_{\lambda_c} \doteq 0.35$ 1/sec, $\tau_e\big|_{\lambda_c} = 0.094$ sec; thus $\alpha\tau_e\big|_{\lambda_c} = 0.037$. The theoretical ratio between the zero margin λ and $1/\tau_e$ is then given by equation (31) as:

$$\lambda\tau_e = 1 - \sqrt{0.037} = 0.81$$

The observed ratio of the autopaced limit $\bar{\lambda}_c$ to $1/\tau_e$ (extrapolated to $\bar{\lambda}_c$) is $\lambda\tau_e = 6.0(0.094) = 0.57$. In other words, given α and λ_c, the theory would indicate $\tau_e = (\lambda\tau)/\bar{\lambda}_c = 0.81/6.0 = 0.135$ sec, while describing function fits indicate $\tau_e = 0.094$ sec.

The apparent discrepancy can be explained by carefully examining the definition of average phase margin and its variation about a mean value. One source of variation in phase angle during a long run is the variation in operator time delay, $\tau_r(t)$. Consider an operator who is tracking with a τ varying every several seconds as shown in the sketch below.

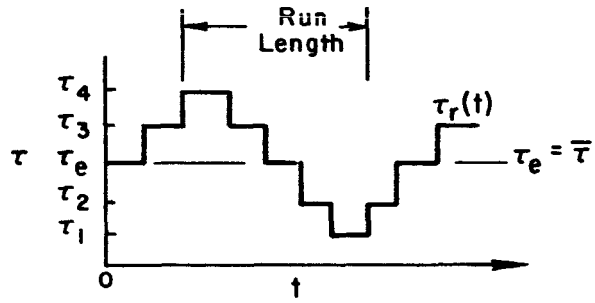

Sketch C. Hypothetical variation in τ

A describing function measure made over a long time compared to the period of the variation would yield a $\overline{\tau} = \tau_e$, or the average of the variation. But imagine short time describing function measures (if it were possible to make such a measure accurately). If the subject were in a subcritical task, a set of successive phase measurements of the describing functions might appear as shown in the following sketch.

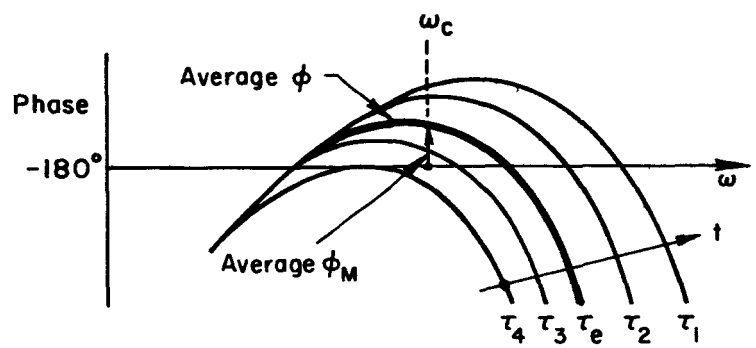

Sketch D. Short time phase plots

Clearly, the subject would lose control whenever his τ became as large as τ_4 because it takes only a fraction of a second for the error to diverge off-scale. The τ_4 is then the value that the critical task measures, while the τ_e is the quantity that the describing function determines.

The actual source of the variation is not too important as long as it is realized that it is an operator-centered limitation. The tentative conclusion is that the critical task measures an upper bound, or limiting value, of τ_e and not the average value. The fact that $\bar{\lambda}_c$ is so repeatable implies that a definite upper bound on τ_e exists. Consideration of the statistical implications of variability on $\bar{\lambda}_c$ is not within the scope of this report. To evolve a thorough treatment requires certain information about remnant which is not yet available, but is another area for further investigation.

The apparent discrepancy between the measured τ_e and value indicated by $\bar{\lambda}_c$ can now be interpreted as a $\Delta\tau$ due to the operator's intrinsic variability.

$$\tau_{e_{\bar{\lambda}_c}} = \tau_{e_{DF}} + \Delta\tau \tag{38}$$

where $\tau_{e_{\bar{\lambda}_c}}$ = the τ computed via equation (31) from autopaced λ_c and α for $\varphi_M = 0$

$\tau_{e_{DF}}$ = the τ obtained from extrapolating the describing function τ_e to $\bar{\lambda}_c$ (fig. 22)

$\Delta\tau$ = a short term increment arising from the operator's basic variability

For continuous describing function runs to be possible, this $\Delta\tau$ requires that a finite average phase margin be maintained. This average

phase margin is given by:

$$\varphi_M = \omega_c \Delta\tau = \omega_c \left(\tau_{e_{\bar{\lambda}_c}} - \tau_{e_{DF}}\right) \tag{39}$$

The measured data for these parameters are:

ω_c = 5.3 rad/sec (from fig. 23)

$\tau_{e_{\bar{\lambda}_c}}$ = 0.135 sec [computed from eq. (31) with $\bar{\lambda}_c = 6.0$ and $\alpha = 0.35$]

$\tau_{e_{DF}}$ = 0.094 sec (from fig. 22)

Then, from equation (39)

$$\varphi_M = 5.3(0.135 - 0.094)57.3 = 12.2 \text{ deg}$$

The extrapolated average phase margin at $\bar{\lambda}_c$ in figure 24 is $\varphi_M \doteq 12$ deg, in, perhaps fortuitously, good agreement with the computation. The conclusion is reached that the difference between the observed τ_e and τ_e predicted from $\bar{\lambda}_c$ is simply a matter of defining short run versus long run values of τ_e.

SECTION VI

CONCLUSIONS

This combined theoretical and experimental investigation of a "critical tracking task" yields the following main conclusions:

1. The behavior of a human operator, while in a compensatory tracking task with a controlled element having a first-order unstable divergence, is accurately predicted by the servo theory of operator response (as given in ref. 2) even near the point of incipient loss of control.

2. As the degree of instability (measured by the inverse time constant, λ) is increased, the closed-loop stability margins decrease and the tracking errors increase, in good agreement with the theory developed herein.

3. As the instability is slowly but continuously increased during one run, a point of incipient loss of control is reached, $\overline{\lambda}_c$, which, for the operator tested, had a consistent level and low variability. A very satisfactory mechanization for automatically measuring λ_c is presented.

4. This critical λ_c is theoretically shown to depend primarily on the operator's effective time delay, τ_e, while tracking. Both the analysis and experiments reveal that there are appreciable secondary influences on λ_c due to the operator's intrinsic stability margin requirements and neuromuscular system artifacts such as kinesthetic phase lags (α effects) and arm/control-stick resonances (ω_N, ζ_N). The experiments were not of sufficient scope to show whether or not these secondary effects would preclude a universal dependence of λ_c on τ_e among all operators.

5. The good agreement between the theoretical and measured operator describing functions proves that one can force

an operator to adopt any form of equalization and gain within his known capabilities by selection of a suitable critical task configuration. This should permit a variety of improved psychomotor tests to be developed in which the experimenter has excellent control over the operator's tracking behavior.

More specific conclusions relating to the various phases of the program are contained at the end of each major subsection.

REFERENCES

1. McRuer, D. T.; and Krendel, E. S.: Dynamic Response of Human Operators [Contracts AF 33(616)-3080 and AF 33(038)-10420]. (WADC-TR-56-524, ASTIA AD-110693) Control Specialistis, Inc., and Franklin Institute Laboratories for Research and Development, Oct. 1957.

2. McRuer, D.; Graham, D.; Krendel, E.; and Reisener, W., Jr.: Human Pilot Dynamics in Compensatory Systems — Theory, Models, and Experiments with Controlled Element and Forcing Function Variations. Tech. Rep. 115-1 (FDL-TR-65-15), Systems Technology, Inc., Jan. 1965.

3. Ashkenas, Irving L.; and McRuer, Duane T.: A Theory of Handling Qualities Derived from Pilot-Vehicle System Considerations. Aerospace Eng., vol. 21, no. 2, Feb. 1962, pp. 60, 61, 83-102.

4. Durand, T. S.; and Jex, H. R.: Handling Qualities in Single-Loop Roll Tracking Tasks: Theory and Simulator Experiments. Tech. Rep. 120-1 (ASD-TDR-62-507, ASTIA AD-293236), Systems Technology, Inc., Nov. 1962.

5. McRuer, D. T.; Ashkenas, I. L.; and Pass, H. R.: Analysis of Multiloop Vehicular Control Systems, Tech. Rept. 123-1 (ASD-TDR-62-1014), Systems Technology, Inc., Mar. 1964.

6. Stark, Lawrence; Kupfer, Carl; and Young, Laurence R.: Physiology of the Visual Control System. NASA CR-238, 1965.

7. Ashkenas, I. L.; and McRuer, D. T.: The Determination of Lateral Handling Quality Requirements from Airframe/Human-Pilot System Studies. Tech. Rep. 3 (WADC-TR-59-135), Systems Technology, Inc., June 1959.

8. McRuer, D. T.; Ashkenas, I. L.; and Guerre, C. L.: A Systems Analysis View of Longitudinal Flying Qualities. Tech. Rep. 6 (WADD-TR-60-43), Systems Technology, Inc., Jan. 1960.

9. Ashkenas, I. L.: A Simple "Critical Task" Test Procedure to Yield Information on Pilot Fitness. Tech. Memo. 46, Systems Technology, Inc., 27 Apr. 1960.

10. Jex, H. R.; and Cromwell, C. H.: Theoretical and Experimental Investigation of Some New Longitudinal Handling Quality Parameters. Tech. Rep. 16 (ASD-TR-61-26), Systems Technology, Inc., Mar. 1961.

11. Tustin, A.: The Nature of the Operator's Response in Manual Control and Its Implications for Controller Design. J. Inst. Elect. and Elec. Eng. (London), vol. 94, pt. IIA, May 1947, pp. 190-202.

12. Okabe, Y.; Rhodes, H. E.; Stark, L.; and Willis, P. A.: Transient Responses of Human Motor Coordination System, Quar. Prog. Rep. 66, Res. Lab. Elec., Mass. Inst. of Tech., July 1962, pp. 389–395.

13. McRuer, Duane; and Graham, Dunstan: Pilot–Vehicle Control Systems Analysis. Paper 63-310, Am. Inst. Aeron. and Astronaut., Aug. 1963.

14. McRuer, Duane T.: Unified Analysis of Linear Feedbacks. Tech. Rep. 14 (ASD-TR-61-118, ASTIA AD-270593), Systems Technology, Inc., July 1961.

15. Phatak, A. V.: Theoretical Performance and Stability of a Single First-Order Critical Task. Working Paper 147-3, Systems Technology, Inc., Jan. 1965.

16. Elkind, J. E.: Characteristics of Simple Manual Control Systems. Tech. Rep. 111, Lincoln Lab., Mass. Inst. of Tech., Apr. 1956.

17. McDonnell, J. D.: Critical Task Configuration Selection and Parameter Choice. Working Paper 147-2, Systems Technology, Inc., 22 Dec. 1964.

18. Graham, Dunstan; and McRuer, Duane: Analysis of Nonlinear Control Systems. John Wiley and Sons, Inc., 1961.

19. Durand, T. S.: Some Preliminary Experiments on the Critical Task for Reaction Time of a Tracking Operator. Working Paper 147-1, Systems Technology, Inc., 25 Aug. 1964.

20. Hoel, Paul G.: Introduction to Mathematical Statistics. Second ed., John Wiley and Sons, Inc., 1954,

21. Tsibulevskii, I. E.: Operator Delay in Processing Visual Signals. Automatika i Telemekhanika, vol. 23, no. 11, Nov. 1962, pp. 1513–1526.

22. Woodworth, Robert S.; and Harold Schlosbert: Experimental Psychology. Rev. ed., Holt, Rinehart and Winston, 1964.

23. Seltzer, L. J.; and D. T. McRuer: Survey of Analog Cross Spectral Analyzers [Contract AF 33(616)-5822]. (WADC-TR-59-241) Systems Technology, Inc., Dec. 1959.

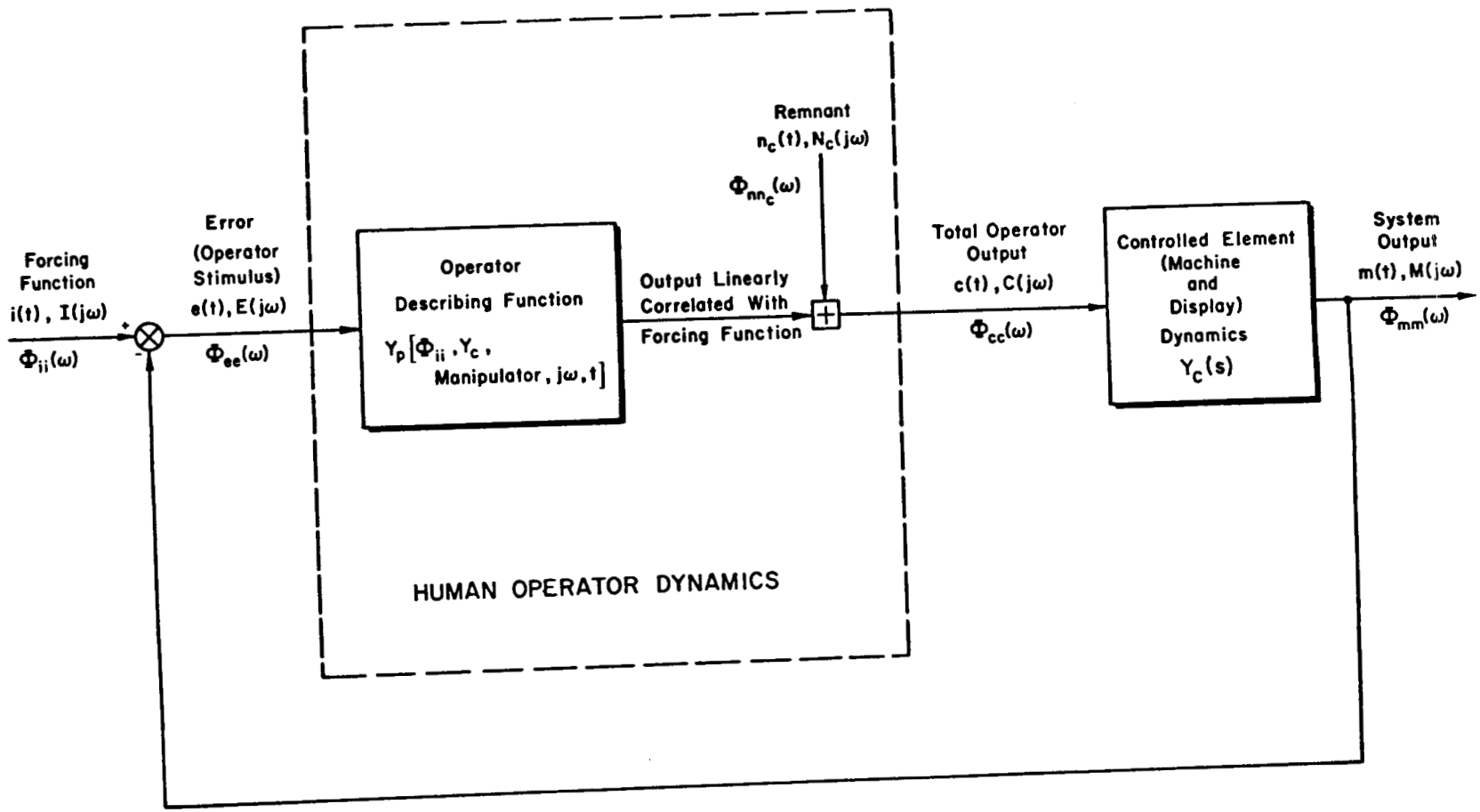

Figure 1. Analytical model for man-machine analysis of compensatory tracking tasks

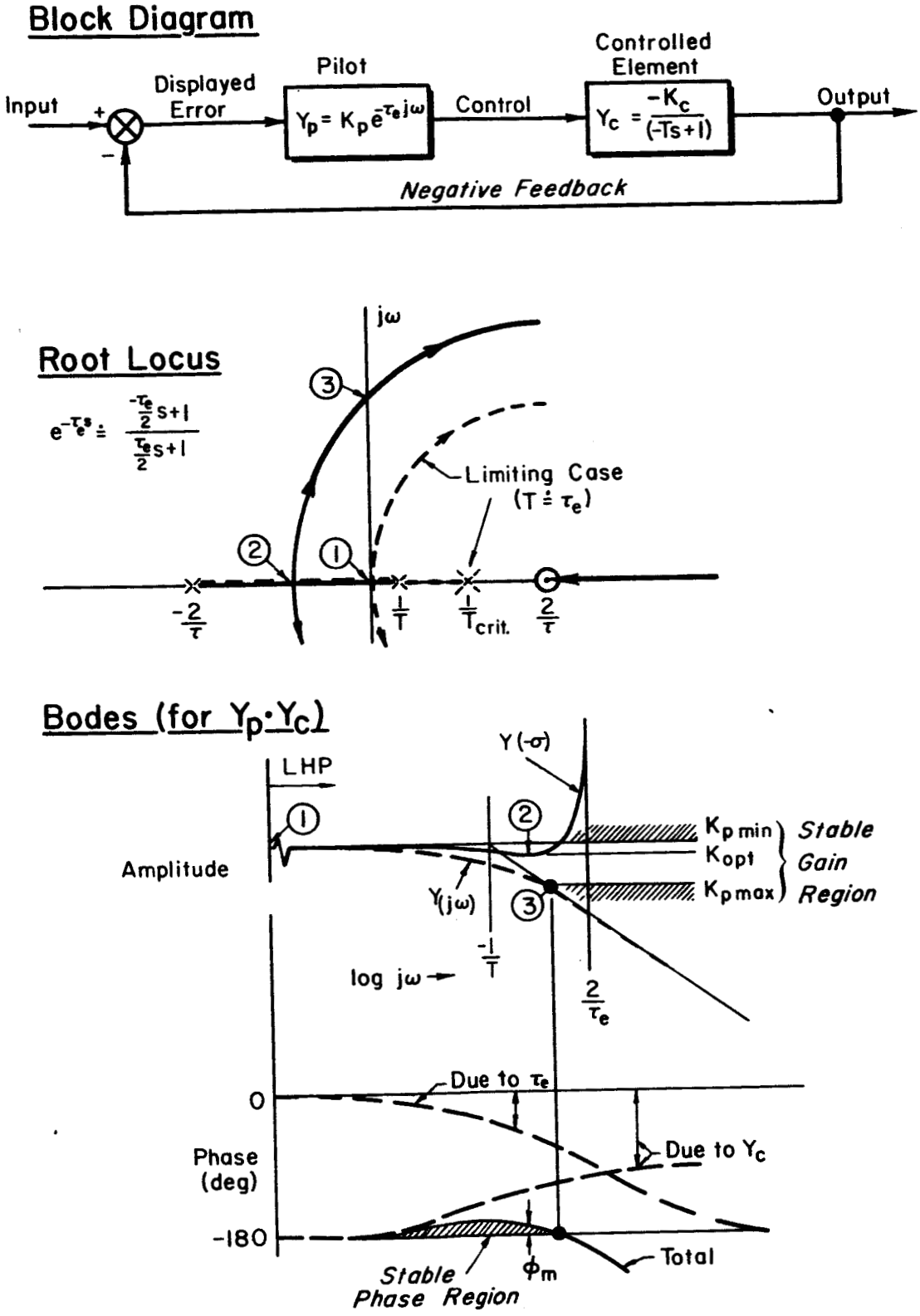

Figure 2. Simplified systems analysis of human operator control of a first-order divergent controlled element

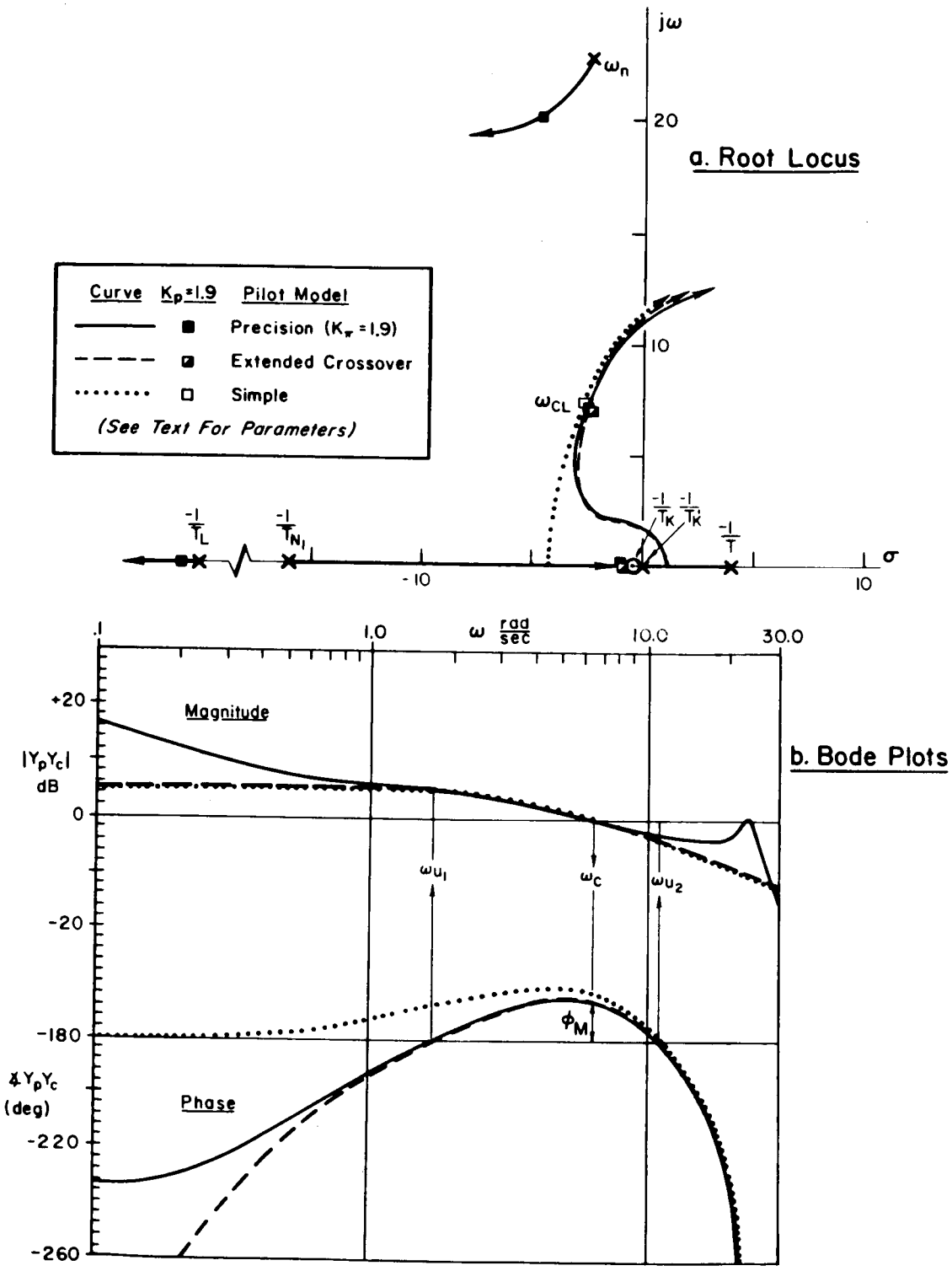

Figure 3. Comparison of Loop Closures for Three Pilot Models

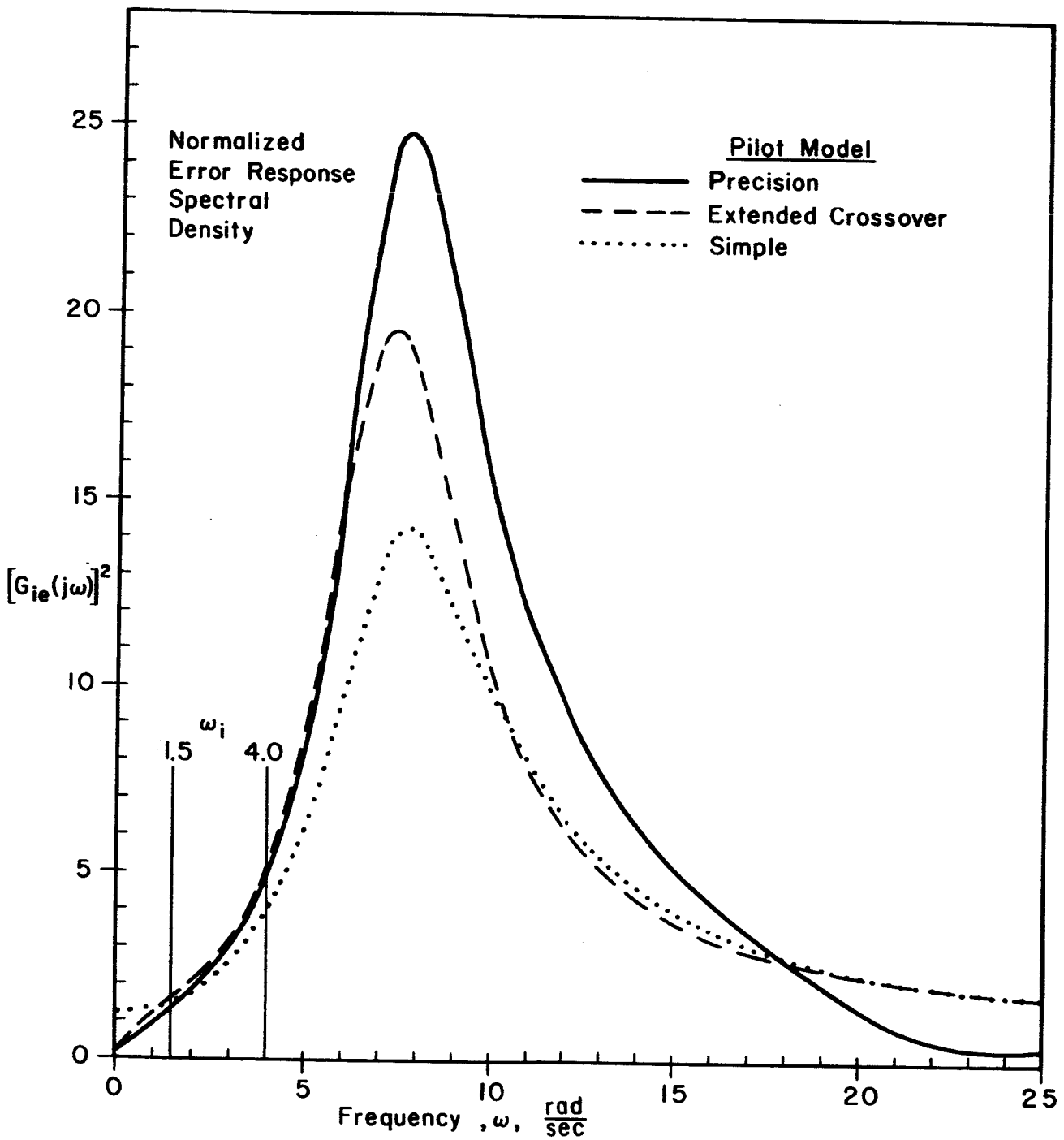

Figure 4. Comparison of normalized error response spectra for three pilot models

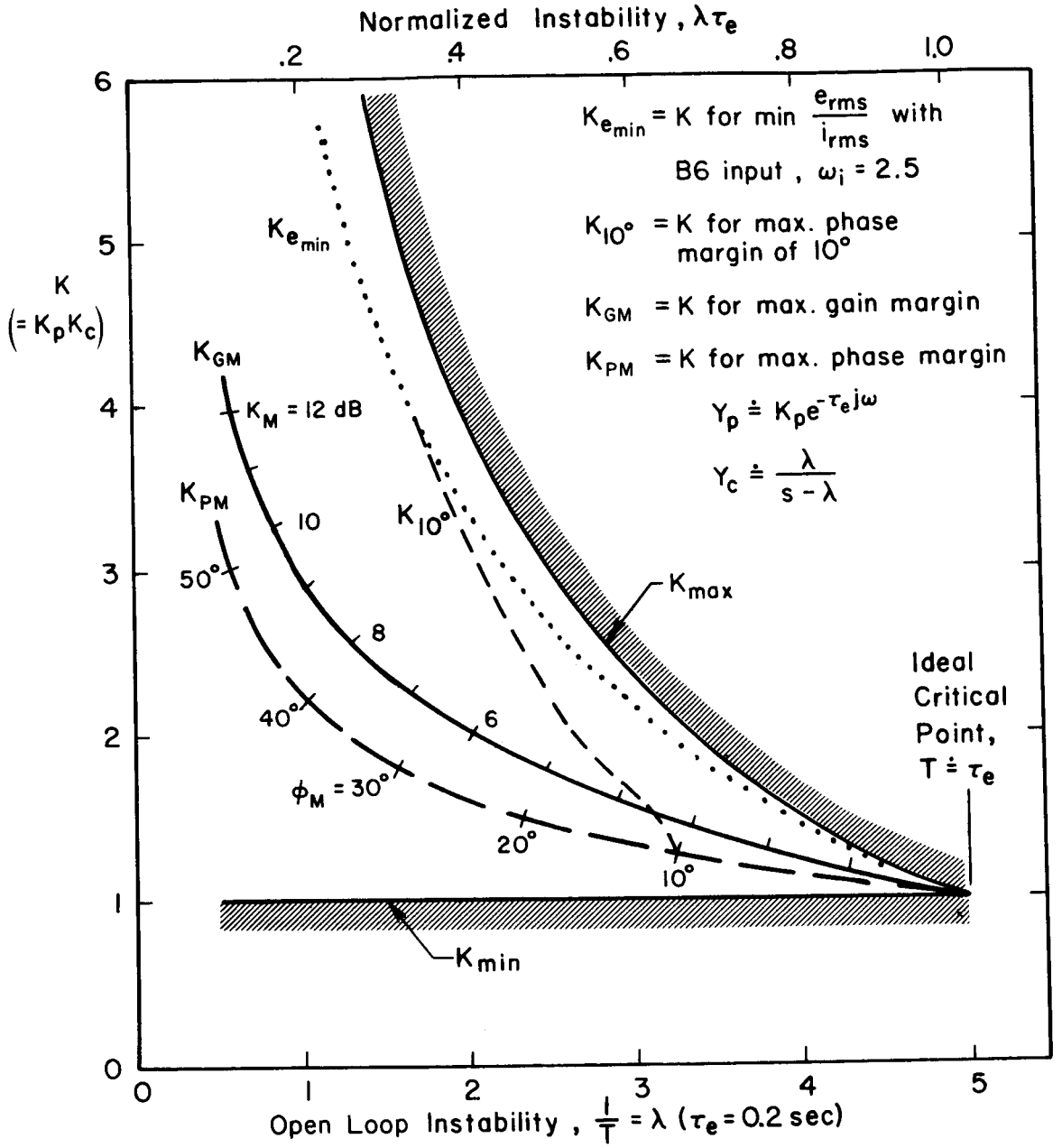

Figure 5. Theoretical constraints on various stability margins as the open-loop instability is increased

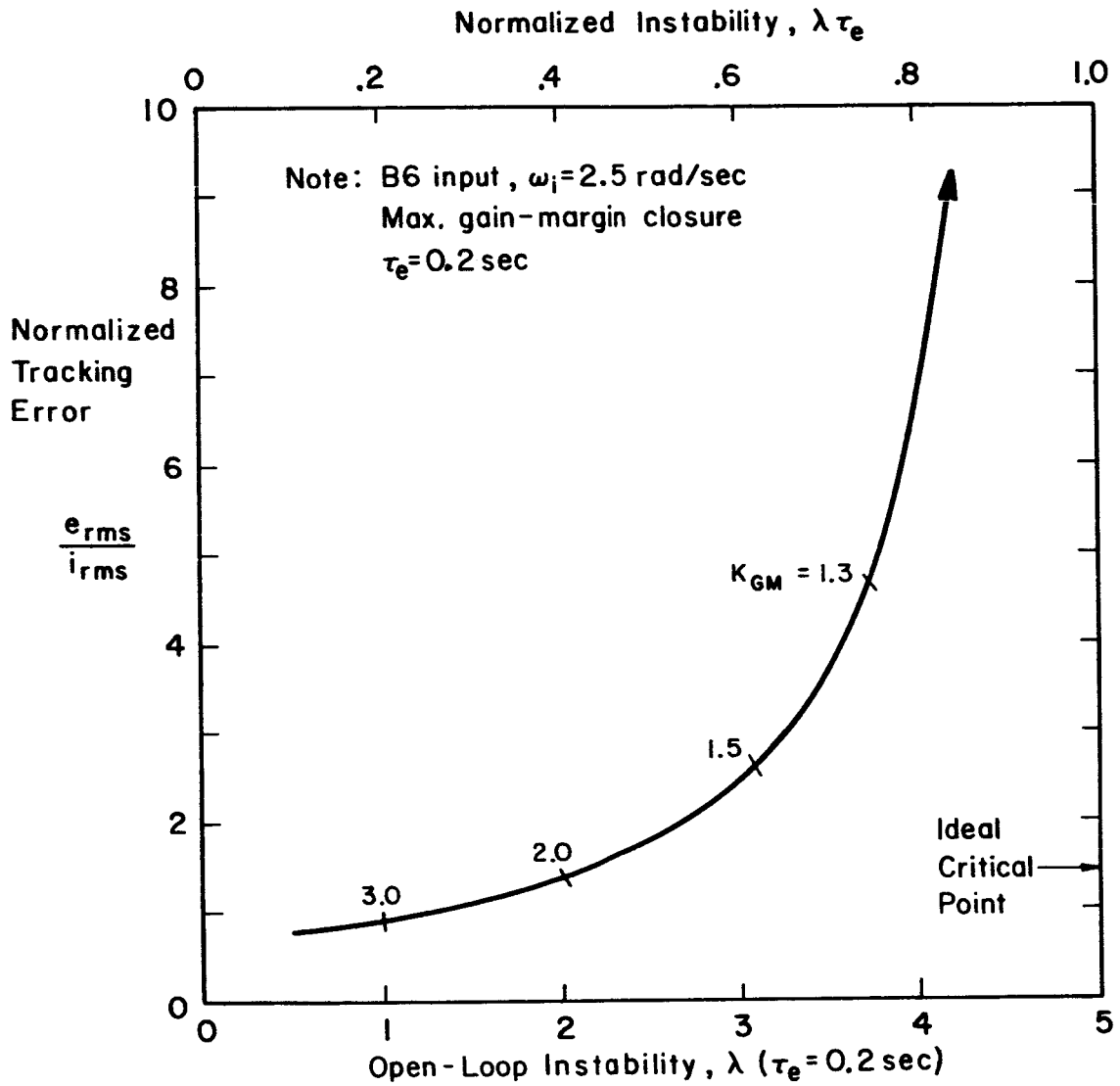

Figure 6. Theoretical tracking error growth as the open-loop instability is increased

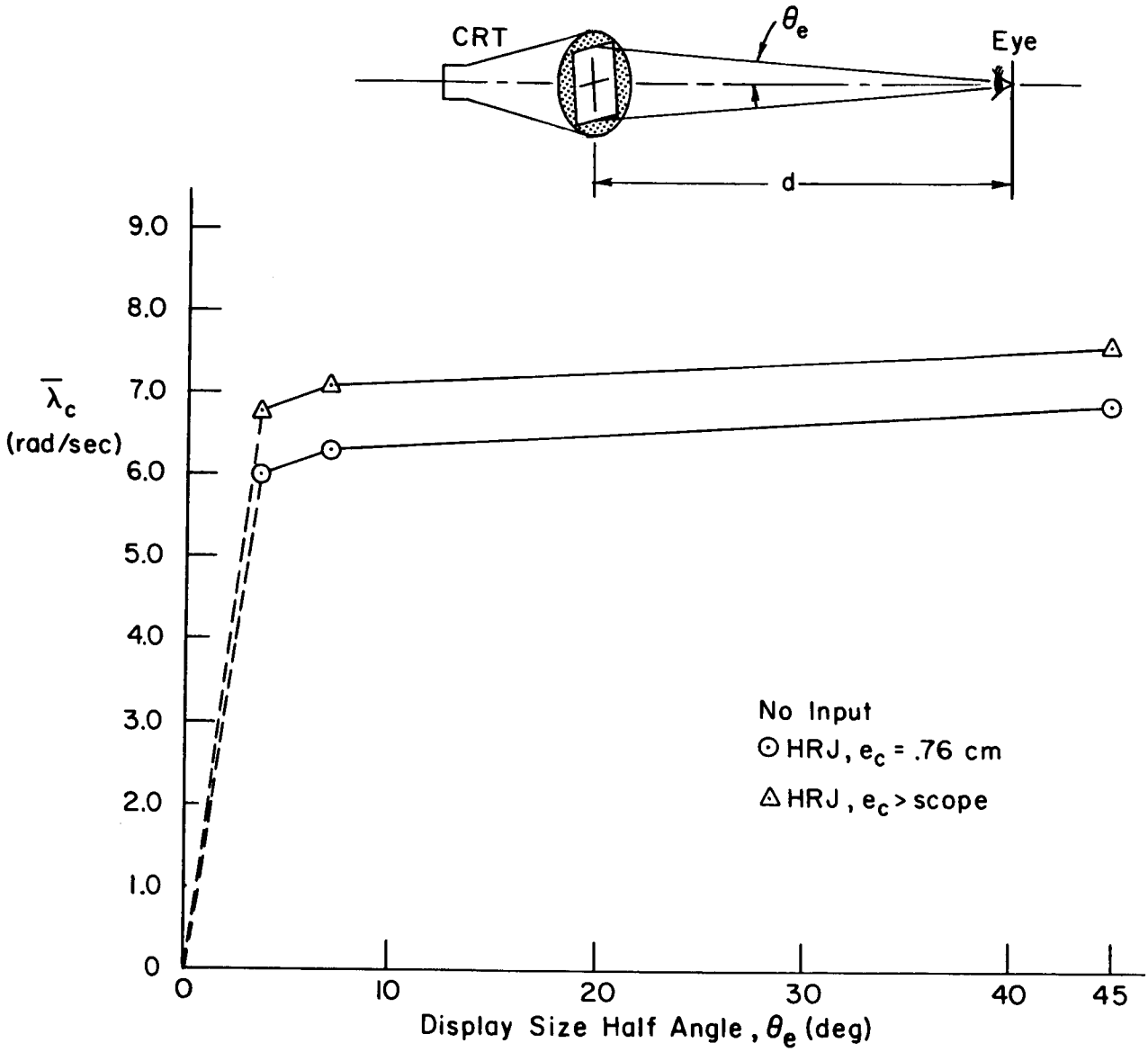

Figure 7. Effects of maximum display size on $\overline{\lambda}_c$

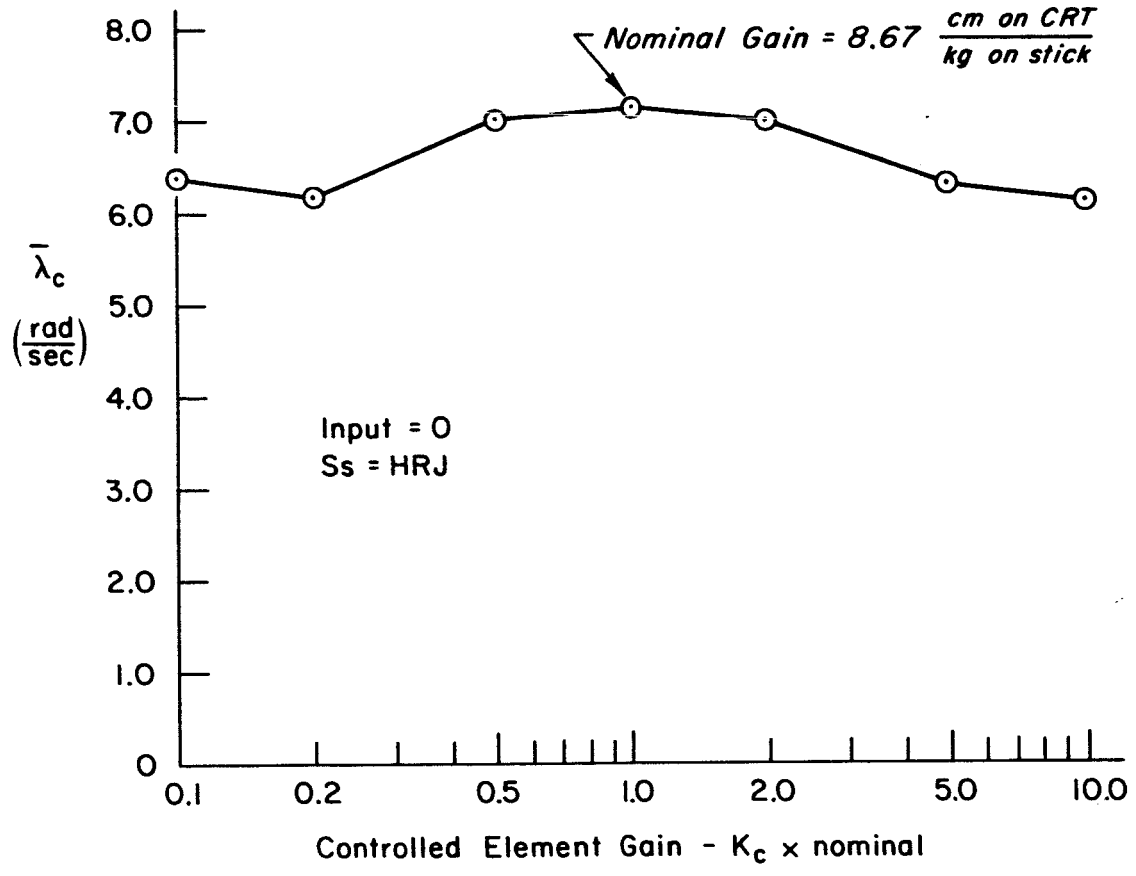

Figure 8. Effects of stick gain on $\bar{\lambda}_c$

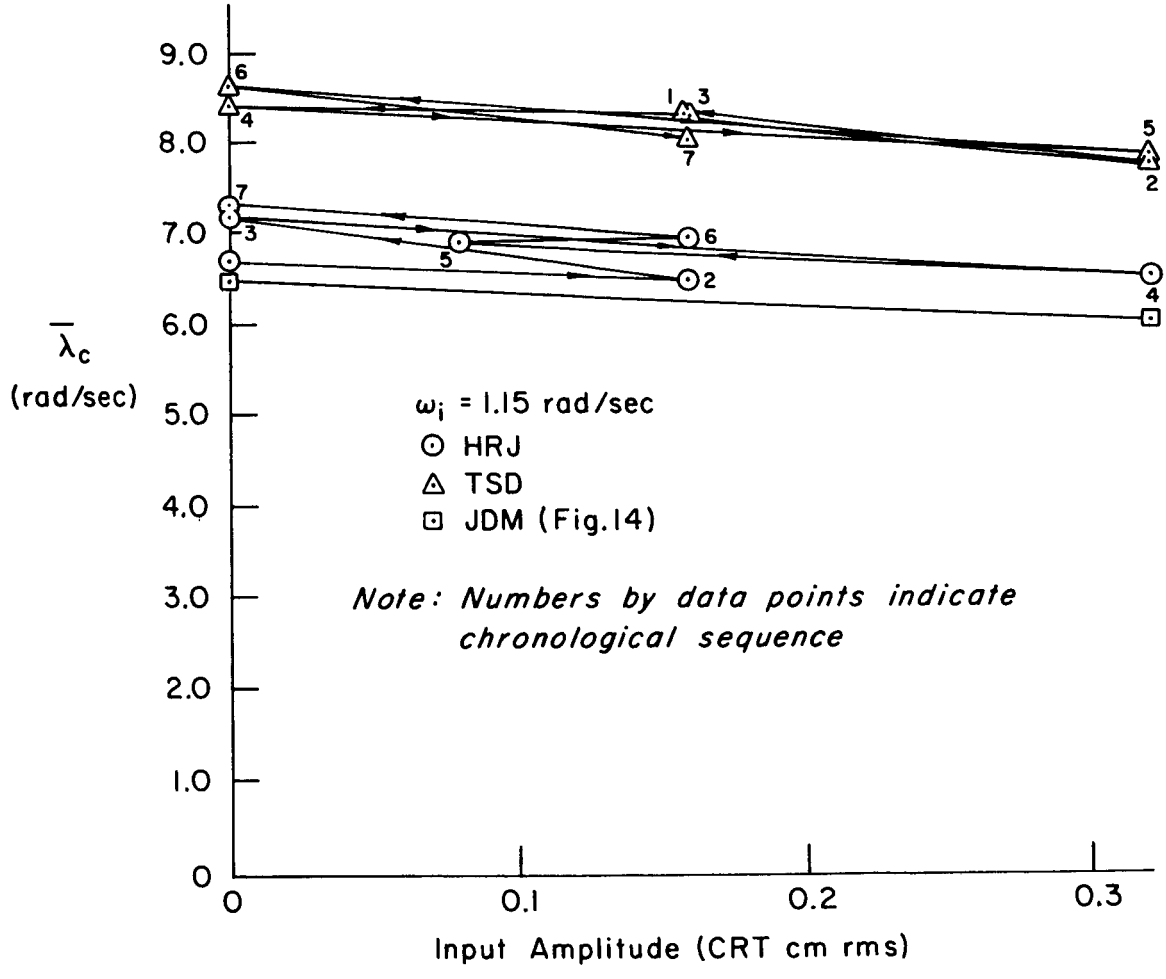

Figure 9. Input amplitude effects

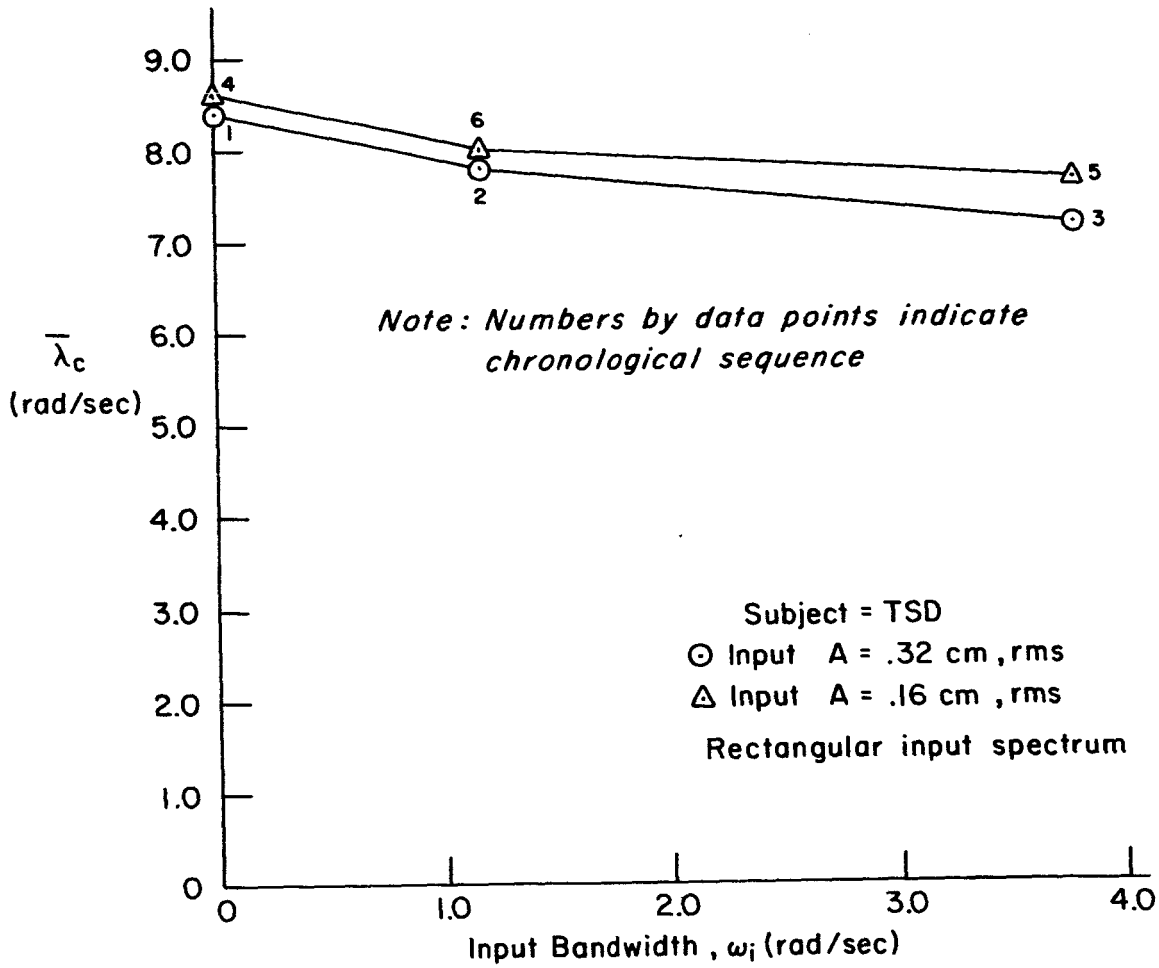

Figure 10. Input bandwidth effects on $\overline{\lambda}_c$

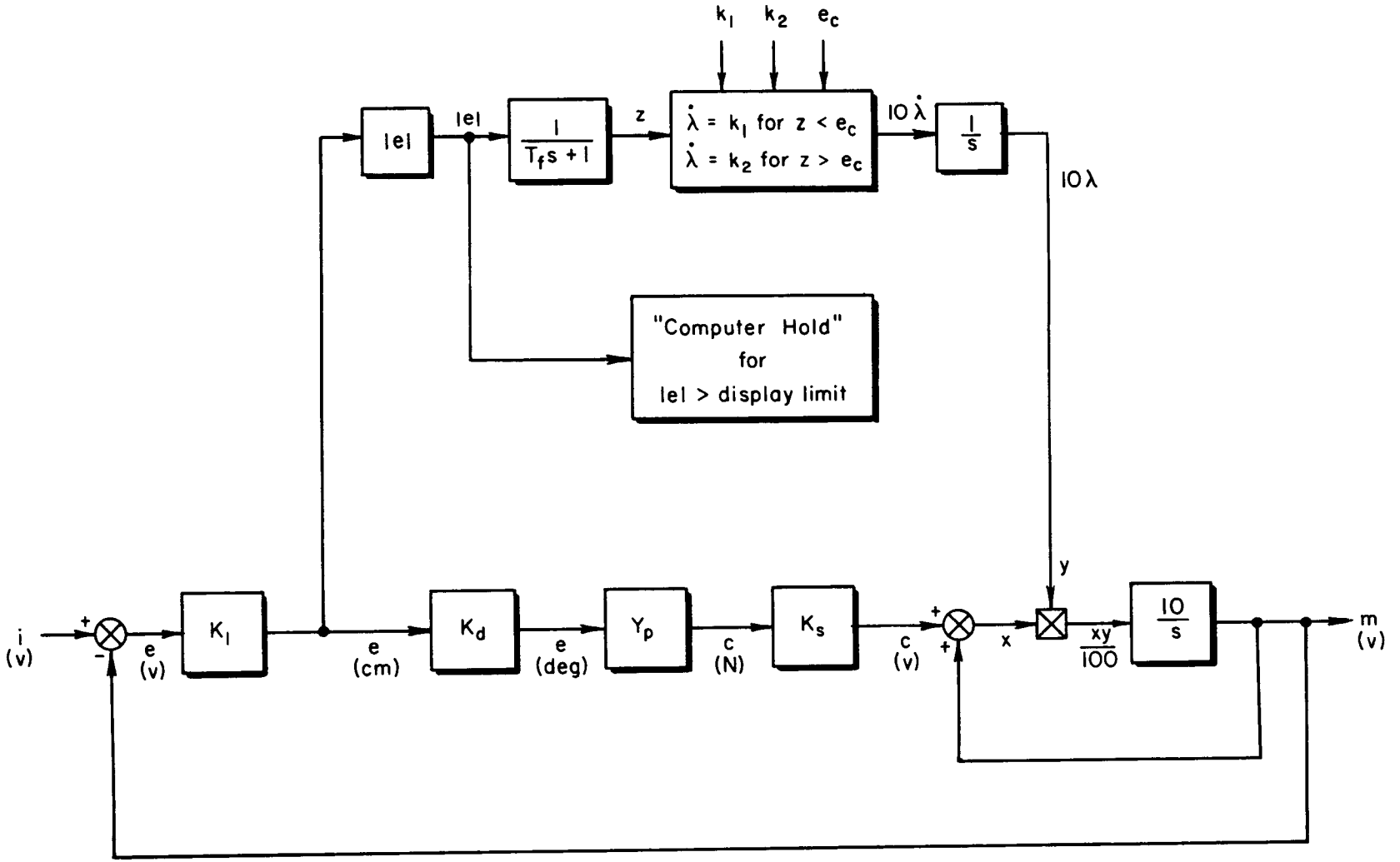

Figure 11. Block diagram of critical task mechanization

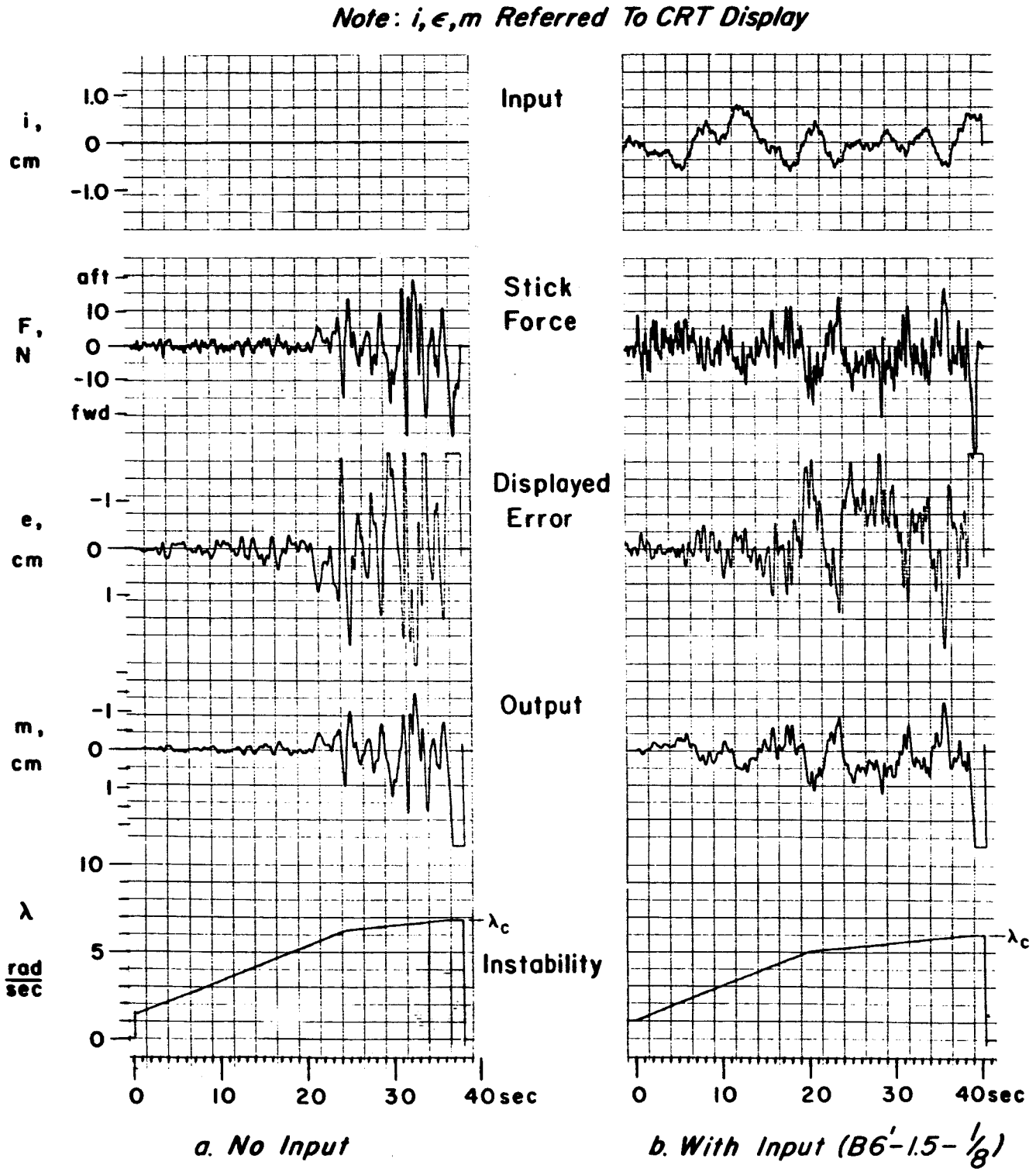

Figure 12. Typical Autopaced Critical Task Time Histories With and Without an Input

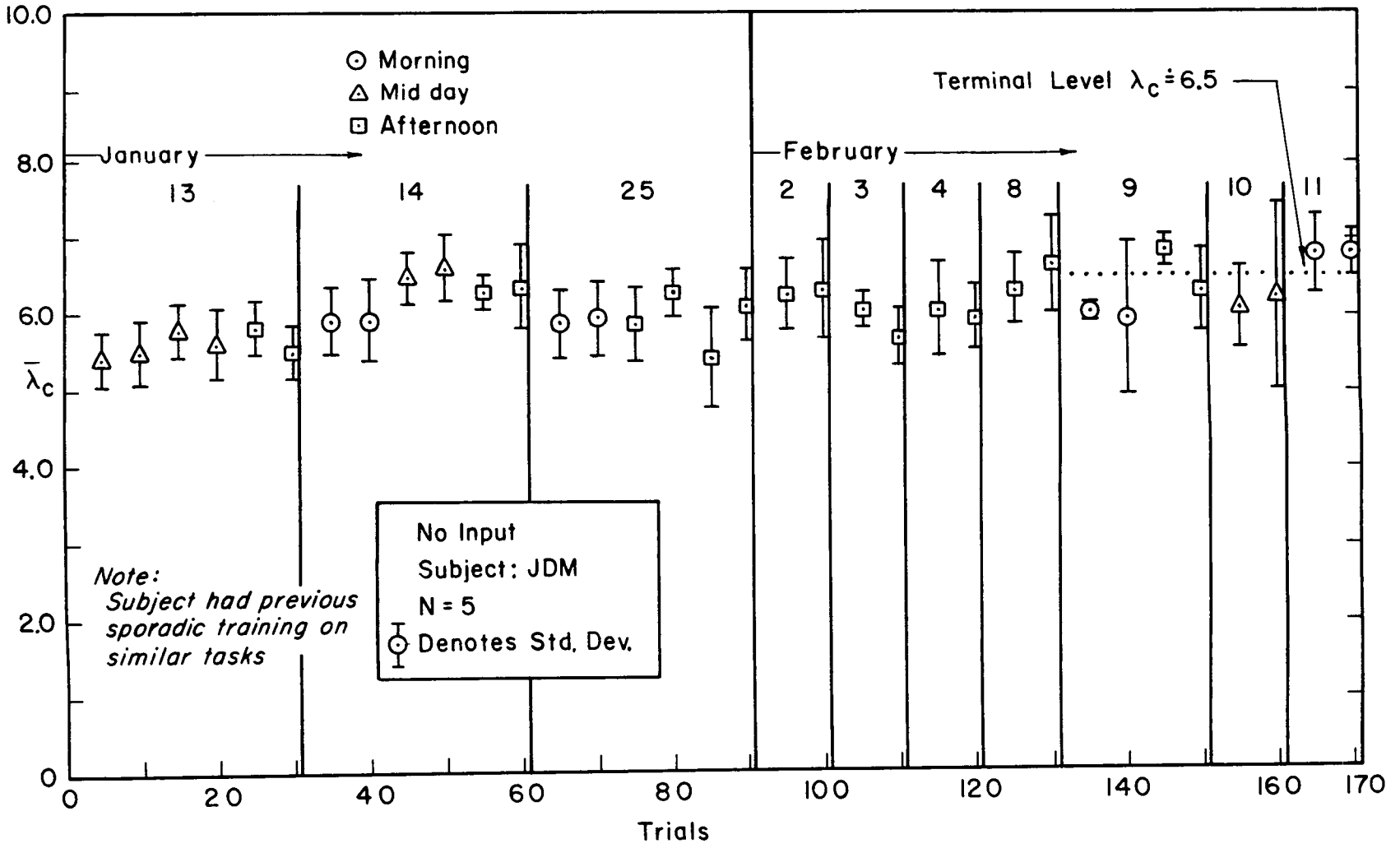

Figure 13. Autopaced sample mean values of λ_c data during training runs

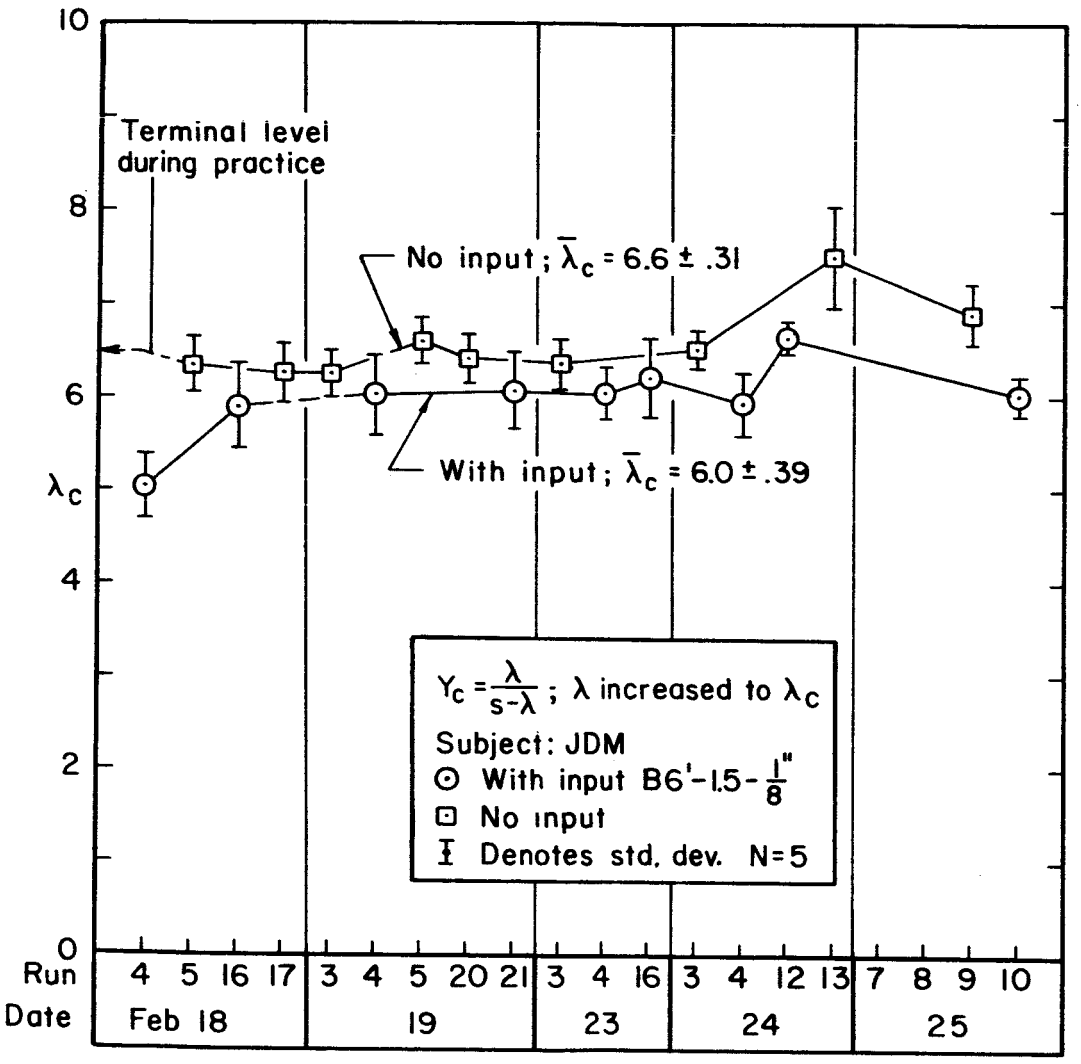

Figure 14. Sample mean levels of $\bar{\lambda}_c$ during the experiments

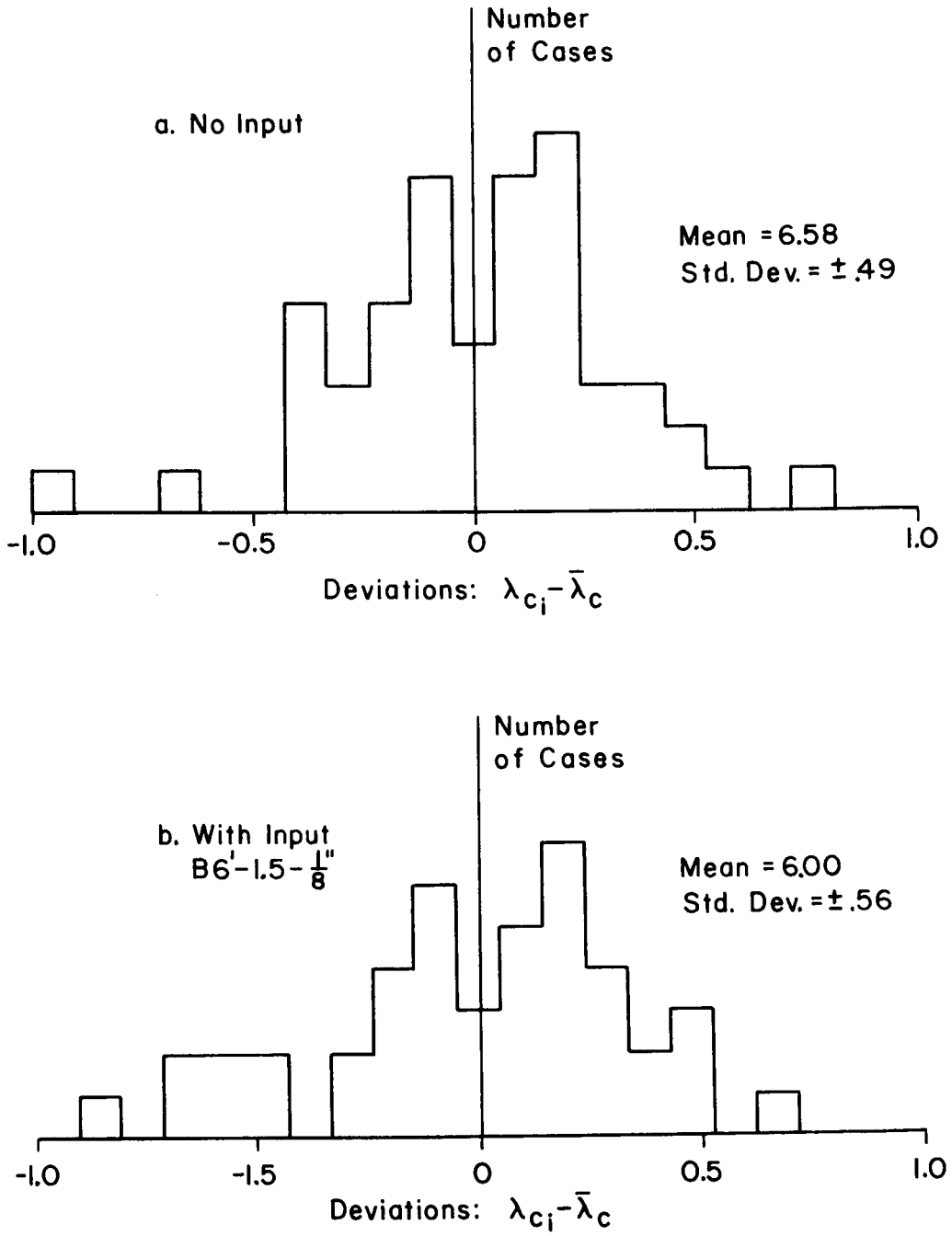

Figure 15. Histograms of the individual λ_c deviations from their five-trial sample means

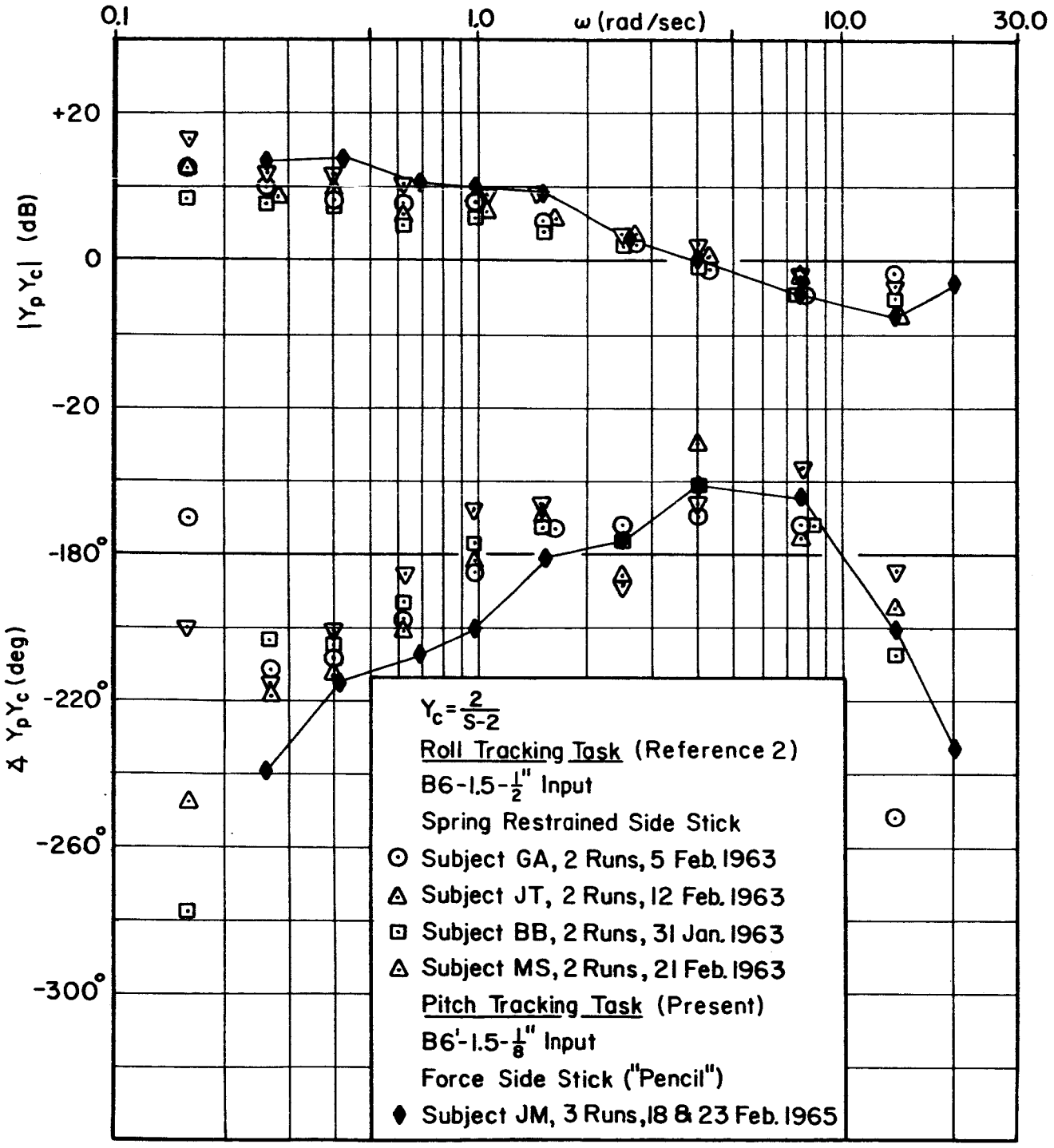

Figure 16. Comparison of present and previous data describing functions for a similar task

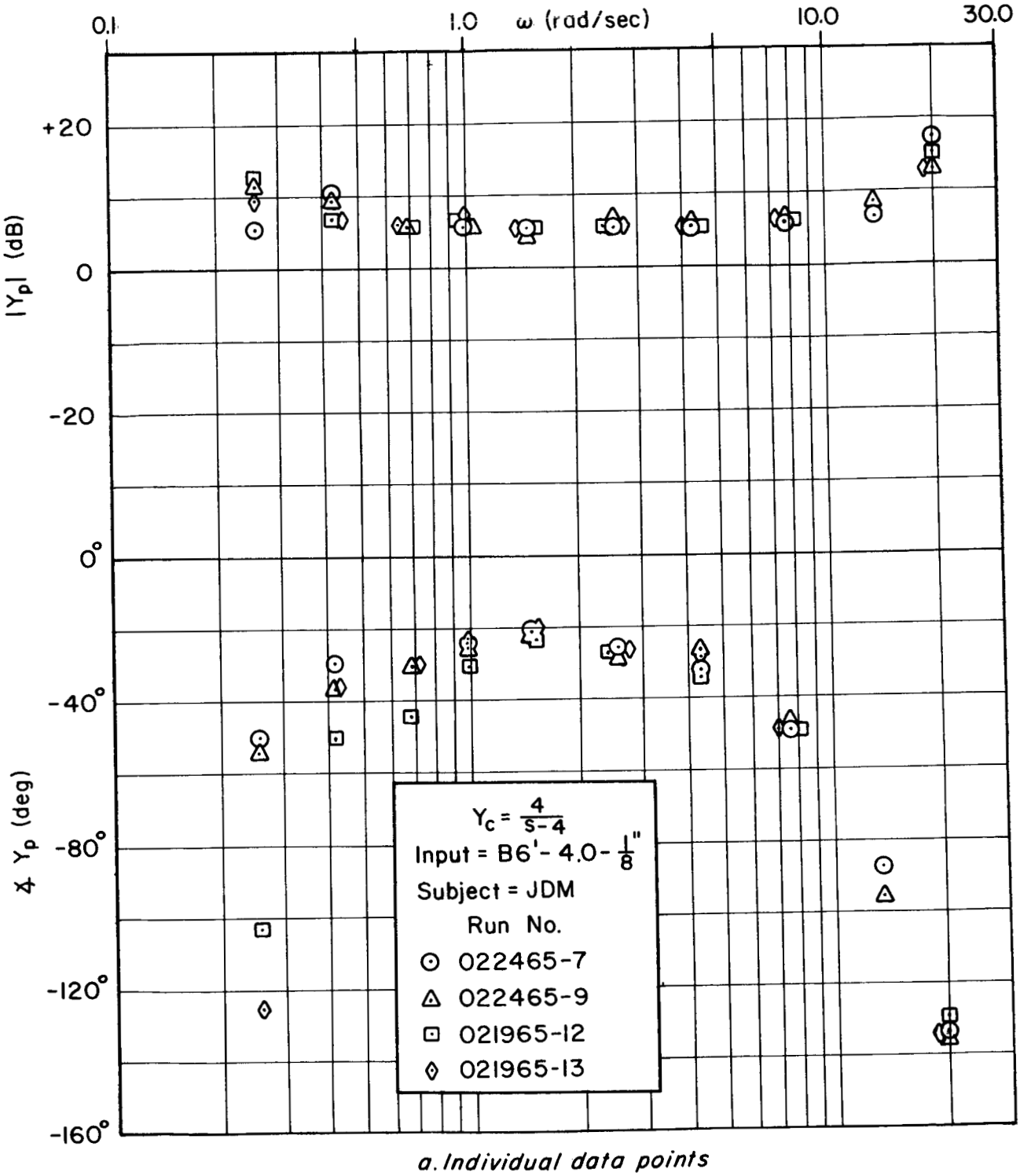

Figure 17. Individual and averaged describing function data at a near-critical value of instability, $\lambda = 4.0$, $\omega_i = 4.0$

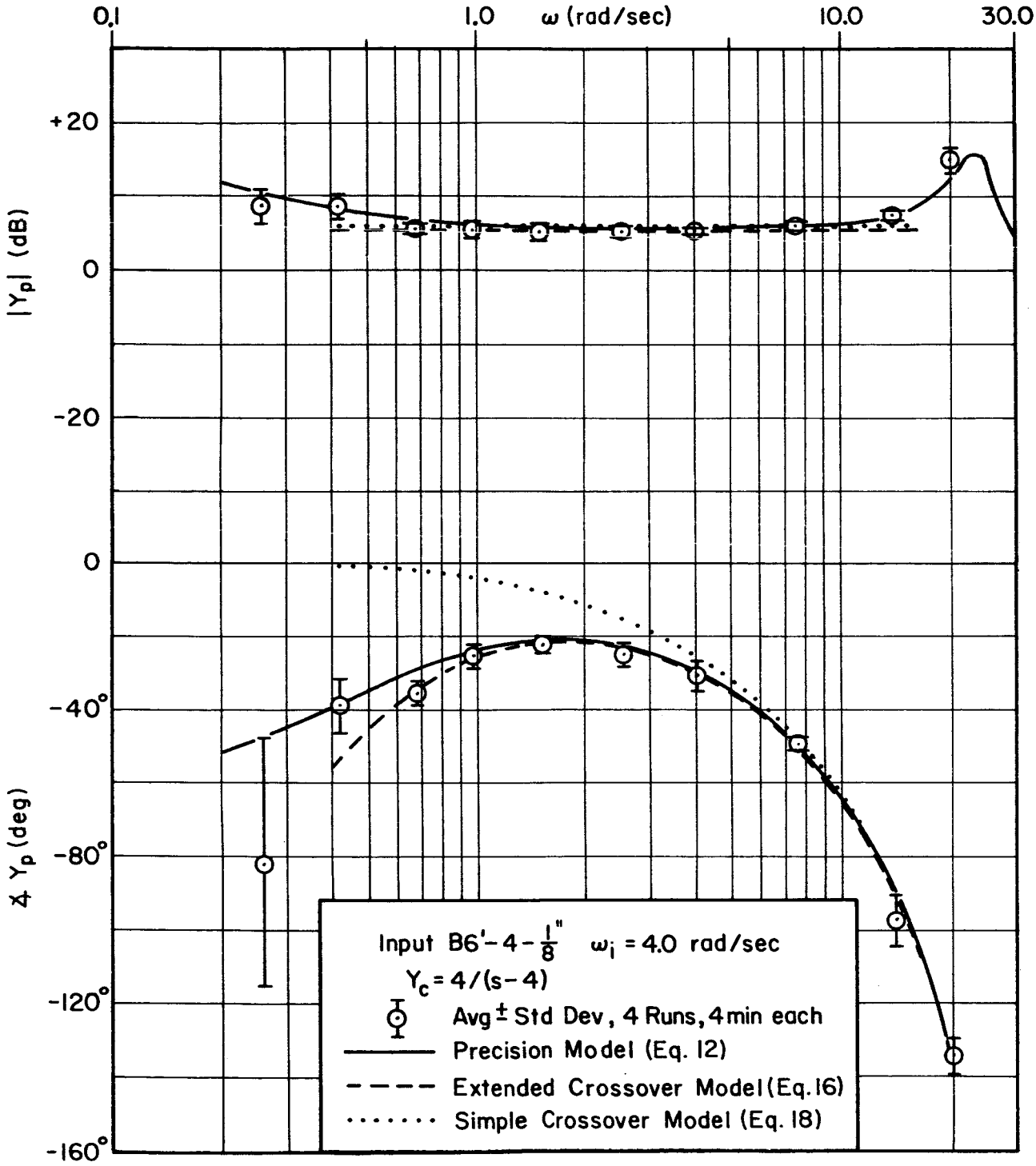

b. Mean data and comparison of model curve fits

Figure 17.– Concluded

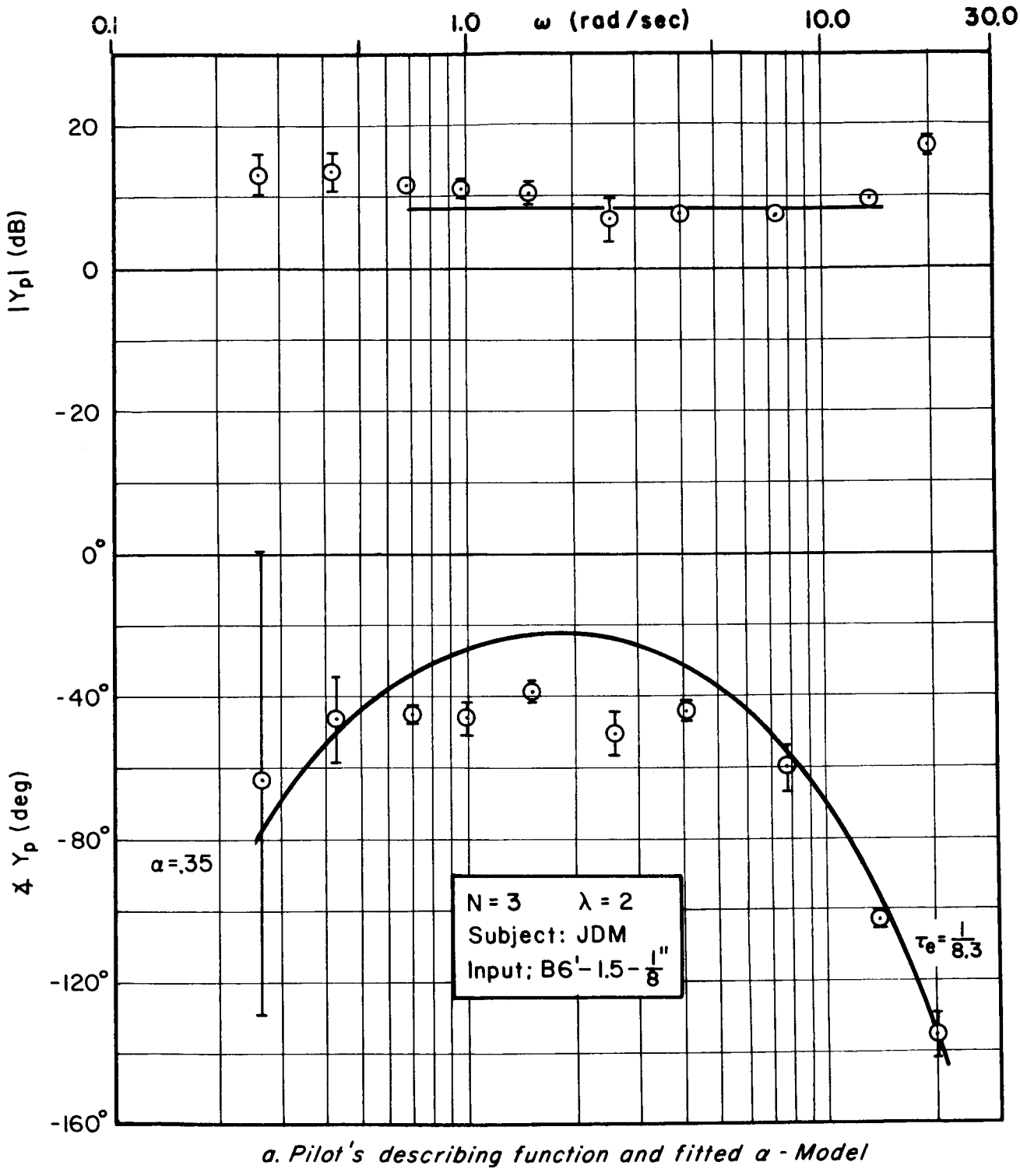

a. Pilot's describing function and fitted α - Model

Figure 18. Describing function data at $\omega_i = 1.5$, $\lambda = 2.0$

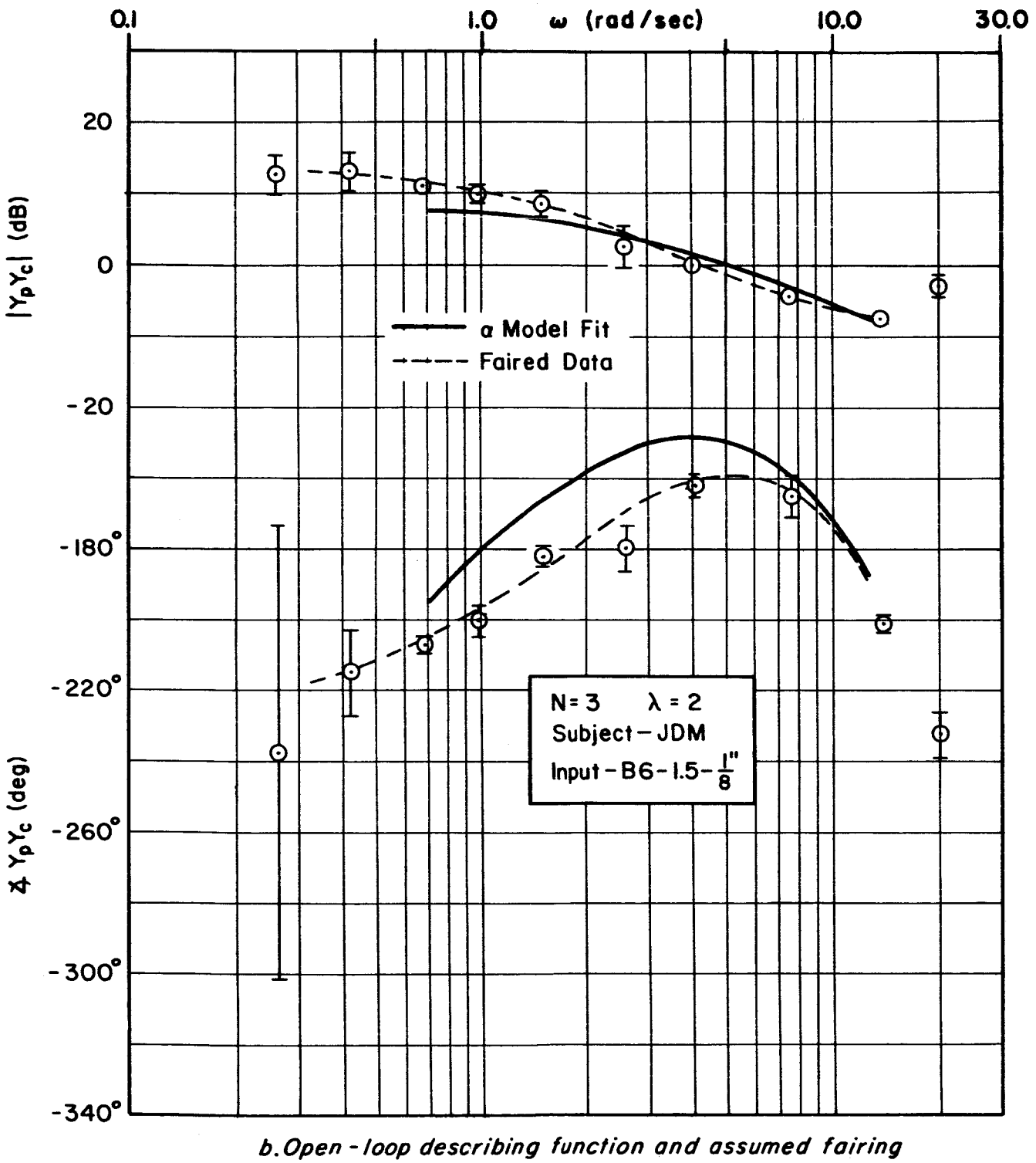

b. Open-loop describing function and assumed fairing

Figure 18.– Concluded

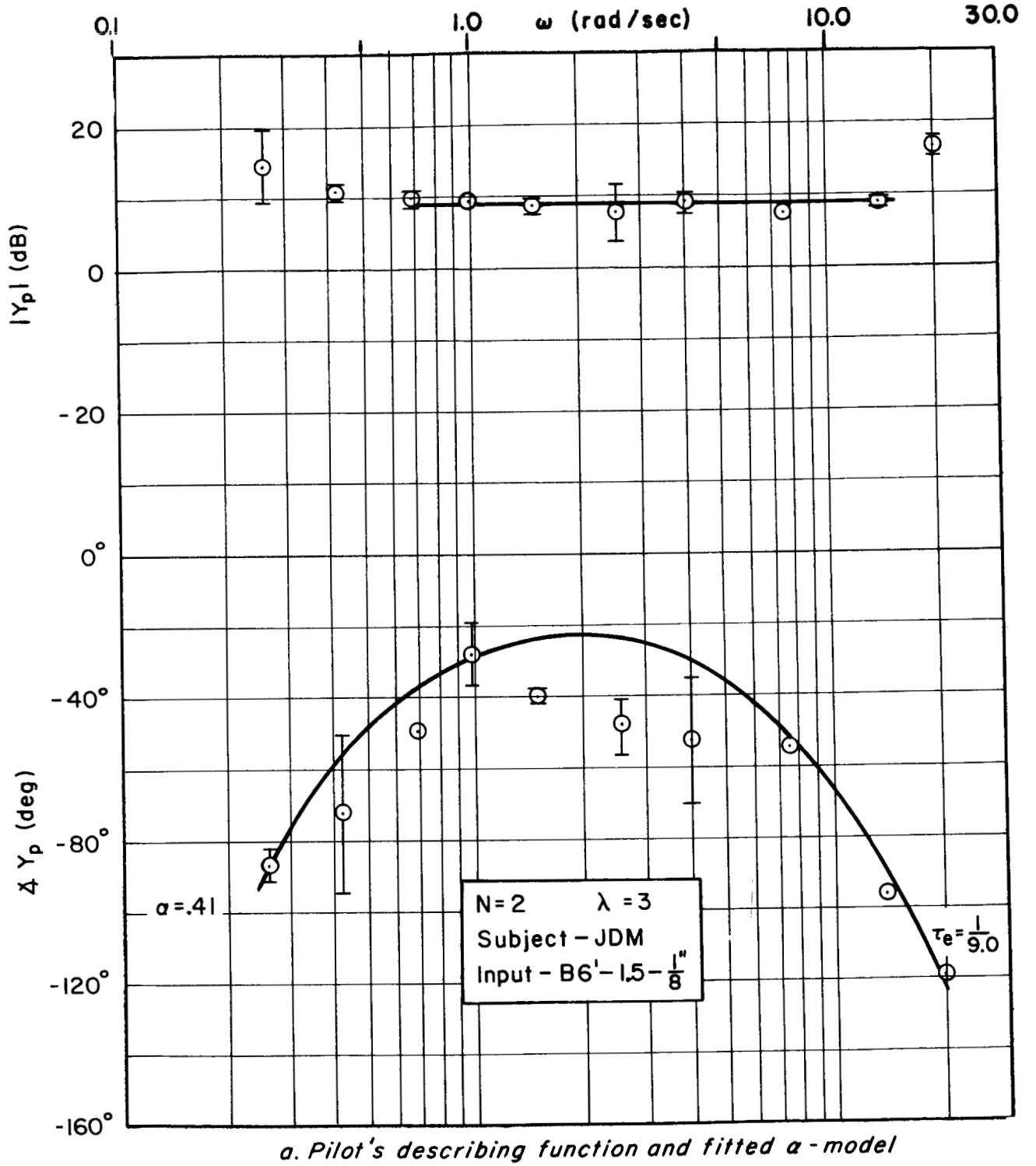

Figure 19. Describing function data at $\omega_i = 1.5$, $\lambda = 3.0$

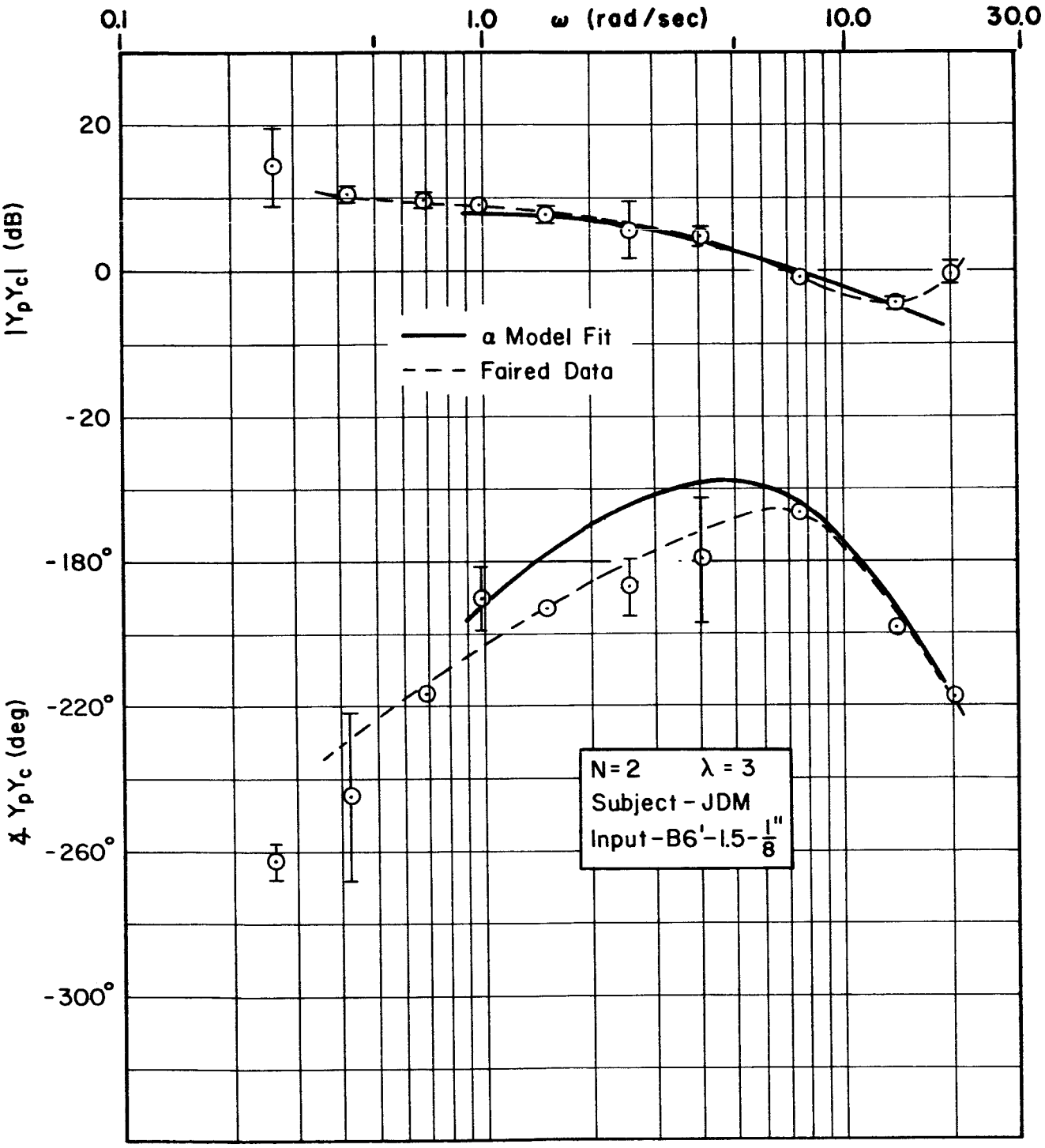

b. Open-loop describing function and assumed fairing

Figure 19.– Concluded

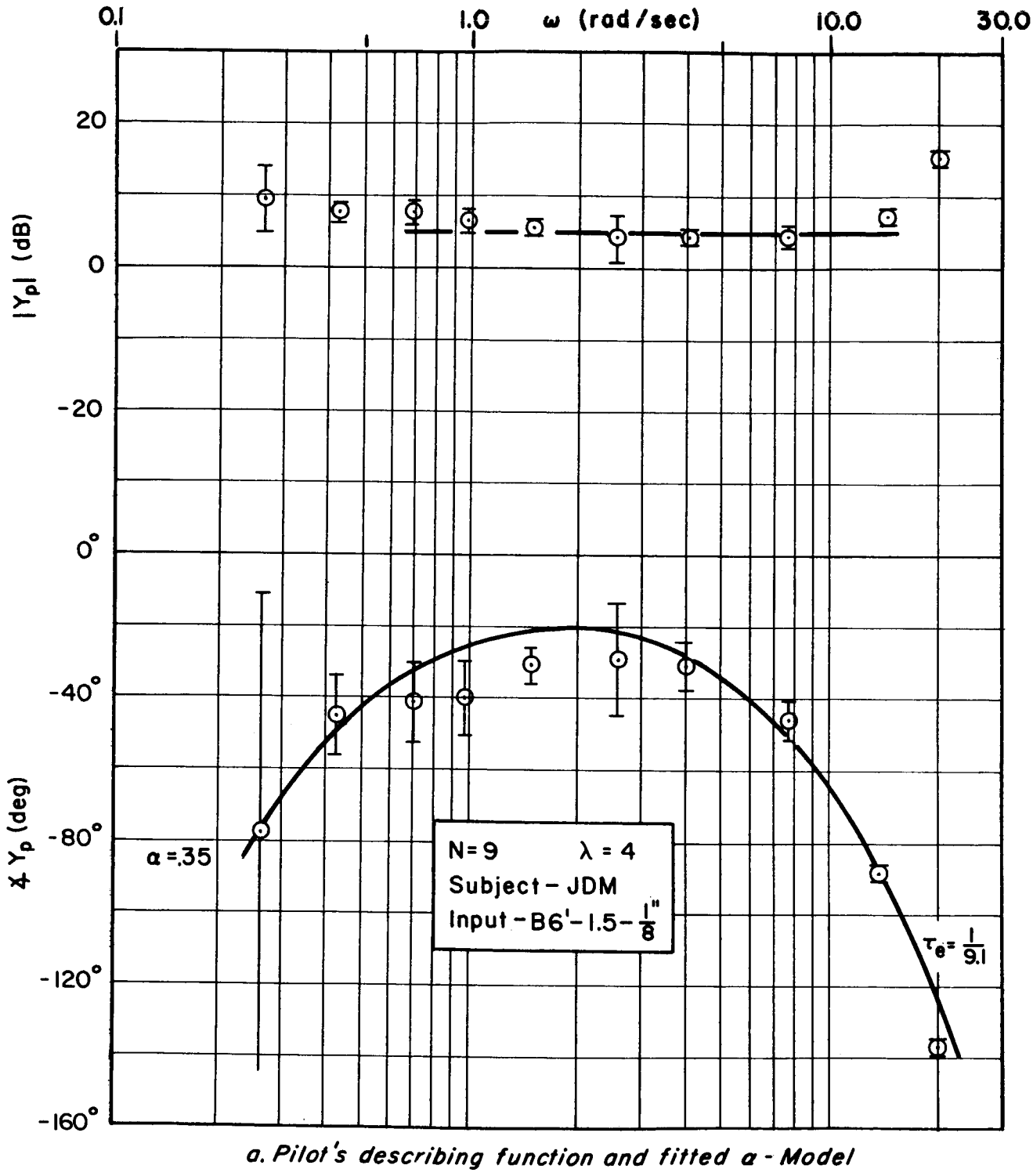

a. Pilot's describing function and fitted α - Model

Figure 20. Describing function data at $\omega_i = 1.5$, $\lambda = 4.0$

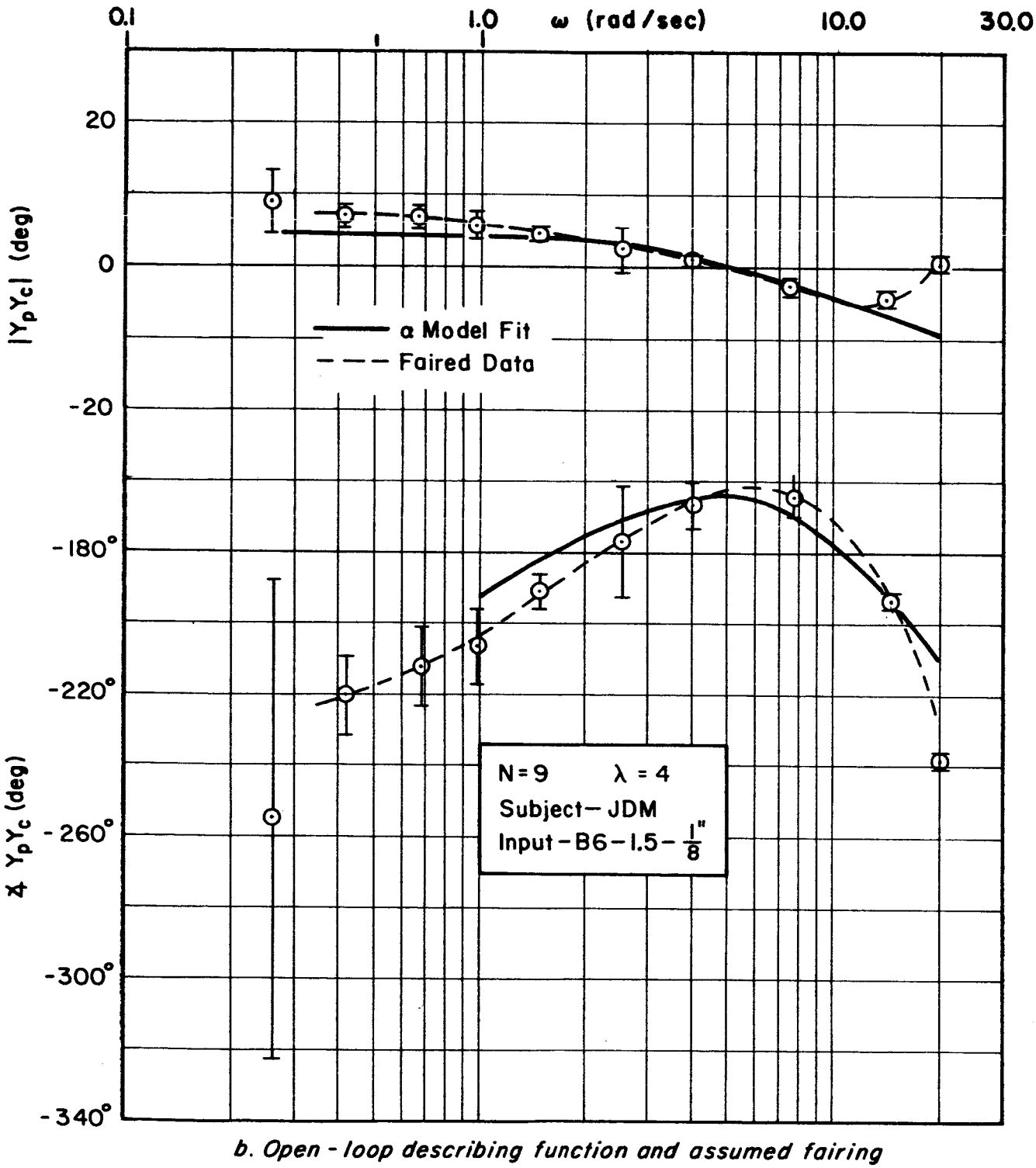

b. Open - loop describing function and assumed fairing

Figure 20.– Concluded

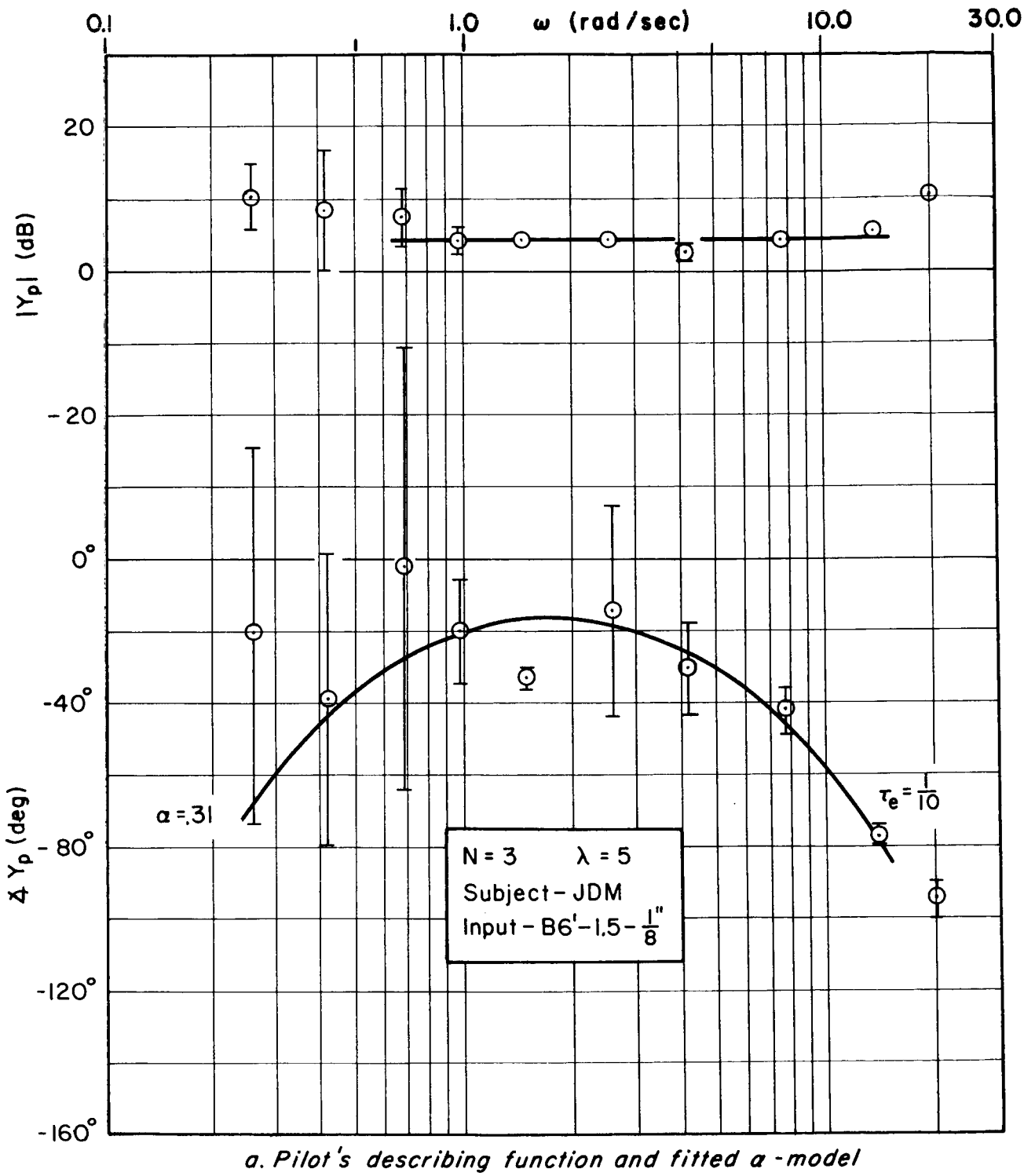

Figure 21. Describing function data at $\omega_i = 1.5$, $\lambda = 5.0$

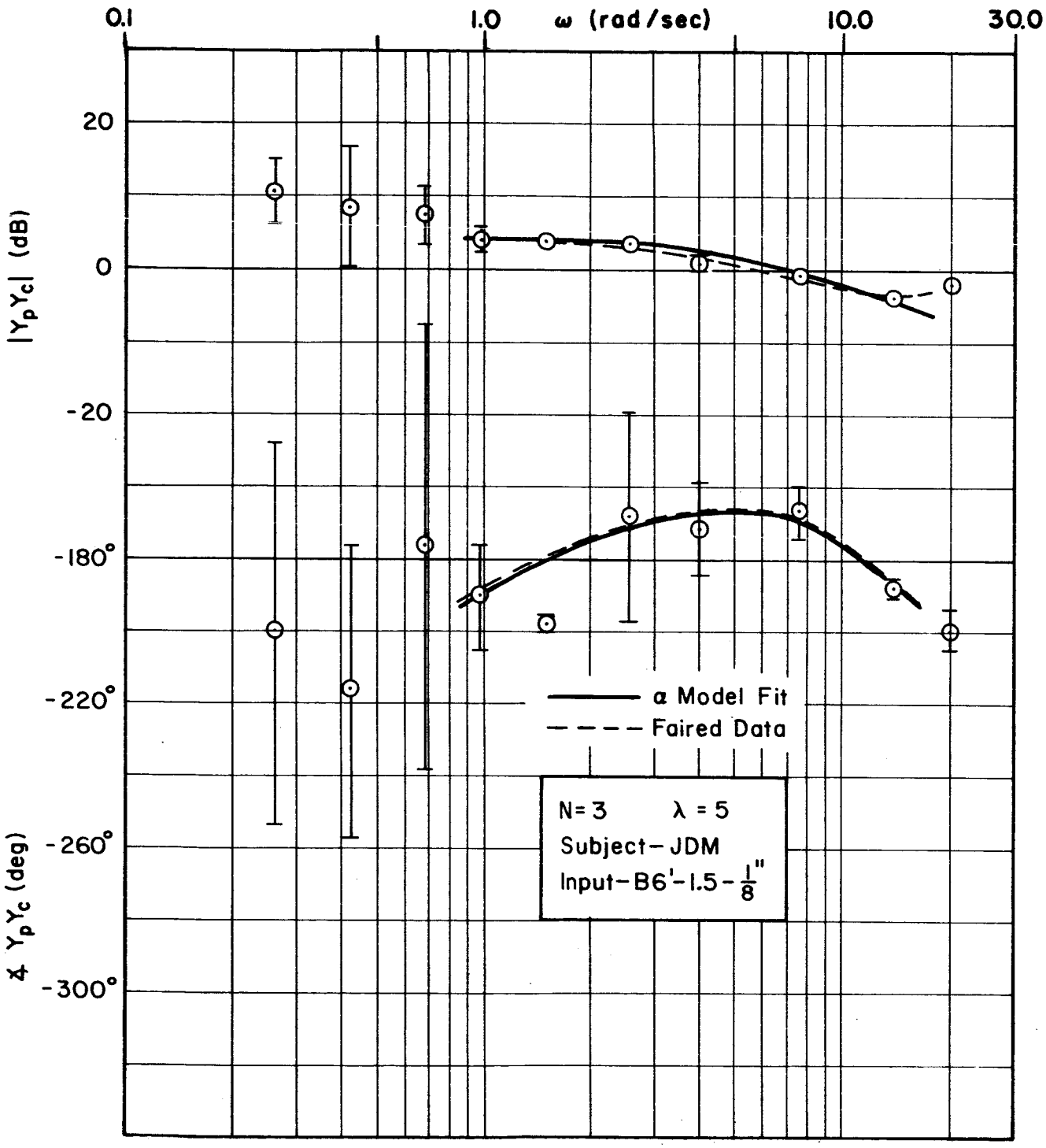

b. Open-loop describing function and assumed fairing

Figure 21.- Concluded

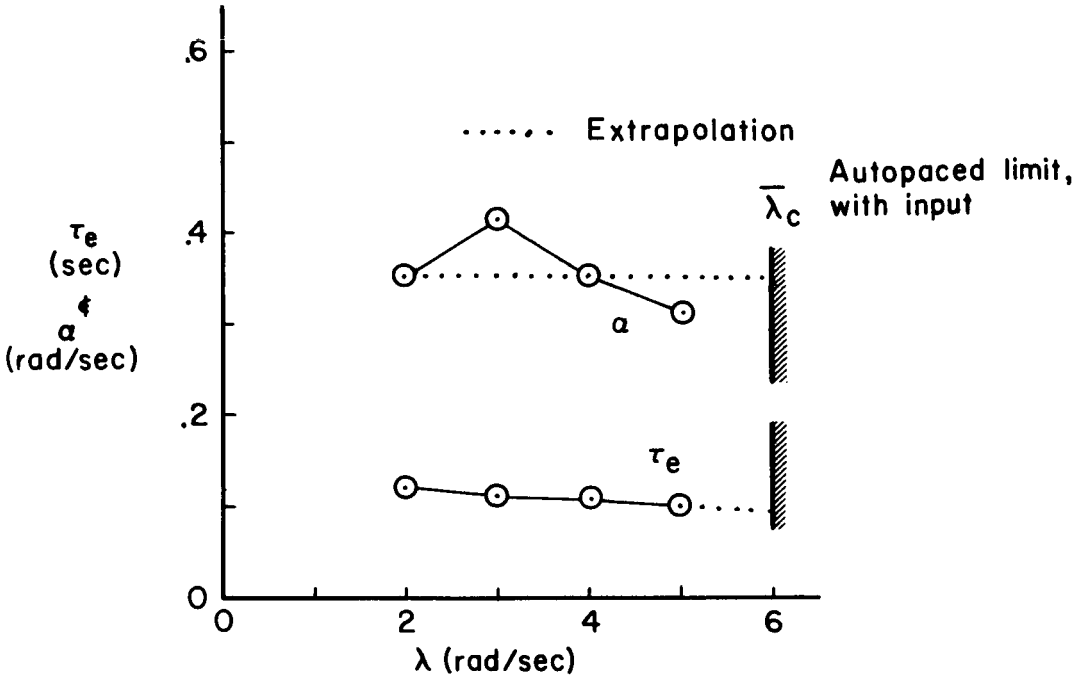

a. Effective delay time and α

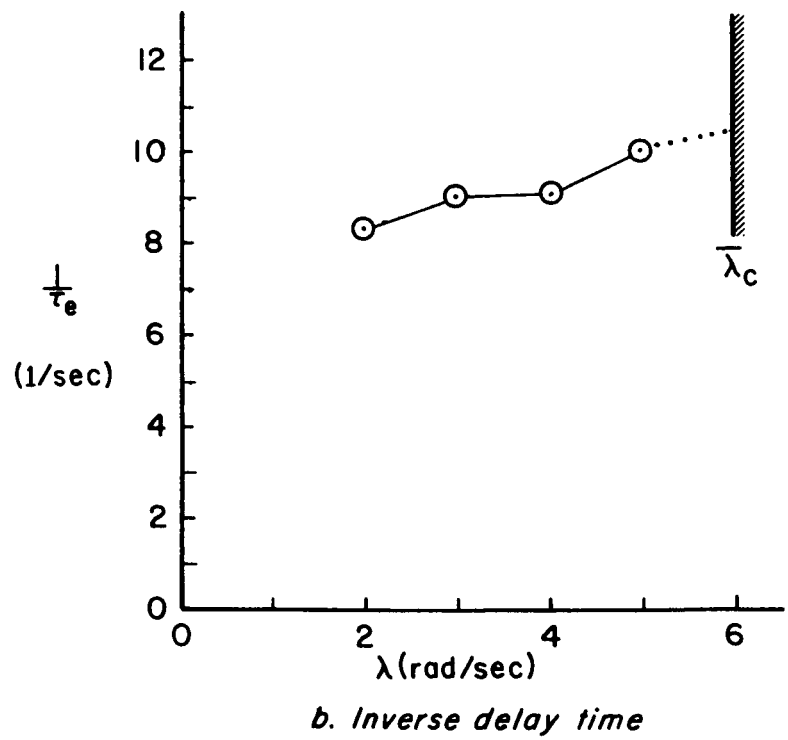

b. Inverse delay time

Figure 22. Fitted α-model parameters (α, τ_e, and $1/\tau_e$) at various levels of instability

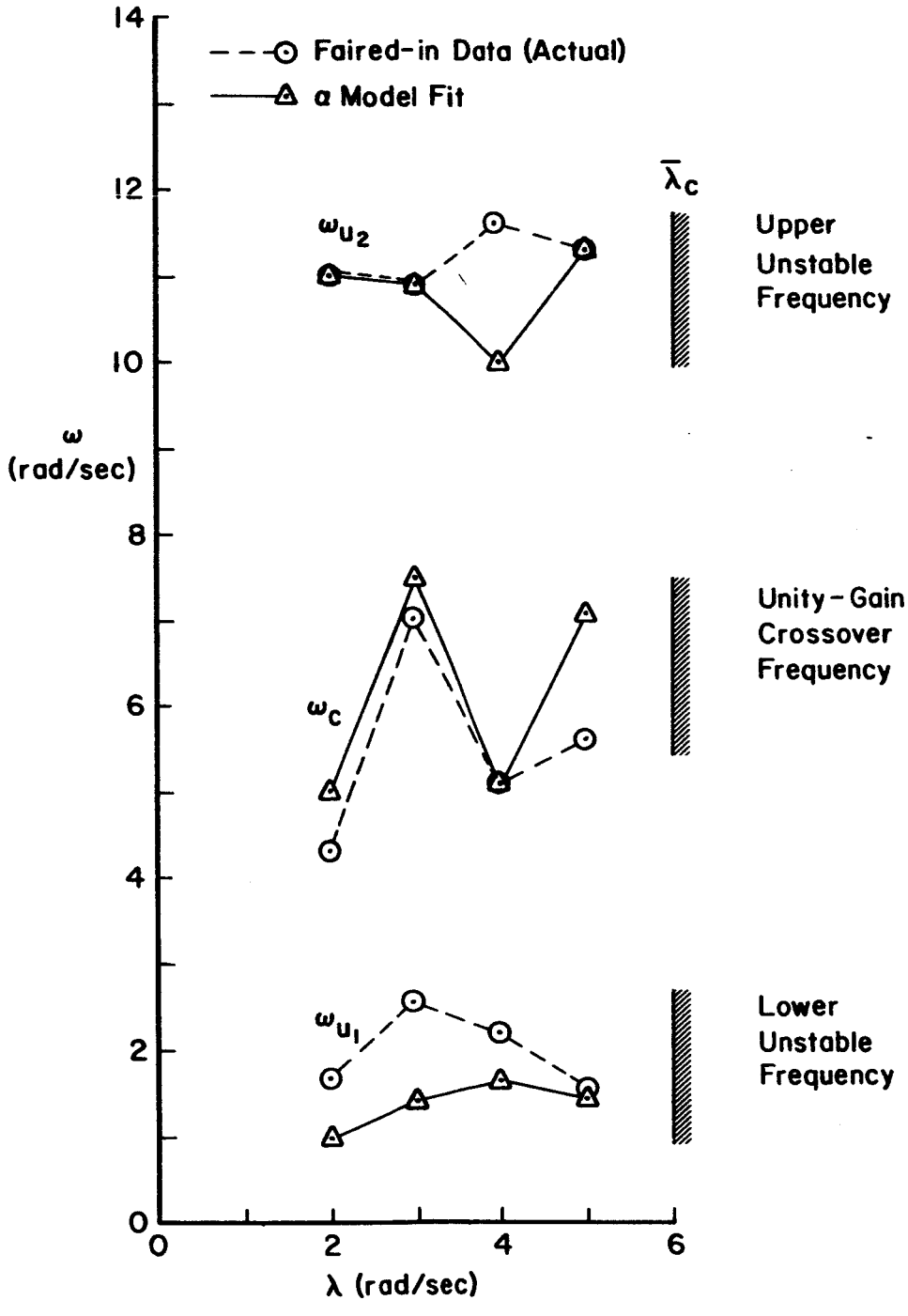

Figure 23. Observed open-loop frequency parameters (ω_{u_1}, ω_{u_2}, and ω_c) at various levels of instability

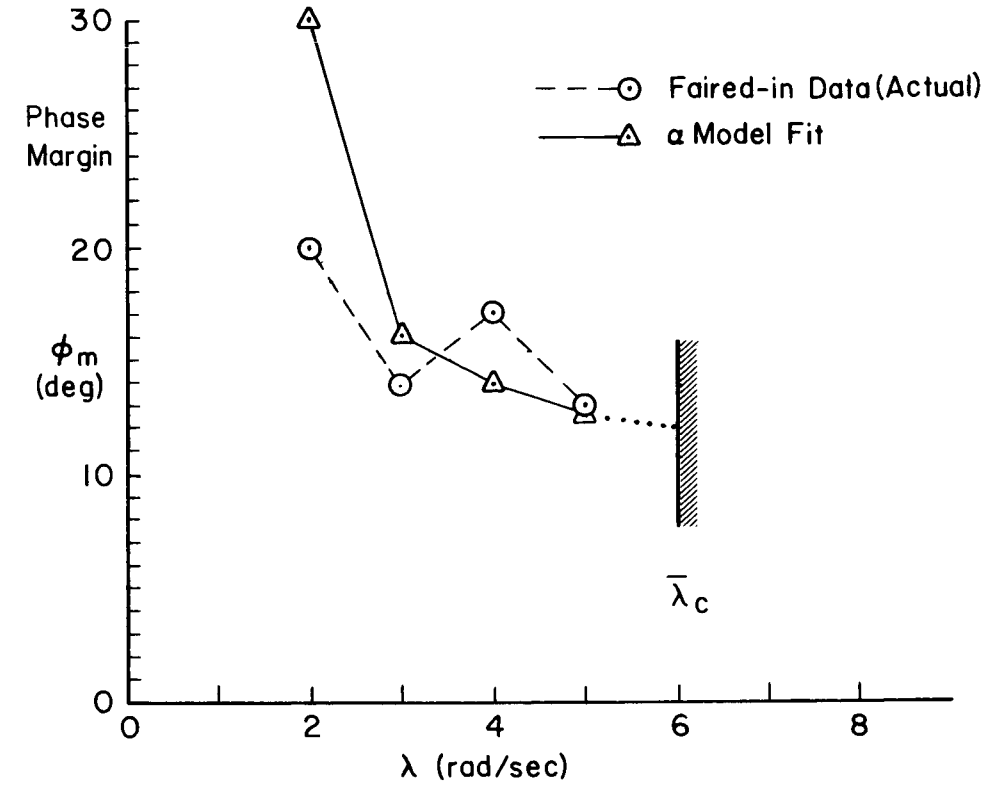

a. Phase Margin

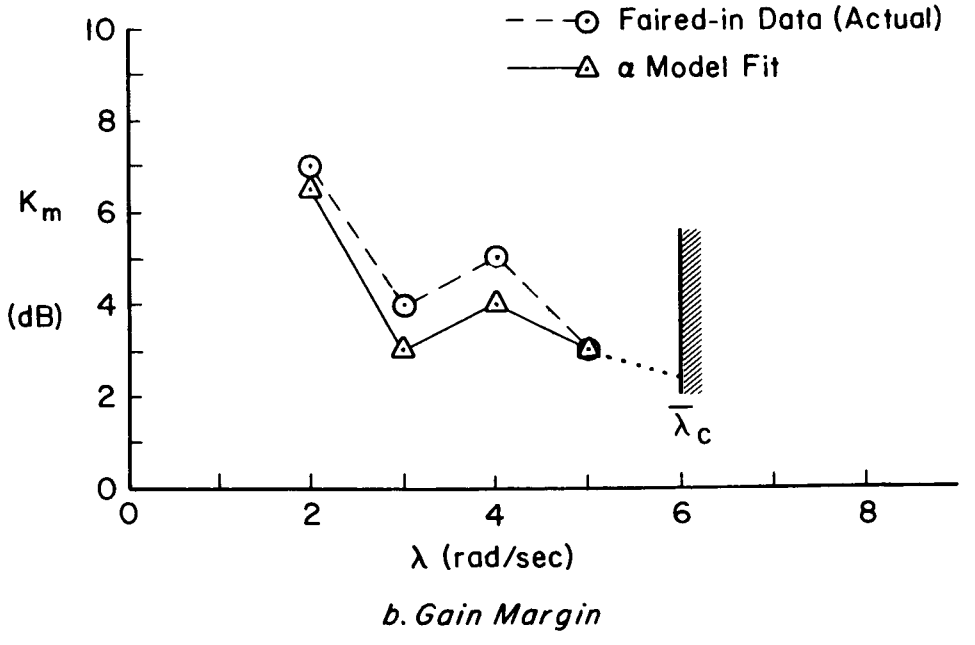

b. Gain Margin

Figure 24. Observed open-loop stability margins (φ_M and K_M) at various levels of instability

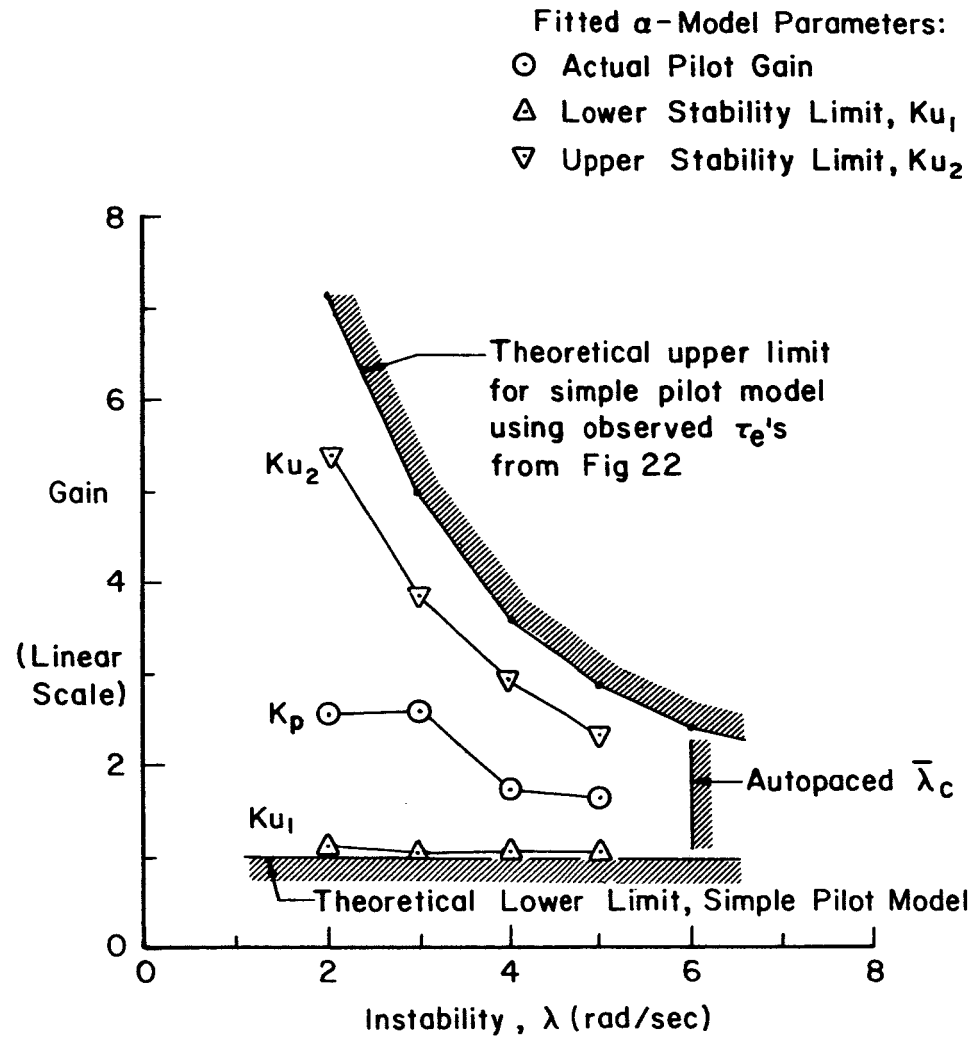

Figure 25. Observed pilot and loop gain parameters (K_{u_1}, K_{u_2}, and K_p) at various levels of instability and comparisons with simple theoretical limits

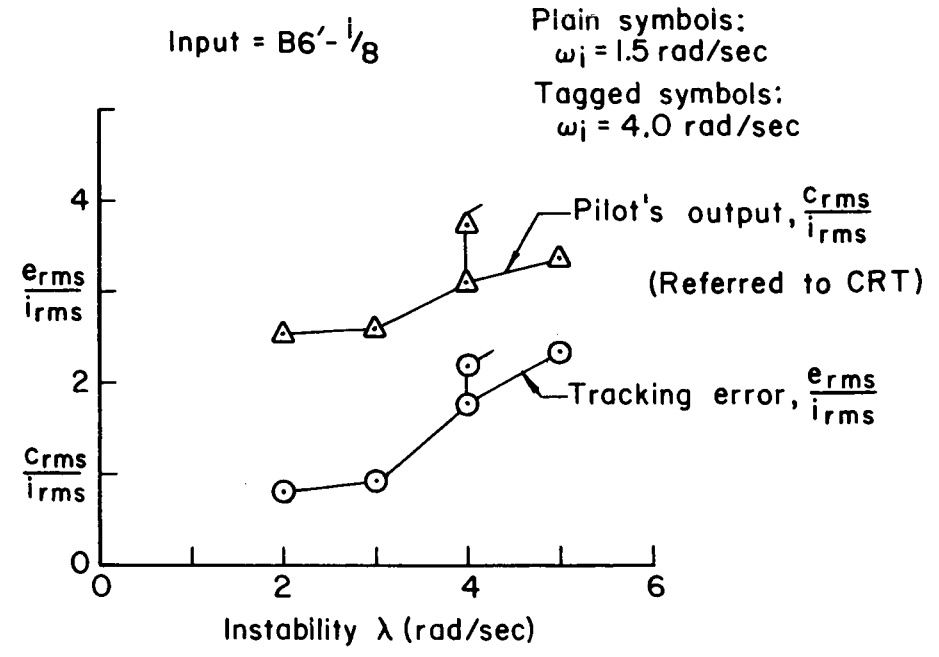

a. Tracking and control measures

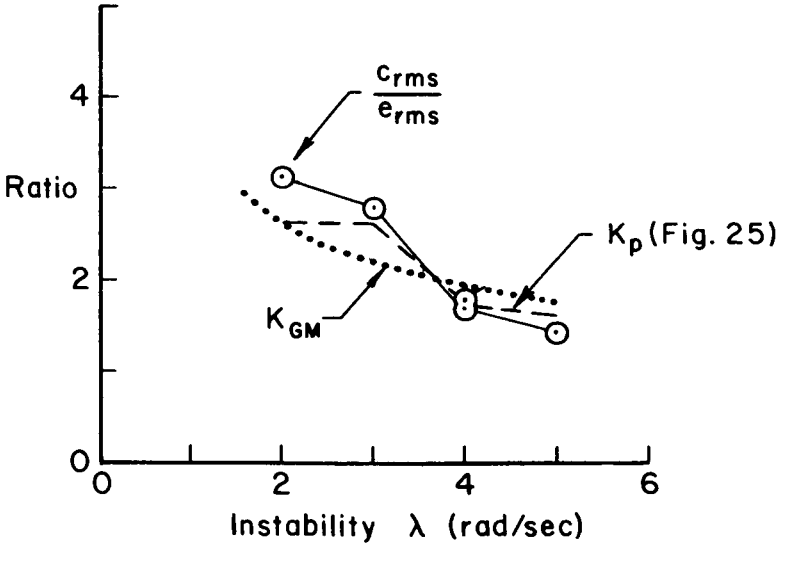

b. Comparison of c_{rms}/e_{rms} and K_p

Figure 26. Relative rms tracking errors and control outputs versus the level of instability

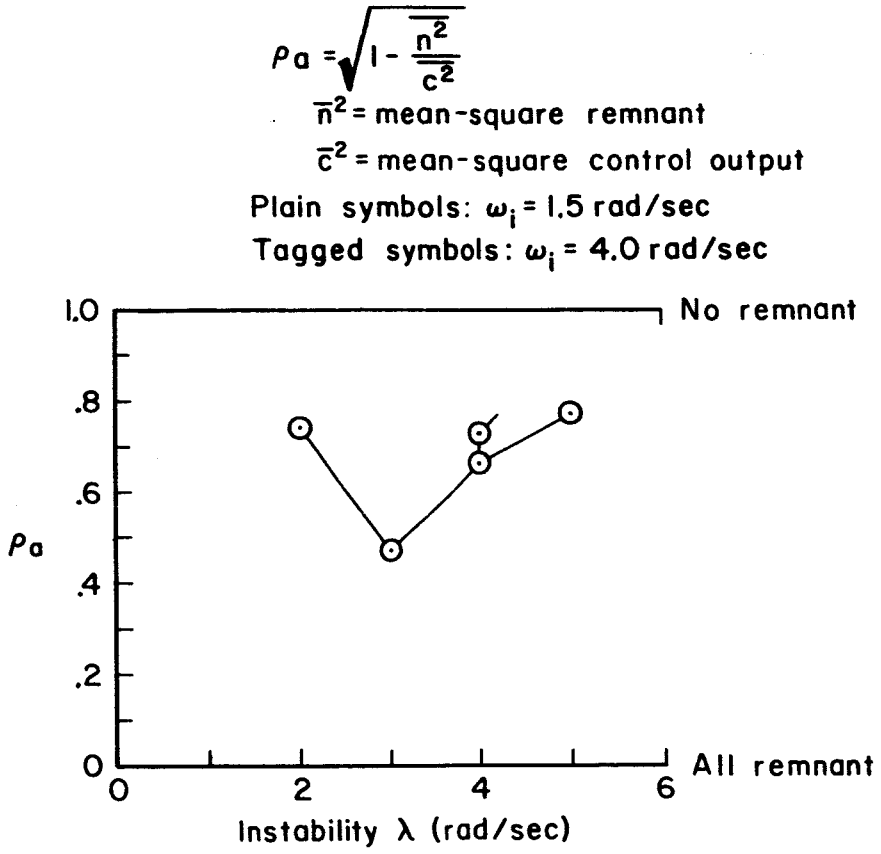

Figure 27. Relative coherence (ρ_a) as a function of λ

APPENDIX A

DERIVATION OF THE CRITICAL TASK LIMIT

The effect of the low frequency kinesthetic lags, as represented by α, on the theoretical relation between the zero margin limit for λ_c and τ_e will be derived. For brevity, most of the subscripts will be dropped.

The total open-loop describing function using the extended crossover model (α-model) of the human operator is given by

$$Y_p Y_c = \frac{-Ke^{-j(\omega\tau + \alpha/\omega)}}{-Ts + 1} \tag{A-1}$$

The limiting conditions for vanishing maximum phase margin are sought. The open-loop phase is

$$\varphi = -\pi + \tan^{-1} T\omega - \tau\omega - \frac{\alpha}{\omega} \tag{A-2}$$

from which the phase margin is

$$\varphi_M = \tan^{-1} T\omega_c - \tau\omega_c - \frac{\alpha}{\omega_c} \tag{A-3}$$

In the ideal limit, the critical condition occurs when <u>both</u> $\varphi_M = 0$ and $d\varphi/d\omega = 0$. The expression for $d\varphi/d\omega$ is

$$\frac{d\varphi}{d\omega} = \frac{T}{1 + (T\omega)^2} - \tau + \frac{\alpha}{\omega^2} = \frac{T\omega^2(1 + \alpha T) + \alpha}{\omega^2\left[(T\omega)^2 + 1\right]} - \tau \tag{A-4}$$

which is zero at the frequency for maximum phase margin, $\omega = \omega_{PM}$. Thus,

$$T\omega_{PM}^2(1 + \alpha T) + \alpha = \tau\omega_{PM}^2\left[(T\omega_{PM})^2 + 1\right] \tag{A-5}$$

Regrouping terms,

$$\left[(T\omega_{PM})^2 + 1\right]\alpha + T\omega_{PM}^2 = \tau\omega_{PM}^2\left[(T\omega_{PM})^2 + 1\right] \qquad \text{(A-6)}$$

from which $$T\omega_{PM}^2 = \left[(T\omega_{PM})^2 + 1\right]\left[\tau\omega_{PM}^2 - \alpha\right] \qquad \text{(A-7)}$$

Generally, $\alpha \ll \tau\omega_{PM}^2$, so

$$\frac{T}{\tau} \doteq (T\omega_{PM})^2 + 1 \qquad \text{(A-8)}$$

Thus, the frequency for maximum phase margin is

$$\omega_{PM}^2 \doteq \frac{T - \tau}{T^2\tau} \qquad \text{(A-9)}$$

Solving for τ in the phase margin expression [eq. (A-3)] for $\varphi_M = 0$, and recognizing this as the limiting crossover frequency, ω_c,

$$\tau = \frac{1}{\omega_c}\tan^{-1} T\omega_c - \frac{\alpha}{\omega_c^2} \doteq T - \frac{\alpha}{\omega_c^2} \qquad \text{(A-10)}$$

Finally, noting that in the limit $\omega_{PM} = \omega_c$, the combination of Eqs. (A-9) and (A-10) into a quadratic in T, plus some algebraic simplification, yields

$$T \doteq \frac{\tau}{1 - \sqrt{\alpha\tau}} \; ; \; T \geq \tau \qquad \text{(A-11)}$$

or $$\lambda_c \doteq \frac{1}{\tau}\left(1 - \sqrt{\alpha\tau}\right) \; ; \; \lambda_c \leq \frac{1}{\tau} \qquad \text{(A-12)}$$

Normalized with respect to τ, the last expression becomes

$$\lambda_c\tau = 1 - \sqrt{\alpha\tau} \qquad \text{(A-13)}$$

APPENDIX B

RUN LOG, AVERAGED AUTOPACED DATA, AND COMPUTER SCHEMATIC

For the reader's reference, a run log of the pertinent runs from which the data of this report were extracted is given in Table B-I. All runs were made at the Engineering Psychology Laboratory at The Franklin Institute under subcontract to Systems Technology, Inc.

The critical values of λ which are plotted in figures 13 and 14 are repeated here in tabular form (Table B-II). The rms variance of the sample is given by

$$\sigma_\lambda = \sqrt{\frac{\sum_{i=1}^{n} (\lambda_i - \bar{\lambda})^2}{n}}$$

where n is the number of trials in the sample.

A schematic of the computer mechanization is shown in figure B-1.

TABLE B-I

CRITICAL TASK RUN LOG

Run no. (a)*	λ (b)*	Input (c)*	Remarks (d, e)*
021865-1	4	2	
-2	4	1	
-4	λ(t)	1	
-5	λ(t)	0	
-6	2	1	
-7	4	1	
-8	3	1	
-9	5	1	2 min. run
-11	5	1	Aborted after 45 sec
-12	5	1	
-13	3	1	
-14	4	1	Data interruped after 2:05 by timer; 4 min. total
-15	2	1	
-16	λ(t)	1	
021965-3	λ(t)	0	
-4	λ(t)	1	
-5	λ(t)	0	
-6	4	1	
-12	4	B6'-4-1/8"	
-13	4	B6'-4-1/8"	
-18	4	1	
-20	λ(t)	0	
-21	λ(t)	1	

*[a]Run number is month-day-year-run of day; i.e., 021865-1 is first run on Feb. 18, 1965.

[b]$Y_c = \lambda/(s-\lambda)$; λ(t) denotes autopaced run.

[c]Input code: 0 = no input; 1 = B6'-1.5-1/8"; 2 = B6-1.6-1/8".

[d]Describing function run length is 4 min. except where noted.

[e]Subject is J. D. McDonnell in all runs.

TABLE B-I.- Concluded

CRITICAL TASK RUN LOG

Run no.	λ	Input	Remarks
022365-3	λ(t)	0	
-4	λ(t)	1	
-7	2	1	
-8	4	1	
-13	4	1	
-14	2	1	
-16	λ(t)	1	
022465-3	λ(t)	0	
-4	λ(t)	1	
-5	4	1	Interrupted at 3:07
-6	4	2	
-7	4	B6'-4-1/8"	Interrupted at 2:42 and 3:47
-9	4	B6'-4-1/8"	
-11	4	1	
-12	λ(t)	1	
-13	λ(t)	0	
022565-9	λ(t)	0	
-10	λ(t)	1	
-11	4	1	

TABLE B-II

TABULATION OF AVERAGED AUTOPACED DATA

Training runs (no input; 5 run samples)			
Trial no.	Date	$\bar{\lambda}_c$	σ_{λ_c}
1 – 5 10	1/13/65, 2:00 PM	5.42 5.48	0.37 0.43
15 20	1/13/65, 2:35 PM	5.76 5.60	0.38 0.48
25 30	1/13/65, 5:15 PM	5.82 5.50	0.37 0.36
35 40	1/14/65, 8:30 AM	5.92 5.90	0.42 0.52
45 50	1/14/65, 11:25 AM	6.46 6.60	0.32 0.41
55 60	1/14/65, 5:30 PM	6.25 6.34	0.21 0.54
65 70	1/25/65, 8:30 AM	5.86 5.94	0.41 0.49
75 80	1/25/65, 5:10 PM	5.84 6.26	0.48 0.30
85 90	1/25/65, 5:23 PM	5.40 6.10	0.65 0.49
95 100	2/2/65, 4:45 PM	6.26 6.30	0.49 0.64
105 110	2/3/65, 4:40 PM	6.02 5.66	0.21 0.38
115 120	2/4/65, 4:40 PM	6.02 5.94	0.60 0.39
125 130	2/8/65, 4:45 PM	6.40 6.62	0.46 0.62
135 140	2/9/65, 10:30 AM	5.98 5.90	0.10 1.01

TABLE B-II.- Concluded

TABULATION OF AVERAGED AUTOPACED DATA

Training runs (no input)			
Trial no.	Date	$\bar{\lambda}_c$	σ_{λ_c}
145 150	2/9/65, 5:15 PM	6.80 6.30	0.21 0.55
155 160	2/10/65, 2:30 PM	6.04 6.20	0.55 1.21
Data runs (from The Franklin Institute)			
No input			
Run no.	Number of trials	$\bar{\lambda}_c$	σ_{λ_c}
021865-5	6	6.36	0.28
-17	5	6.28	0.30
021965-3	5	6.27	0.22
-5	5	6.62	0.22
-20	5	6.40	0.27
022365-3	5	6.36	0.26
022465-3	4	6.51	0.22
-13	5	7.50	0.52
022565-9	5	6.91	0.28
B6'-1.5-1/8" input			
Run no.	Number of trials	$\bar{\lambda}_c$	σ_{λ_c}
021865-4	6	5.05	0.36
-16	5	5.90	0.45
021965-4	5	6.02	0.41
-21	4	6.08	0.46
022365-4	5	6.04	0.26
-16	5	6.22	0.42
022465-4	4	5.95	0.33
-12	5	6.66	0.15
022565-10	5	6.06	0.17

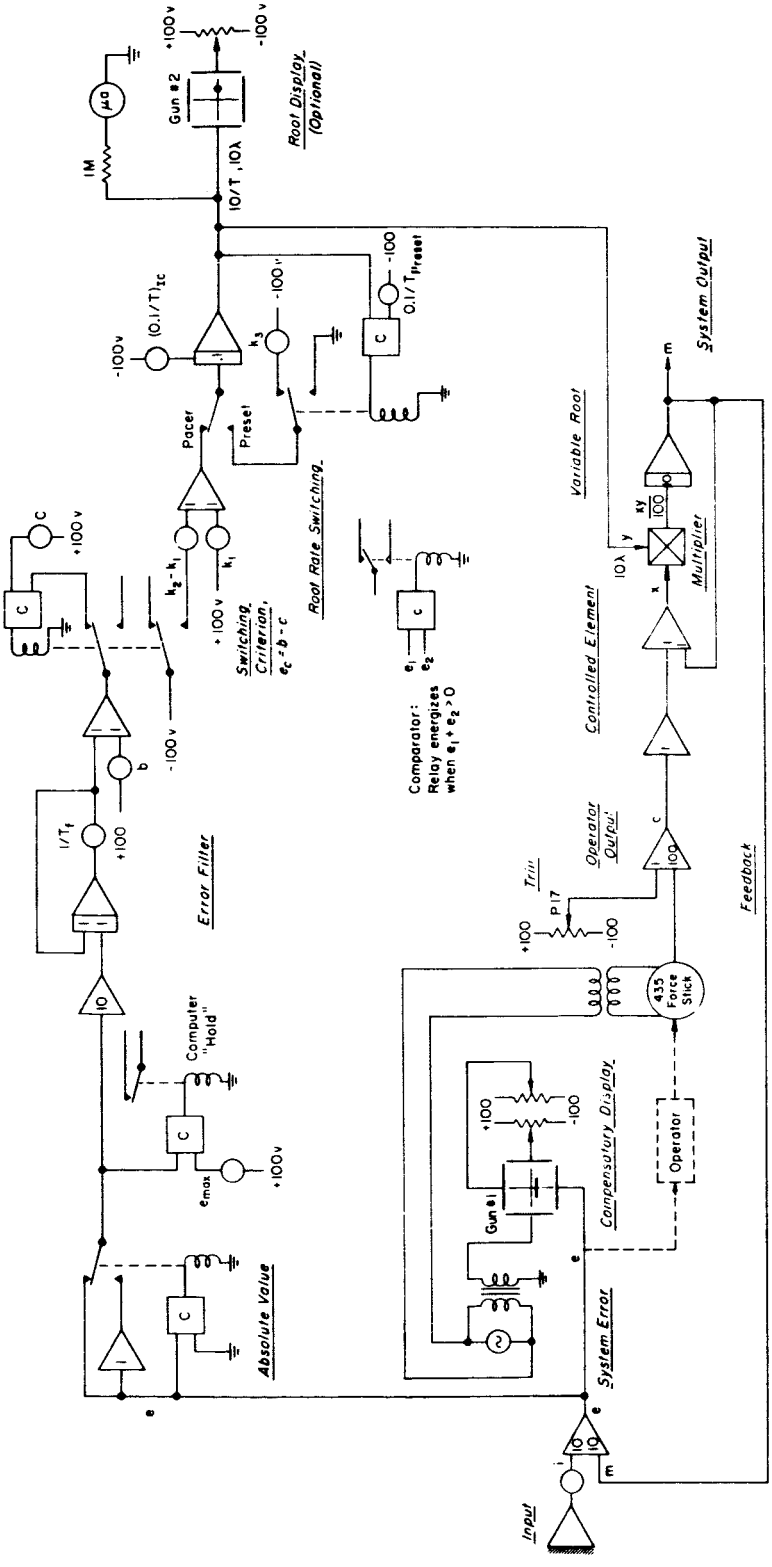

Figure B-1. Detailed Computer Mechanization for the Autopaced Critical Task